

AD-A111 575

VIRGINIA POLYTECHNIC INST AND STATE UNIV BLACKSBURG --ETC F/6 11/2
THERMO-MECHANICAL AND THERMAL BEHAVIOR OF HIGH-TEMPERATURE STRU--ETC(U)
DEC 81 D P HASSELMAN, L D BENTSEN N00014-78-C-0431

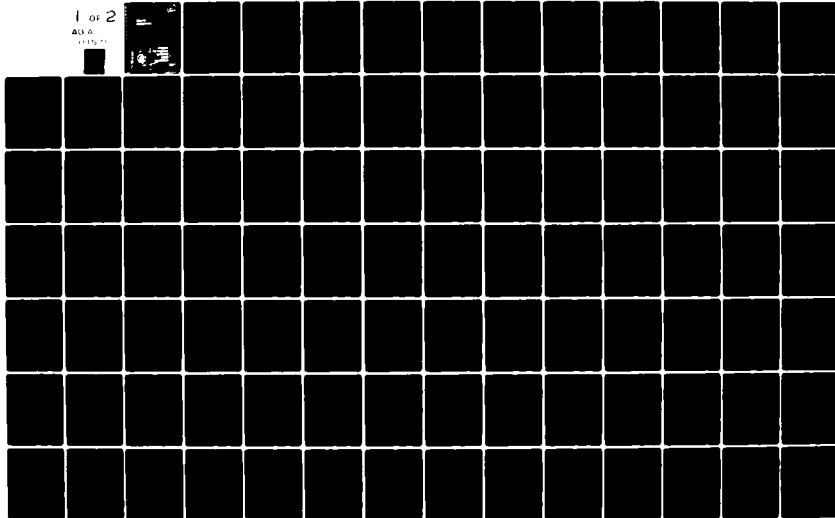
UNCLASSIFIED

NL

1 of 2

AD A

11/7/75



AD A 111575



THERMO-MECHANICAL AND THERMAL
BEHAVIOR OF HIGH-TEMPERATURE STRUCTURAL MATERIALS

Interim Report to

Office of Naval Research

Contract No.: N00014-78-C-0431

January 1, 1981 - December 31, 1981

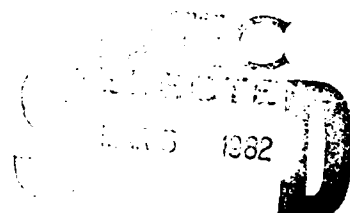
by

D. P. H. Hasselman
Virginia Polytechnic Institute and State University
Blacksburg, Virginia 24061

and

L. D. Bentsen, J. J. Brennan, N. Claussen, C. E. Knight
K. Mazdidasni, K. Niihara, T. Ozyener, K. Satyamurthy,
C. Shih, J. P. Singh, M. Srinivasan, J. R. Thomas, Jr.,
and G. Ziegler

Reproduction in whole or in part is permitted for any
purpose of the United States Government.



A

Approved
for release by the
Department of Defense
on 11/11/81

Unclassified

SECURITY CLASSIFICATION OF THIS PAGE (When Data Entered)

REPORT DOCUMENTATION PAGE		READ INSTRUCTIONS BEFORE COMPLETING FORM
1. REPORT NUMBER	2. GOVT ACCESSION NO.	3. RECIPIENT'S CATALOG NUMBER
4. TITLE (and Subtitle) Thermo-Mechanical and Thermal Behavior of High-Temperature Structural Materials		5. TYPE OF REPORT & PERIOD COVERED Interim Report Jan. 1, 1981 - Dec. 31, 1981
		6. PERFORMING ORG. REPORT NUMBER
7. AUTHOR(s) D. P. H. Hasselman		8. CONTRACT OR GRANT NUMBER(s) N00014-78-C-0431
9. PERFORMING ORGANIZATION NAME AND ADDRESS Virginia Polytechnic Institute and State University, Blacksburg, Virginia 24061		10. PROGRAM ELEMENT, PROJECT, TASK AREA & WORK UNIT NUMBERS
11. CONTROLLING OFFICE NAME AND ADDRESS Office of Naval Research, Code 471 Arlington, VA 22217		12. REPORT DATE December 31, 1981
		13. NUMBER OF PAGES 178
14. MONITORING AGENCY NAME & ADDRESS (if different from Controlling Office)		15. SECURITY CLASS. (of this report) Unclassified
		15a. DECLASSIFICATION/DOWNGRADING SCHEDULE
16. DISTRIBUTION STATEMENT (of this Report) See distribution list. [redacted] release to NTIS		
17. DISTRIBUTION STATEMENT (of the abstract entered in Block 20, if different from Report)		
18. SUPPLEMENTARY NOTES		
19. KEY WORDS (Continue on reverse side if necessary and identify by block number) Absorption coefficient, composites (SiC-Si, MgO-SiC, Al ₂ O ₃ -SiC, BeO-SiC, SiC-glass ceramic, Si ₃ N ₄ -BN), crack propagation and interaction, fracture, micro-cracking, fluidized bed, quench testing, thermal conductivity and diffusivity, radiation, thermal stress and shock.		
20. ABSTRACT (Continue on reverse side if necessary and identify by block number) This report contains preprints of studies, completed during the reporting period, on the thermo-mechanical and thermal behavior of high-temperature structural materials, as follows:		

This document has been approved for public release and sale; its distribution is unlimited.

Technical Articles

- I. K. Niihara, J. P. Singh, and D. P. H. Hasselman, "Observations on the Characteristics of a Fluidized Bed for the Thermal Shock Testing of Brittle Ceramics,"
- II. T. Ozyener, K. Satyamurthy, C. E. Knight, G. Ziegler, J. P. Singh, and D. P. H. Hasselman, "Effect of ΔT - and Spatially Varying Heat Transfer Coefficient on Thermal Stress Resistance of Brittle Ceramics Measured by the Quenching Method."
- III. J. P. Singh, C. Shih and D. P. H. Hasselman, "Analysis of Effect of Crack Interaction on Nature of Strength Loss in Thermally Shocked Brittle Ceramics,"
- IV. J. P. Singh, K. Niihara and D. P. H. Hasselman, "Analysis of Thermal Fatigue Behavior of Brittle Structural Materials."
- V. J. R. Thomas, Jr., J. P. Singh and D. P. H. Hasselman, "Thermal Stresses in a Partially Absorbing Plate Asymmetrically Heated by Cyclic Thermal Radiation and Cooled by Convection,"
- VI. K. Niihara, L. D. Bentsen and K. Mazdidasni, "Anisotropy Effects in the Thermal Diffusivity of Si_3N_4 -BN Composites."
- VII. M. Srinivasan, L. D. Bentsen and D. P. H. Hasselman, "Thermal Diffusivity of Silicon Carbide-Silicon Composites."
- VIII. L. D. Bentsen, D. P. H. Hasselman and N. Claussen, "Effect of Microcracking on the Conduction of Heat in Brittle Composites,"
- IX. J. J. Brennan, L. D. Bentsen and D. P. H. Hasselman, "Measurement of the Thermal Conductivity and Diffusivity of Fine Silicon Carbide Fibers by the Composite Technique,"

Review

- X. J. R. Thomas, Jr., J. P. Singh, and D. P. H. Hasselman, "Thermal Stress in Materials Heated Internally by Radiation Absorption."



Letter on file

A

THERMO-MECHANICAL AND THERMAL
BEHAVIOR OF HIGH-TEMPERATURE STRUCTURAL MATERIALS

PREFACE

Technical ceramics because of their chemical inertness, high melting point, good wear resistance, excellent mechanical stability at high temperature and other unique properties, represent a class of materials eminently suited for many critical engineering applications. Unfortunately, because of their brittleness and unfavorable combination of pertinent material properties, technical ceramics generally are highly susceptible to catastrophic failure in non-uniform thermal environments, which give rise to thermal stresses of high magnitude.

Thermal stress failure analysis of structural materials represents a multi-disciplinary problem which involves the principles of heat transfer, mechanics and materials engineering. Over the last few decades much general understanding of the nature of thermal stress failure of brittle materials has been generated. However, due to the multi-disciplinary nature of the problem, the ability to predict thermal stress failure quantitatively for design or other purposes has lagged behind the progress made in other engineering fields. The objective of the present program is to improve the qualitative and quantitative understanding of the nature of thermal stress failure of brittle structural materials, including the experimental as well as theoretical variables. In order to achieve this objective, the participating investigators and scope of the program are organized such that full advantage is taken of the combined inputs from a number of engineering disciplines. In a similar spirit, a number of studies were conducted in cooperation with investigators at other institutions.

The effort of this program consists of four main themes, including: experimental thermal shock testing with supporting analyses, measurement of thermophysical properties relevant to thermal stress failure, the analysis of mechanisms of thermal stress failure and the dissemination of information on thermal stresses in the form of review articles, conferences, etc.

Studies completed within the period covered by this report are presented as individual chapters in the main body of this report. The title of these chapters within their main theme together with a brief comment are as follows:

A. Experimental Thermal Shock Testing and Supporting Analyses

Chapter I: "Observation on the Characteristics of a Fluidized Bed for the Thermal Shock Testing of Brittle Ceramics"

This study indicates that the heat transfer coefficient of a fluidized bed depends strongly on air flow rate and powder particle size. The absolute values for the heat transfer coefficient for the fluidized bed are below those for silicone oils and aqueous media. For this reason fluidized beds extend the range of values of heat transfer coefficient available to the investigator.

Chapter II: "Effect of ΔT - and Spatially Varying Heat Transfer Coefficient on Thermal Stress Resistance of Brittle Ceramics Measured by the Quenching Method"

Commonly, analyses of experimental data for the thermal stress resistance of brittle ceramics measured by the quenching method assume that the heat transfer coefficient is Newtonian in nature and is spatially uniform over the whole surface of the specimen. In practice, these assumptions generally are not realized. The results of this study shows that for an accurate assessment of thermal shock data, these effects must be taken into account.

Chapter III: "Analysis of Effect of Crack Interaction on Nature of Strength Loss in Thermally Shocked Brittle Ceramics"

The results of this study indicate that co-planar crack interaction during thermal stressing of brittle ceramics can lead to crack coalescence and complete disintegration, not predicted by fracture theories which do not take crack interaction into account.

Chapter IV: "Analysis of Thermal Fatigue Behavior of Brittle Structural Materials"

The purpose of this study was to define the proper role of the various fracture mechanical parameters such as stress intensity factor exponent and activation energy on the thermal fatigue resistance of brittle structural materials for a range of defined thermal environments.

B. Analysis of Mechanisms of Thermal Stress Failure

Chapter V: "Thermal Stresses in a Partially Absorbing Plate Asymmetrically Heated by Cyclic Thermal Radiation and Cooled by Convection"

This study is a continuation of a series of analyses of thermal stresses in partially absorbing ceramics subjected to radiation heating. The present study focussed on the effect of cyclic radiation. The results obtained show that for the same average radiative flux, cyclic radiation will result in thermal stresses of higher magnitude than steady-state radiation.

C. Measurement of Thermophysical Properties Relevant to Thermal Stress Failure

Chapter VI: "Anisotropy Effects in the Thermal Diffusivity of Si_3N_4 -BN Composites"

Experimental data for the thermal diffusivity of hot-pressed Si_3N_4 -BN composites show that the heat conduction properties of these composites can be highly anisotropic due to the preferred orientation of the BN inclusions.

Chapter VII: "Thermal Diffusivity of Silicon Carbide-Silicon Composites"

The results of this study indicate that the room temperature thermal diffusivity of silicon carbide-silicon composites is strongly dependent on the impurity content of the silicon carbide and silicon used for their manufacture.

Chapter VIII: "Effect of Microcracking on the Conduction of Heat in Brittle Composites"

The thermal diffusivity of composites of silicon carbide dispersions in matrices of aluminum oxide, beryllium oxide or magnesium oxide is lowered significantly by the formation of microcracks which result from the mismatch in the coefficients of thermal expansion. The experimental results also indicate that microcrack formation is a highly sensitive function of pore content.

Chapter IX: "Measurement of the Thermal Conductivity and Diffusivity of Fine Silicon Carbide Fibers by the Composite Technique"

Values were obtained for the thermal conductivity and diffusivity of amorphous silicon carbide fibers from corresponding experimental data for composites composed of these fibers contained in a lithium-alumino-silicate glass ceramic matrix.

D. Reviews

Chapter X: "Thermal Stress in Materials Heated Internally by Radiation Absorption"

The results of Chapter V and earlier analysis of thermal stresses in semi-absorbing ceramics were primarily aimed at electro-magnetic radiation such as solar or laser radiation. However, the results obtained are identical to the thermal stresses which would result from the absorption of nuclear radiation. This chapter (X) represents an overview of all relevant results, presented to the technical community interested in fusion research.

For the convenience of the reader, Table 1 lists the status of publications presented in earlier reports. For most of these studies, reprints are available and will be sent on request.

Table 1. Publication Status of Technical Reports Prepared during Program to Date (4/1/78 - 12/31/81)

1. D. P. H. Hasselman and W. A. Zdaniewski, "Thermal Stress Resistance Parameters of Brittle Materials Subjected to Thermal Stress Fatigue," J. Am. Ceram. Soc., 61 (7-8) 375 (1978).
2. D. P. H. Hasselman, "Effect of Cracks on Thermal Conductivity," J. Comp. Mat., 12, 403-07 (1978).
3. W. Zdaniewski, H. Knoch, J. Heinrich and D. P. H. Hasselman, "Thermal Diffusivity of Reaction-Sintered Silicon Nitride," Ceram. Bull, 58, 539 (1979).
4. D. P. H. Hasselman, "Figures-of-Merit for the Thermal Stress Resistance of High-Temperature Brittle Materials," Ceramurgia International, 4, 147 (1979).
5. K. Chyung, G. E. Youngblood and D. P. H. Hasselman, "Effect of Crystallization on the Thermal Diffusivity of a Cordierite Glass-Ceramic," J. Amer. Ceram. Soc., 61, 530 (1978).

6. D. P. H. Hasselman, "Role of Physical Properties in the Resistance of Brittle Ceramics to Fracture in Thermal Buckling," J. Am. Ceram. Soc., 62, 125 (1979).
7. D. P. H. Hasselman and J. P. Singh, "Analysis of Thermal Stress Resistance of Micro-cracked Brittle Materials," Ceramic Bull., 58, 856 (1979).
8. G. E. Youngblood, L. Bentsen, J. W. McCauley and D. P. H. Hasselman, "Thermal Diffusivity of Ba-Mica/Alumina Composites," J. Amer. Ceram. Soc., 58, 620 (1979).
9. D. P. H. Hasselman and Y. Tree, "On the Thermal Fracture of Ice," J. Mat. Sc., 14, 1499 (1979).
10. D. P. H. Hasselman, J. C. Swearingen, E. K. Beauchamp and W. A. Zdaniewski, "Effect of Alumina Dispersions on the Thermal Conductivity/Diffusivity and Thermal Stress Resistance of a Borosilicate Glass," J. Mat. Sc., 15, 518-20 (1980).
11. D. P. H. Hasselman, J. R. Thomas, Jr., M. P. Kamat and K. Satyamurthy, "Thermal Stress Analysis of Partially Absorbing Brittle Ceramics Subjected to Radiation Heating," J. Am. Ceram. Soc., 63, 21-25 (1980).
12. J. P. Singh, J. R. Thomas, Jr., and D. P. H. Hasselman, "Analysis of Effect of Heat Transfer Variables on Thermal Stress Resistance of Brittle Ceramics Measured by Quenching Experiments," J. Am. Ceram. Soc., 63, 140-44 (1980).
13. K. Satyamurthy, M. P. Kamat, J. P. Singh and D. P. H. Hasselman, "Effect of Spatially Varying Thermal Conductivity on Magnitude of Thermal Stress in Brittle Ceramics Subjected to Convective Heating," J. Am. Ceram. Soc., 63, 363 (1980).
14. G. Ziegler and D. P. H. Hasselman, "Effect of Data Scatter on Apparent Thermal Stress Failure Mode of Brittle Ceramics," Ceramurgia, 5, 126 (1979).
15. K. Satyamurthy, J. P. Singh, M. P. Kamat and D. P. H. Hasselman, "Effect of Spatially Varying Porosity on Magnitude of Thermal Stress During Steady-State Heat Flow," J. Amer. Ceram. Soc., 62, 432 (1979).
16. Bob R. Powell, Jr., G. E. Youngblood, D. P. H. Hasselman and Larry D. Bentsen, "Effect of Thermal Expansion Mismatch on the Thermal Diffusivity of Glass-Ni Composites," J. Amer. Ceram. Soc., 63, 581 (1980).
17. D. P. H. Hasselman, P. F. Becher and K. S. Mazdidasni, "Analysis of the Resistance of High-E, Low-E Brittle Composites to Failure by Thermal Shock," Materials Technology, 11, 82 (1980).

18. K. Satyamurthy, J. P. Singh, M. P. Kamat and D. P. H. Hasselman, "Thermal Stress Analysis of Brittle Ceramics with Density Gradients Under Conditions of Transient Convective Heat Transfer," Proc. Brit. Ceram. Soc., 80, 10 (1980).
19. J. R. Thomas, Jr., J. P. Singh and D. P. H. Hasselman, "Analysis of Thermal Stress Resistance of Partially Absorbing Ceramic Plate Subjected to Asymmetric Radiation, I: Convective Cooling at Rear Surface," J. Am. Ceram. Soc., 63, 163 (1981).
20. J. P. Singh, K. Satyamurthy, J. R. Thomas and D. P. H. Hasselman, "Analysis of Thermal Stress Resistance of Partially Absorbing Ceramic Plate Subjected to Asymmetric Radiation, II: Convective Cooling at Front Surface," J. Am. Ceram. Soc., 63, 169 (1981).
21. J. P. Singh, D. P. H. Hasselman, W. M. Su, J. A. Rubin and R. Palicka, "Observations on the Nature of Micro-Cracking in Brittle Composites," J. Mat. Sc., 16, 141 (1981).
22. J. P. Singh, Y. Tree and D. P. H. Hasselman, "Effect of Bath and Specimen Temperature on the Thermal Stress Resistance of Brittle Ceramics Subjected to Thermal Quenching," J. Mat. Sc., 16, 2109 (1981).
23. N. Claussen and D. P. H. Hasselman, "Improvement of Thermal Shock Resistance of Brittle Structural Ceramics by a Dispersed Phase of Zirconia," pp. 381-395, Proc. Conf. on Thermal Stress in Severe Environments, Ed. by D. P. H. Hasselman and R. A. Heller, Plenum Press (1980).
24. G. Ziegler and D. P. H. Hasselman, "Effect of Phase Composition and Microstructure on the Thermal Diffusivity of Silicon Nitride," J. Mat. Sc., 16, 495 (1981).
25. G. Ziegler, L. D. Bentsen and D. P. H. Hasselman, "Orientation Effects on the Thermal Diffusivity of Hot-Pressed Silicon Nitride," Comm. Am. Ceram. Soc., 64, 35 (1981).
26. K. Niihara, J. P. Singh, L. D. Bentsen and D. P. H. Hasselman, "Observations on the Sub-Critical Growth and Healing of Micro-cracks in Brittle Ceramics," pp. 323-34, Proc. Conf. on Surfaces and Interfaces in Ceramic and Ceramic-Metal Systems, Plenum Press (1981).
27. J. P. Singh, J. R. Thomas and D. P. H. Hasselman, "Thermal Stresses in Partially Absorbing Flat Plate Symmetrically Heated by Thermal Radiation and Cooled by Convection," J. of Thermal Stresses, 3, 341, (1980).
28. K. Satyamurthy, D. P. H. Hasselman and J. P. Singh, "Effect of Nature of Concavity of Temperature Distribution on Position and Sign of Maximum Thermal Stress, A Short Note," J. Thermal Stresses, 3, 551 (1980).
29. C. Shih, J. P. Singh and D. P. H. Hasselman, "Effect of Crack Interaction on the Fracture Initiation and Crack Propagation in Brittle Ceramics Subjected to Severe Thermal Shock," High-Temp.-High Pressures, 12, 477 (1980).

30. Proc. Conf. Thermal Stresses in Materials and Structures in Severe Thermal Environments. Co-edited by D. P. H. Hasselman and R. A. Heller, Plenum Press (1980).
31. K. Satyamurthy, D. P. H. Hasselman, J. P. Singh, and M. P. Kamat, "Effect of Spatial Variation of Thermal Conductivity on Magnitude of Tensile Thermal Stresses in Brittle Materials Subjected to Convective Heating," pp. 325-342, Proc. Conf. Thermal Stresses in Materials and Structures in Severe Thermal Environments, Ed. by D. P. H. Hasselman and R. A. Heller, Plenum Press (1980).
32. J. P. Singh, J. R. Thomas, Jr., and D. P. H. Hasselman, "Stresses Due to Thermal Trapping in Semi-Absorbing Materials Subjected to Intense Radiation," pp. 157-168, Proc. Conf. Thermal Stresses in Materials and Structures in Severe Thermal Environments, Ed. by D. P. H. Hasselman and R. A. Heller, Plenum Press (1980).
33. D. P. H. Hasselman, "Effect of Micro-Cracking on Thermal Conductivity: Analysis and Experiment," Proc. 16th Int. Conf. Thermal Conductivity (in press).
34. J. R. Thomas, J. P. Singh and D. P. H. Hasselman, "Role of Thermal Expansion in the Thermal Stress Resistance of Semi-Absorbing Brittle Materials Subjected to Severe Thermal Radiation," Proc. 7th Int. Thermal Expansion Symposium (in press).
35. K. Niihara, J. P. Singh and D. P. H. Hasselman, "Observations on the Characteristics of a Fluidized Bed for the Thermal Shock Testing of Brittle Ceramics," J. Mat. Sc., (in review).
36. T. Ozyener, K. Satyamurthy, C. E. Knight, G. Ziegler, J. P. Singh and D. P. H. Hasselman, "Effect of ΔT - and Spatially Varying Heat Transfer Coefficient on Thermal Stress Resistance of Brittle Ceramics Measured by the Quenching Method," J. Amer. Ceram. Soc., (in review).
37. J. P. Singh, C. Shih and D. P. H. Hasselman, "Analysis of Effect of Crack Interaction on Nature of Strength Loss in Thermally Shocked Brittle Ceramics," J. Amer. Ceram. Soc., 64, C106 (1981).
38. J. P. Singh, K. Niihara and D. P. H. Hasselman, "Analysis of Thermal Fatigue Resistance of Brittle Structural Materials," J. Mat. Sc., 16, 2789 (1981).
39. J. R. Thomas, Jr., J. P. Singh and D. P. H. Hasselman, "Thermal Stresses in a Partially Absorbing Plate Asymmetrically Heated by Cyclic Thermal Radiation and Cooled by Convection," J. Thermal Stresses (in press).
40. K. Niihara, L. D. Bentsen, K. Mazdidasni, "Anisotropy Effects in the Thermal Diffusivity of Si_3N_4 -BN Composites," J. Amer. Ceram. Soc., 64, C-117 (1981).

41. M. Srinivasan, L. D. Bentsen and D. P. H. Hasselman, "Thermal Diffusivity of Silicon Carbide-Silicon Composites," Proc. 17th Int. Thermal Conductivity Conference (in press).
42. L. D. Bentsen, D. P. H. Hasselman and N. Claussen, "Effect of Microcracking on the Conduction of Heat in Brittle Composites," pp. 369-82 in Proc. Conf. Environmental Degradation of Engineering Materials in Aggressive Environments, Virginia Polytechnic Institute (1981).
43. J. J. Brennan, L. D. Bentsen and D. P. H. Hasselman, "Measurement of the Thermal Conductivity and Diffusivity of Fine Silicon Carbide Fibers by the Composite Technique," J. Mat. Sc., (in review).
44. J. R. Thomas, Jr., J. P. Singh and D. P. H. Hasselman, "Thermal Stress in Materials Heated Internally by Radiation Absorption," J. of Nuclear Materials (in press).

CHAPTER I

OBSERVATIONS ON THE CHARACTERISTICS OF A FLUIDIZED
BED FOR THE THERMAL SHOCK TESTING OF BRITTLE CERAMICS

By

K. Niihara, J. P. Singh and D. P. H. Hasselman

Department of Materials Engineering
Virginia Polytechnic Institute and State University
Blacksburg, VA. 24061 USA

OBSERVATIONS ON THE CHARACTERISTICS OF A FLUIDIZED
BED FOR THE THERMAL SHOCK TESTING OF BRITTLE CERAMICS

K. Niihara, J. P. Singh, D. P. H. Hasselman

Department of Materials Engineering
Virginia Polytechnic Institute and State University
Blacksburg, VA. 24061 USA

The heat transfer characteristics of a fluidized bed used as a quenching medium for the thermal stress testing of brittle ceramics, were determined by measurements of the thermal shock behavior of rods of a soda-lime-silica glass. The heat transfer coefficient was found to be strongly dependent on the mean particle size of the powder and air flow rate, and was relatively independent of the position within the bed. The results indicate that the heat transfer coefficient during thermal shock fracture may have a value lower than that obtained under heat transfer conditions which more closely resemble steady-state. The heat transfer data inferred from the quenching experiments with the glass, gave excellent agreement between calculated and measured values for the thermal shock behavior for rods of a polycrystalline aluminum oxide. It is concluded that fluidized beds are excellent inert quenching media with variable heat transfer coefficient controlled by particle size and flow rate.

1. INTRODUCTION

Technical ceramics, because of their combination of high melting point and chemical stability are excellent candidate materials for engineering applications involving extreme thermal and chemical environments. However, due to an unfavorable combination of values

for such properties as thermal conductivity, Young's modulus, coefficient of thermal expansion and tensile strength, many technical ceramics exhibit low resistance to failure by thermal stresses, frequently encountered during transient or steady-state heat flow [1]. Due to the inherent brittleness of ceramic materials, such failure can be highly catastrophic. For reliable engineering design and optimum material selection, it is imperative that the thermal stress behavior of technical ceramics be well understood. This can be accomplished on the basis of theoretical principles or by actual testing. One popular test method, in view of its simplicity, consists of quenching specimens in the form of circular or square cylinders from a pre-selected higher temperature into a fluid medium at lower temperature. Such a fluid medium can consist of either silicone oil [2], a eutectic salt mixture [3,4], water [5], liquid metals [6] or fluidized powders [7]. For purposes of the quantitative evaluation of the test results, the heat transfer characteristics of these fluid media must be well understood. In this respect, a number of experimental studies [8,9,10,11] have shown that water as a quenching medium can be highly variable in its heat transfer characteristics, primarily due to nucleate boiling and/or steam film formation which are dependent not only on the temperature but also on the surface condition of the material. The decrease of the viscosity of silicone oils with increasing temperature causes a corresponding increase in the heat transfer coefficient [11]. Increased turbulence of eutectic salts with increasing temperature tends to create a corresponding increase in the rate of heat transfer [4]. A recent analysis showed that the results of quenching experiments also depend on whether the heat transfer occurs by natural or forced convection [12]. Water has the disadvantage

of promoting stress corrosion [13]. Oils are subject to decomposition which can lead to the formation of strongly adhering coatings on the specimen surface and subsequent changes in mechanical or other properties [14].

Fluidized beds which use ceramic powders as the fluid medium offer the advantage of chemical inertness over a wide range of temperature. Literature data [7,15] show considerable differences in the heat transfer characteristics of fluidized beds used for thermal shock testing. These differences, as indicated by the experimental data of Callahan [15] for the heat transfer coefficient of fluidized beds obtained by a direct method, may be attributable to differences in the way these fluidized bed were being operated. In this respect, then, the primary objective of this study was to investigate the effect of gas flow rate and powder particle size on the heat transfer characteristics of fluidized beds used for the thermal shock testing of brittle ceramics. The secondary objective of this study was to compare the values of the heat transfer coefficient inferred indirectly from the thermal shock data with those measured by direct means.

2. EXPERIMENTAL

2.1 Test Materials

A soda-lime-silica glass^{*} and a polycrystalline alumina^{**} were selected as materials appropriate for testing of the fluidized bed. Both these materials were used in a number of previous studies [11,13] which facilitated comparison of the experimental data. The materials were

* R-6, Owens-Corning Fiberglass Corp., Toledo, Ohio

**998 Alumina, McDanel Refractory Porcelain Co., Beaver Falls, PA.

supplied by the manufacturers in the form of circular rods. Their property values and diameter are given in Table 1. Because of the ease of crack detection in the glass by visual means, most tests were conducted with this material. The aluminum oxide specimens were used for the purpose of illustration of the use of data obtained.

2.2 Equipment and Test Procedures

The fluidized bed of commercial design[§], suitable for operation at elevated temperatures, if desired, consisted of a vertical stainless-steel hollow cylinder with inner diameter of approximately 0.1 m and height of approximately 0.15 m. In order to extend the range of the rates of air flow and to minimize the loss of the fluidizing powder, a silica tube approximately 0.5 m high and 0.09 m in inner diameter was placed inside the steel cylinder. Air was used as the fluidizing agent. The rate of air flow was controlled by a flow meter. To assure a uniform flow of air across the width of the fluidizing bed, the perforated bottom was covered with a fiberglass cloth pad, which also prevented the loss of finer powders through the bed bottom between experiments. For all tests, the fluidized bed was maintained at room temperature.

An aluminum oxide powder^{*} was selected as an appropriate fluidizing medium. By screening, the powder was divided into a number of size fractions corresponding to screen sizes of 60 to 65, 100 to 115, 200 to 270 and 325-400 mesh, to give average particle sizes of 231, 138, 69 and 38 μm .

[§]TECAM Fluidized Bath Model FBS, Techne Incorp., 661 Brunswick Pike, Princeton, N.J.

^{*}Calcined alumina powder (-230 mesh), Aluminum Corporation of America.

TABLE 1. Properties of Test Materials

	<u>Soda-Lime Glass</u> [*]	<u>Alumina</u> ^{**}
Young's modulus (GPa)	69	393
Coeff. of thermal expansion, α ($^{\circ}\text{C}^{-1}$) $\times 10^{-6}$	9.3	9 (725 $^{\circ}\text{C}$)
Poisson's ratio, ν	0.25	0.265
Thermal conductivity, k (cal.cm. $^{-1}$ $^{\circ}\text{C}^{-1}$.s $^{-1}$) $\times 10^3$	2.5	21.9 (725 $^{\circ}\text{C}$)
Flexural strength (MPa)	194 (Liq. N ₂ temp.)	271 (Room temp.)
Diameter, $d(\text{m}) \times 10^{-3}$	5.3	6.35
Weibull parameter, m	8	16

* See refs. 11, 13.

** Young's modulus value was supplied by the manufacturer, Poisson's ratio and coeff. of thermal expansion were obtained from ref. 16, and other properties values were obtained in the writer's laboratory.

Prior to quenching, the specimens were preheated in an electrically heated, thermostatically controlled ($\pm 0.5^\circ\text{C}$) tube furnace with internal diameter of ≈ 0.05 m, mounted vertically above the fluidized bed. The specimens in the form of circular cylinder with length ≈ 0.06 m were attached to the lower end of a quartz rod mounted vertically along the center line of the furnace tube. In the upper position of the rod, during preheating, the specimens were located in the axial and radial center of the hot zone of the furnace. In the lower position of the rod, the specimen was located within the fluidized bed. This lower position was adjustable to permit measurement of the heat transfer characteristics as a function of the vertical position within the bed. Caps mounted over the ends of the furnace tube assured temperature uniformity and eliminated possible specimen cooling due to the upward flow of air through the tube furnace. Thermal equilibrium immediately prior to quenching was obtained by holding the specimens for at least 15 min. at the level of preselected temperature. Quenching of the specimens was accomplished by dropping the rod from the upper to lower position under the influence of gravity without any mechanical constraint. Following the quenching, the specimens were held in the fluidized bed for approximately 5 min. after which they were removed and examined. All specimens were tested singly, in order to assure that the heat transfer was not affected by the presence of other specimens. However, in order to take account of possible specimen-to-specimen variation, a total of five (5) specimens were tested for any given temperature difference and operating condition of the fluidized bed. To eliminate any fatigue effects on the results obtained each specimen was tested only once.

The critical temperature difference (ΔT_c) required to induce thermal stress fracture in the specimens for a given air flow rate and alumina particle size was established by varying the temperature difference between the tube furnace and the fluidized bed. To reflect the variation from specimen to specimen, ΔT_c for the glass was reported in terms of the temperature range required to fracture one and four of the five specimens tested. For the alumina specimens in which the cracks were not easily detected by visual or other means, ΔT_c was determined by measuring the fracture strength of the quenched specimens at room temperature in four-point bending with an inner and outer span of 0.016 and 0.05 m, respectively. For these specimens, ΔT_c was defined as the value of quenching temperature difference which caused a 50% or greater decrease in strength compared to the non-quenched specimens.

The heat transfer characteristics of the fluidized bed were determined by indirect as well as direct means. Indirectly, the heat transfer coefficient was determined from the experimental data for ΔT_c for the glass specimens with the aid of thermoelastic theory. Thermal stress failure in brittle materials generally occurs under the influence of the tensile stresses. For the quenching conditions of the present study, the maximum tensile thermal stresses occur in the specimen surface. For a solid circular cylinder and $0 < Rh/k < 10$, from the solutions of Jaeger [17] the magnitude of these stresses to a very good approximation can be described by:

$$\sigma_{\max}^{-1}(r = R) = \frac{1.45(1-\nu)}{\alpha E} \left\{ 1 + \frac{3.41K}{Rh} \right\} \quad (1)$$

where α , E , K and ν are defined in Table 1, R is the radius of the cylinder and h is the heat transfer coefficient. At $\Delta T = \Delta T_c$, the maximum value

of tensile thermal stress equals the tensile fracture stress. Following the approach of Becher et al. [10] and Singh, Tree and Hasselman [11], the heat transfer coefficient was calculated by substitution of the values for the material properties, R and ΔT_c into equation 1. In the calculations, the relative temperature dependence of the strength of the glass specimen was assumed to be identical to the strength data of Shand [18]. Using the strength of 194 MPa at liquid nitrogen temperature [13], an estimate of the strength of the present glass specimens at different temperatures was easily made.

The direct measurement of the heat transfer coefficient relied on the method of Callahan [15] and Crantina [14], which consisted of measuring the transient temperature response of a small, preheated specimen quenched in the fluidized bed. For the present study the specimen consisted of an alumina sphere of diameter 1.25 cm, with a thermocouple in a hole drilled to the exact center of the sphere. For the alumina, the thermal conductivity and diffusivity were established independently by the laser-flash method. A plot of the non-dimensional transient temperature at the center of the sphere, on comparison with the charts of Schneider [19], yields the appropriate value of Rh/K from which the value of h can be calculated.

The value of h obtained from the data for ΔT_c may possibly reflect the highly transient nature (if any) of the heat transfer during the quench. The value of h obtained by the immersed-sphere method requires a time period in excess of 40 seconds well in excess of the time period of < 0.1 seconds of insertion of the specimen in the fluidized bed or the time period of ~ 0.3 sec. [20] for the tensile thermal stress to

reach its maximum value. For this reason, the value of h obtained by the latter method more closely corresponds to the steady-state heat transfer conditions.

3. EXPERIMENTAL RESULTS AND DISCUSSION

Figure 1 shows the values of ΔT_c for the glass specimens as a function of air flow rate for four values of mean particle size of the aluminum oxide powder. At approximately $0.8 \text{ l min.}^{-1} \text{ cm}^{-2}$ the air flow rate was sufficiently high that some of the powder with the lowest value of mean particle size was carried out of the bed. The data indicate that ΔT_c depends strongly on the air flow rate as well as particle size. Such variation can only be attributed to the strong dependence of the heat transfer coefficient (h) on flow rate and particle size.

The validity of this latter conclusion is substantiated by the values of the heat transfer coefficient shown in Fig. 2 evaluated from the data for ΔT_c of Fig. 1. These values of h vary by nearly as much as a factor of three. At the lower range of flow rate, the increasing value of h with increasing flow rate most likely is the result of the corresponding increasing degree of fluidization of the bed. The decrease in h with increasing flow rate at the higher values of flow rate probably results from the decrease in net density of the bed, which as judged by the observed increase in relative bed height for the highest flow rate could amount to as much as 30%. The relative dependence of heat transfer coefficient on flow rate as shown in Fig. 2, is similar to the findings of Callahan [15].

Figure 3 shows the dependence of the heat transfer coefficient inferred from corresponding data for ΔT_c for the glass specimens as a function of the depth of the bed for the specific value of air flow rate of $0.47 \text{ l.min}^{-1} \text{ cm}^{-2}$ and average alumina particle size of $138 \text{ }\mu\text{m}$. For convenience, the depth of the bed was defined as the distance from the bottom of the bed to the center of the vertical specimens of length $\sim 6 \text{ cms}$. Experimentally, it was observed that the specimen did not undergo fracture at a preferred location along their length. This observation combined with the relative independence of the heat transfer coefficient on depth of the bed suggests that the heat transfer appears to be relatively uniform along the length of the specimen. Of practical significance is that the position of the specimen in the bed is not critical to the results obtained. Of course, insertion of the specimens close to or in direct contact with the side-walls should be avoided.

Figure 4 shows the experimental data for the heat transfer coefficients obtained by the sphere immersion method for three of the identical batches of powders used to establish the data shown in Figs. 1 and 2. Comparison of Figs. 2 and 4 shows that the values of the heat transfer coefficient obtained by both methods show the same relative dependence on the air flow rate. Quantitatively, however, the maximum values of h inferred from the data for ΔT_c significantly exceed the corresponding values obtained by the sphere immersion method. In explaining this discrepancy at least two major effects must be considered. The first effect results from the differences in the geometry of the test specimens. As presented by Gebhart [21], the forced convection heat transfer coefficients, h_c and h_s for a cylinder and sphere, respectively can be expressed by:

$$h_c = 0.69(Re)^{0.466}(Pr)^{1/3}K_f/d_c \quad \text{for } 40 < Re < 4,000 \quad (2)$$

$$h_s = [2.0 + 0.6(Re)^{0.5}(Pr)^{1/3}]K_f/d_s \quad \text{for } 1 < Re < 70,000 \quad (3)$$

where $Re = Vd/\eta$ is the Reynolds number, V is the fluid velocity, η is the fluid viscosity and d is the specimen diameter. Pr is the Prandtl number, K_f is the thermal conductivity of the fluid and d_c and d_s are the diameters of the cylinder and the sphere respectively.

Taking the case that $2 \ll 0.6(Re)^{0.5}(Pr)^{1/3}$ and assuming no significant difference between the exponents of 0.466 and 0.5 for the Reynolds number in eqs. 2 and 3, yields the ratio

$$h_c/h_s = 1.15 (d_s/d_c)^{1/2} \quad (4)$$

which for the present specimens with $d_s/d_c \approx 2.29$ yields:

$$h_c/h_s \approx 1.74 \quad (5)$$

This result suggests that an upward adjustment of the data of Fig. 4 for the spherical geometry by a factor 1.74 yields the appropriate values for the heat transfer coefficient for the vertical glass circular cylinders. For example, the value of $0.0145 \text{ cal.cm.}^{-2}\text{°C}^{-1}\text{s.}^{-1}$ (Fig. 4) inferred from immersed sphere data for fluidized bed with particle size of $69 \mu\text{m}$ and air flow rate of $0.47 \text{ l.min.}^{-1}\text{cm.}^{-2}$ must be multiplied by 1.74 in order to account for geometry effect. This brings the peak value to about $0.025 \text{ cal.cm.}^{-2}\text{°C}^{-1}\text{s.}^{-1}$ which is still only about 71% of the corresponding value for h determined from ΔT_c (Fig. 2).

The second effect to which the remaining discrepancy between the data of Fig. 2 and the adjusted data of Fig. 4, can be attributed is based on the statistical nature of brittle fracture, which states that the strength of a brittle solid is a function of the volume of the stressed material as

well as the stress distribution. Theoretical analyses of this effect have been presented by Weibull [22] and others. As a result of this statistical effect, the tensile fracture stress of the glass specimens under conditions of thermal shock with a uniform biaxial stress distribution in the specimen surface is expected to differ from the strength under conditions of 4-point bending on which the data of Fig. 2 were based.

In a previous study [13] of the thermal fatigue behavior of the identical glass specimens of the present study, it was shown that the ratio of the tensile fracture stress (σ_{ts}) during thermal shock to the corresponding fracture stress in 4-point bending (σ_b) for a population of surface flaws, by means of the Weibull theory can be calculated to be:

$$\sigma_{ts}/\sigma_b \approx 0.59 \quad (6)$$

This result suggests that multiplication of the data shown in Fig. 2 by the factor 0.59, will yield values of the heat transfer coefficient which more closely correspond to the magnitude of the tensile failure stress encountered during quenching in the fluidized bed. The peak value for the heat transfer coefficient h determined from ΔT_c for the glass specimens then becomes approximately $2.1 \times 10^{-2} \text{ cal.cm}^{-2} \text{ } ^\circ\text{C}^{-1} \text{ .s}^{-1}$. The corresponding h value obtained by the correction for geometry of the results in Fig. 4 evaluated from the sphere-immersion data is $2.5 \times 10^{-2} \text{ cal.cm}^{-2} \text{ } ^\circ\text{C}^{-1} \text{ .s}^{-1}$, which is higher than the corrected value inferred from ΔT_c . In view of the total uncertainties in establishing both values, possibly no major significance should be attached to this discrepancy. Nevertheless, the lower value of h inferred from ΔT_c may possibly reflect

the highly transient nature of the heat transfer in the very brief time period required for fracture to occur. Possibly in this brief period, the transfer of heat from the specimen can not benefit from the motion of the fluidized powder. A detailed analysis of this effect is beyond the scope of the present discussion.

Figure 5 shows the results for the strength behavior of the alumina specimens quenched into the fluidized bed with mean particle size of 138 μm and air flow rate of $0.47 \text{ l.min.}^{-1} \text{ cm}^{-2}$. The dependence of strength on temperature difference indicates a value of $\Delta T_c \approx 800$. From the data of Figs. 2 and 4, the values appropriately adjusted for the statistical and geometry effects as discussed earlier are approximately 2.0 and $2.5 \times 10^{-2} \text{ cal.cm}^{-2} \text{ }^\circ\text{C.s}^{-1}$, respectively. Using these latter values, the data in Table 1 and ratio of strength under thermal shock to the strength in bending, $\sigma_{ts}/\sigma_b \approx 0.79$ inferred from the Weibull parameter for a distribution of surface flaws, the values for ΔT_c can be calculated to be 830°C and 675°C . The value of 725°C for the property values listed in Table 1, corresponds to the mean specimen temperature at the instant of fracture for $\Delta T_c \approx 800^\circ\text{C}$. The much better agreement between this latter value and 830°C predicted from the h value inferred from ΔT_c for the glass specimen than that predicted from the value obtained from the sphere-immersion method, provides confirmation for the earlier suggestion that the heat transfer in a fluidized bed during a thermal quench is less severe than under conditions which more closely resemble steady-state conditions.

A comparison of data shows that the peak value of the heat transfer coefficient of approximately 2.1 to $2.5 \times 10^{-2} \text{ cal.cm}^{-2} \text{ }^\circ\text{C.s}^{-1}$ found in the present study, agrees quite well with the value of approximately

$2.0 \times 10^{-2} \text{ cal.cm.}^{-2} \text{ C.s}^{-1}$ reported by Ammann et al [23] and Callahan [15]. The much lower value of about $8 \times 10^{-3} \text{ cal.cm.}^{-2} \text{ C.s}^{-1}$ found by Trantina [14] probably can be attributed to differences in experimental conditions.

Comparison of the values found in the present study with those for other quenching media, show that even the peak values for the heat transfer coefficient for the fluidized bed is less than the corresponding values for the effective heat transfer coefficients for silicone oils or water obtained in a previous study [11]. This statement holds even if these latter data are adjusted downward by the factor 0.59 to account for the statistical nature of brittle fracture. It appears then that fluidized beds for purposes of thermal shock testing of brittle ceramics extend the range of heat transfer coefficients available to the researcher. As indicated by the results of the present study as well as those of Callahan [15] a particular advantage of fluidized beds is that they offer considerable flexibility in adjusting the heat transfer coefficient by modification of gas flow rate and particle size.

ACKNOWLEDGMENT

This study was supported by the Office of Naval Research under contract: N00014-78-C-0431. The donation of the fluidized bed by the Corning Glass Works, Corning, New York is greatly appreciated.

REFERENCES

1. W. D. Kingery, J. Am. Ceram. Soc. 38 (1955) 3-15.
2. J. Gebauer, D. A. Krohn and D. P. H. Hasselman, J. Am. Ceram. Soc. 55 (1972) 198.
3. W. B. Crandall and J. Ging, J. Am. Ceram. Soc. 38 (1955) 44.
4. D. P. H. Hasselman and W. B. Crandall, J. Am. Ceram. Soc., 46 (1963) 434.
5. D. P. H. Hasselman, J. Am. Ceram. Soc. 53 (1970) 490.
6. C. Y. King and W. W. Webb, J. Appl. Phys 42 (1971) 2386.
7. D. P. H. Hasselman, E. P. Chen, C. L. Ammann, J. E. Doherty and C. C. Nessler, J. Am. Ceram. Soc., 58 (1975) 513.
8. S. S. Manson and R. W. Smith, Trans. ASME, 78 (1956) 533.
9. E. Glenny and M. G. Royston, Trans. Brit. Ceram. Soc. 57 (1958) 645.
10. P. F. Becher, D. Lewis III, K. R. Carman and A. C. Gonzalez, Am. Ceram. Soc. Bull. 59 (1980) 542.
11. J. P. Singh, Y. Tree and D. P. H. Hasselman, J. Mat. Sc., 16 (1981) 2109.
12. J. P. Singh, J. R. Thomas and D. P. H. Hasselman, J. Am. Ceram. Soc. 63 (1980) 140.
13. D. P. H. Hasselman, R. Badalian, K. R. McKinney and C. H. Kim, J. Mat. Sc. 11 (1976) 458.
14. G. G. Trantina, pp. 229-244 in Thermal Stresses in Severe Environments. Ed. by D. P. H. Hasselman and R. A. Heller, Plenum Press (1980).
15. J. T. Callahan, Trans. ASME, J. of Basic Engineering, (1971) 165.
16. Engineering Properties of Selected Ceramic Materials, American Ceramic Society, Columbus, Ohio (1966).
17. J. C. Jaeger, Phil. Mag. 36 (1945) 418.
18. E. B. Shand, Glass Engineering Handbook, McGraw-Hill Inc., New York, 1958.

19. P. J. Schneider, Temperature Response Charts, John Wiley, NY (1963).
20. R. Badalian, D. A. Krohn and D. P. H. Hasselman, J. Am. Ceram. Soc. 57 (1974) 432.
21. Benjamin Gebhart, Heat Transfer, McGraw Hill Book Company, New York (1971)
22. W. W. Weibull, J. Appl. Mech (1951) 293.
23. C. L. Ammann, J. E. Doherty and C. G. Nessler, Mat. Sc. Engr., 22 (1976) 15.

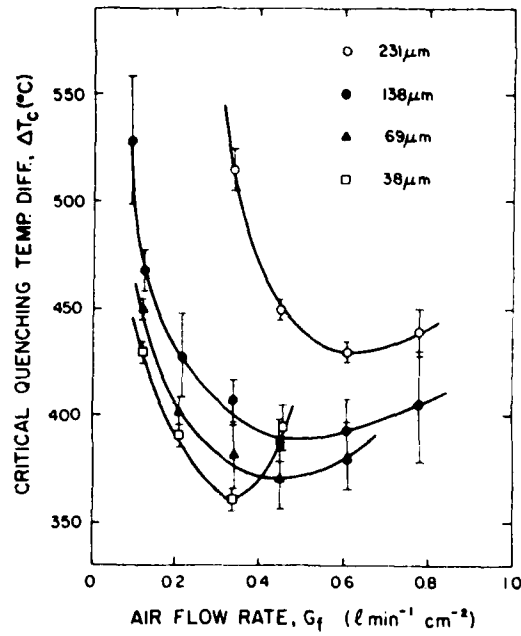


Fig. 1. Effect of air flow rate and alumina particle size on the critical quenching temperature difference (ΔT_C) for soda-lime glass rods ($d = 0.53 \text{ cm}$) quenched in fluidized bed.

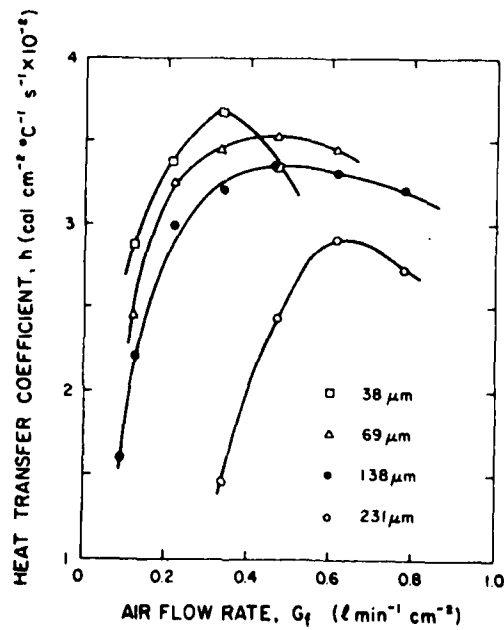


Fig. 2. Effect of air flow rate and alumina particle size on the heat transfer coefficient h for fluidized bed as inferred from the results for ΔT_C in figure 1.

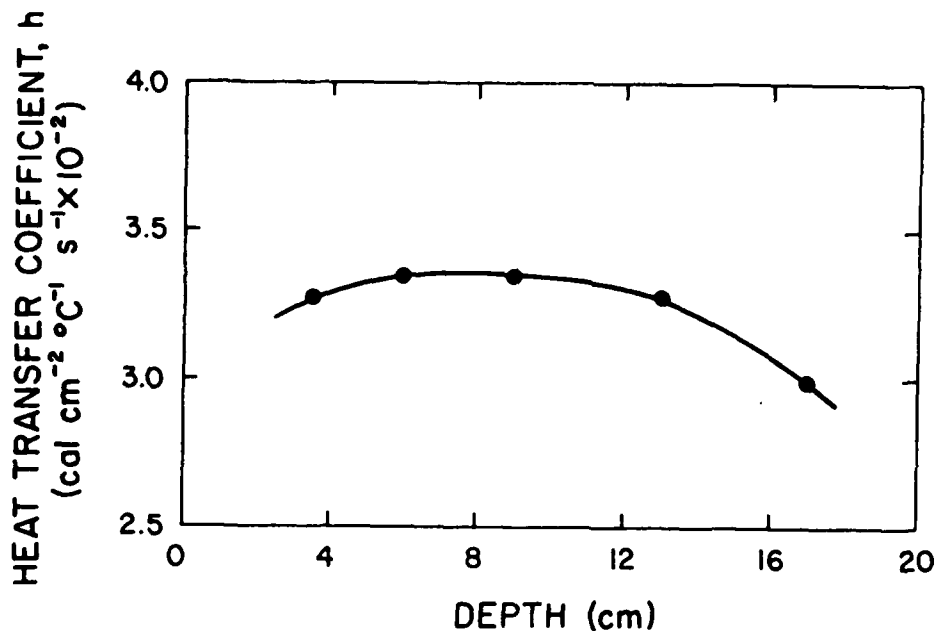


Fig. 3. Heat transfer coefficient h as a function of specimen position in the fluidized bed for air flow rate of $0.47 \text{ l.min.}^{-1} \text{ cm.}^{-2}$ and mean alumina particle size of $138 \text{ } \mu\text{m}$ inferred from values of ΔT_c for soda-lime glass rods.

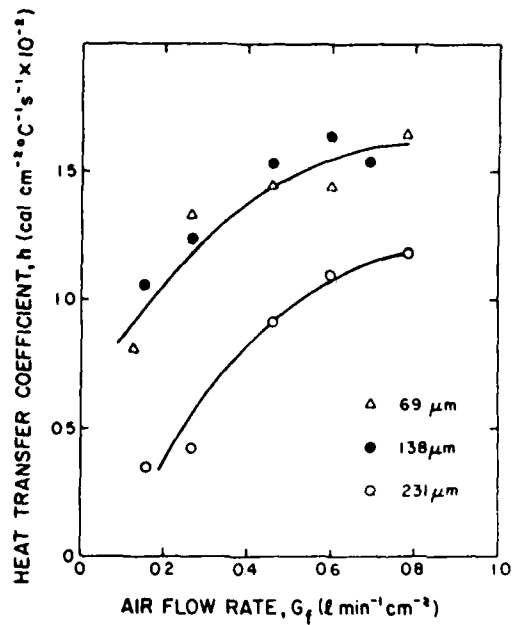


Fig. 4. Heat transfer coefficient h for the fluidized bed obtained by sphere-immersion method as a function of air flow rate and alumina particle size.

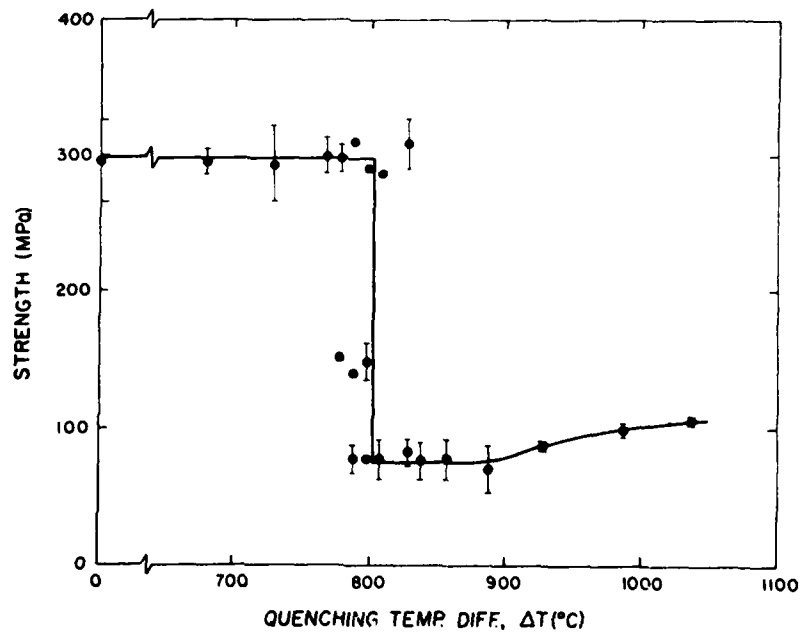


Fig. 5. Strength as a function of quenching temperature difference for alumina rods ($d = 0.63$ cm) quenched in fluidized bed with air flow rate of 0.47 l.min.⁻¹.cm.⁻² and mean alumina particle size of 138 μm.

CHAPTER II

EFFECT OF ΔT - AND SPATIALLY VARYING HEAT TRANSFER
COEFFICIENT ON THERMAL STRESS RESISTANCE OF BRITTLE CERAMICS
MEASURED BY THE QUENCHING METHOD

T. Ozyener*, K. Satyamurthy*, C. E. Knight*,
G. Ziegler†, J. P. Singh* and D. P. H. Hasselman*

*Departments of Mechanical and Materials
Engineering, Virginia Polytechnic Institute
and State University, Blacksburg, Virginia 24061, USA

†Institute for Materials Research, DFVLR
Cologne, Federal Republic of Germany

ABSTRACT

A study was conducted for the effect of a spatial variation in heat transfer coefficient during forced convection and the effect of temperature dependence of the heat transfer coefficient during free convection on the magnitude of thermal stress encountered during the thermal shock testing of brittle ceramics by the quenching method. For specimens with circular geometry, the results obtained by the finite element method indicate that depending on the value of Biot number, a factor of three spatial variation in heat transfer coefficient changes the tensile thermal stresses on cooling by a maximum of about 17% over the value for spatially uniform heat transfer. On heating, the corresponding tensile thermal stresses are lower by a maximum of about 6%.

In free convection for a heat transfer coefficient, h , proportional to $\Delta T_i^{1/4}$, where ΔT_i is the instantaneous temperature difference between the specimen and quenching medium, the stresses are appreciably less than those for ΔT_i -independent heat transfer for the same initial value of h at the onset of the thermal quench. The validity of the dependence of h on ΔT_i was established experimentally. The relevance of the above result to the interpretation of thermal quenching studies are discussed.

I. INTRODUCTION

Brittle ceramic materials generally are highly susceptible to catastrophic fracture under conditions of thermal shock which gives rise to thermal stresses of high magnitude.^{1,2} For purpose of the reliable performance of ceramics for structural applications their response to thermal stress failure must be well understood, both qualitatively as well as quantitatively. For any given structure or component one approach to this is to calculate the magnitude of thermal stresses from the known heat transfer conditions and pertinent material property data. Alternately, the thermal shock response can be established experimentally.

One such method, very popular in view of its simplicity consists of quenching appropriate specimens at some predetermined initial temperature into a fluid medium at lower or higher temperature. Such fluid media can consist of water, liquid metal, eutectic salt mixtures, oil, fluidized powders and stationary or flowing air.³⁻⁹ For quantitatively meaningful evaluation of the results of such quenching test, it is imperative that the heat transfer characteristics of these fluid media are well understood. For any given medium, literature data suggest considerable variation in heat transfer coefficient. In this respect, water as a quenching medium shows a large variation in heat transfer, due to nucleate boiling and film-formation, which is anticipated to depend on the temperatures of both the specimen as well as the water itself.^{3,6,9,10} Silicon oils as thermal quenching media, also show considerable variation in heat transfer behavior, attributable in large part to the temperature dependence of the viscosity.⁶ Literature data for the heat transfer characteristics of fluidized beds show an order of magnitude variation, presumably due to differences in the flow rate of the fluidizing gas, the particle size of the fluidized powder and other variables.^{7,11,12}

In the analysis of quenching data, it is generally assumed that the transfer of heat occurs in a Newtonian manner such that the heat flux is directly proportional to the instantaneous difference in temperature of the specimen surface and the fluid medium. It is also assumed that the transfer of heat is spatially uniform over the specimen surface. Both these assumptions permit the use of analytical solutions for the thermal stresses in circular solid or hollow cylinders,^{13,14} flat plates or spheres⁵ subjected to instantaneous changes in ambient temperature with Newtonian convective heat transfer.

The transfer of heat, however, is Newtonian only in the case of forced convection, in which the fluid medium is passed over the ceramic specimen or during the movement of a specimen through a stationary fluid. This latter condition occurs during the type of quenching in which the specimen is permitted to fall through the fluid by gravity. On the other hand, if a ceramic specimen is held stationary in a stationary fluid, as frequently is the case in automated thermal fatigue studies, the specimen is subjected to natural convection, with the exception of the brief period during which the specimen is inserted in the fluid, where forced convection is the primary mode of heat transfer.

The heat transfer coefficient under conditions of natural-convection is a function of the instantaneous difference in temperature of the specimen surface and the fluid medium.¹⁵ This implies that the heat transfer coefficient is a maximum at the onset of the thermal quench and decreases as the specimen approaches thermal equilibrium. For this reason, the magnitude of the thermal stresses for natural and forced convective heat transfer are not expected to be equal. The validity of this latter conclusion was demonstrated in an earlier study¹⁶ by approximate analytical expressions

valid for very low values of the Biot number. Ceramic specimens of large size and low values of thermal diffusivity (such as glasses) can exhibit time periods to maximum thermal stress which can be quite large compared to the time period required for insertion of the specimen into the fluid medium. In this case, for a specimen held stationary in a stationary fluid, the transfer of heat will occur primarily by natural convection.

A variable which further complicates analyses of thermal quenching results is that the heat transfer coefficient for both natural and forced convection can be spatially highly non-uniform.¹⁷ This effect is well known in the heat transfer literature. However, its role during the thermal shock testing of ceramic materials by the quenching method does not appear to have been investigated.

For the proper analysis of the results of quenching studies, quantitative data for the transient thermal stresses for natural convection and for forced convection with a spatially variable heat transfer coefficient are required. No such information appears to be available in the literature, probably because it is not easily obtained by either analytical or experimental means. The purpose of this study was to obtain the required information by numerical means.

II. GEOMETRY, BOUNDARY CONDITIONS, NUMERICAL PROCEDURES AND EXPERIMENT

A solid circular cylinder was chosen as the geometry appropriate for this study, since this specimen shape frequently is chosen for thermal quenching experiments. For simplicity, the cylinder was assumed to be of infinite length which eliminates the complexity of possible end-effects. In practice, thermal fracture near the center of finite-sized specimens

is promoted by thermal insulation of the end.¹⁸ All relevant material properties of the cylinder such as the thermal conductivity, density, specific heat, coefficient of thermal expansion, Young's modulus of elasticity and Poisson's ratio were assumed to be independent of temperature and position. In order to obtain information on the separate effects of the ΔT - and position-dependent h , these effects were not superposed in the calculations of the temperatures and thermal stress. This was justified in retrospect, as the effect of the spatial variation in heat transfer coefficient on the magnitude of thermal stress was found to be relatively small. Furthermore, superposition of these two effects would have rendered the calculations quite lengthy and prohibitively expensive. The natural and forced convection modes of heat transfer during thermal quench are both expected to be accompanied by transient effects. Equations in the literature for these two modes of heat transfer are generally applicable to steady state conditions. For the purpose of present analysis, it is assumed that during the thermal quench, the steady state conditions prevail. For transient effects, the reader is referred to studies such as those cited by Lin.¹⁹

For natural convection the dependence of the average heat transfer coefficient on the instantaneous temperature difference ΔT_i between the surface of the cylinder and the fluid was chosen to be of the form:¹⁶

$$h = C(\Delta T_i)^{1/4} \quad (1)$$

where

$$C = C'(g\gamma_f\rho_f c_f/\nu_f)^{1/4} d^{-1/4} k_f^{-3/4} \quad (2)$$

In which C' is a constant which depends on the values of the Grashof and Prandtl numbers, g is the gravitational acceleration, γ_f is the coefficient of volume thermal expansion of the fluid, ρ_f is the density of the fluid, c_f is the specific

heat of the fluid, ν_f is the fluid viscosity, d is the diameter of the cylinder and k_f is the thermal conductivity of the fluid.

The spatial variation of the heat transfer coefficient h depends on the experimental conditions.¹⁷ For this study the spatial variation of h was taken as described by the experimental data of Krall and Eckert¹⁷ for a cylinder with its axis oriented perpendicular to the direction of fluid flow for the value of the Reynolds number, $R_e = 4640$. These data are included in Fig. 6, expressed in terms of the angular position around the surface, relative to the average value of h . Since the heat transfer is symmetric about the diameter parallel to the fluid flow, the data for h are given over 180° only. The spatial variation of the heat transfer coefficient as described in Fig. 6, would correspond to a quench specimen falling through the quenching medium. Axial variation of heat transfer was assumed to be negligible.

The temperatures and thermal stresses were calculated by the finite element method with the aid of a computer program used for a number of previous studies.^{20,21} The program was modified to incorporate the boundary conditions for the heat transfer described above. The model consisted of 150 triangular elements forming a half solid cylinder with the smallest elements being near the cylinder surface where the temperature and stress gradients are highest. Thirty of these elements lay along the half cylinder circumference yielding good spatial resolution of the heat transfer coefficient. The coefficient's distribution given in Fig. 6 was interpolated to give the values on the surface elements of the model. The computed temperatures at the model node points provided the thermal loading on the stress model. Generalized plane strain conditions were assumed throughout. The rod used in quenching tests generally has its ends unconstrained. For this reason, no net axial load or flexural bending

moment due to the axial stress distribution was permitted. The axial stresses were first computed from the in-plane stress components assuming the cylinder ends to be fully constrained (plane strain conditions). The axial load and bending moment due to the constrained axial stress distribution were then calculated. The net thermal stresses in the unconstrained cylinder were then obtained by subtraction of the latter values from the stress values for the fully constrained cylinder.

For the calculations, the numerical values of the materials and fluid properties were chosen to be typical of a polycrystalline alumina or a soda-lime-glass¹⁸ quenched into fluid media over a range of quenching temperature difference required to induce thermal stress fracture.⁶ Variation of the radius and thermal conductivity of the cylinder permitted calculations of the thermal stresses over a range of values of the Biot number, $\beta = Rh/k_c$ where R is the cylinder radius and k_c is the thermal conductivity of the cylinder.

In order to facilitate comparison, the stress results for the ΔT -dependent h (eq. 1) were reported in terms of the Biot number (β_0) calculated using the value of the heat transfer coefficient (h_0) at the beginning of the thermal quench, i.e., the value of h in eq. 1 corresponds to the value of ΔT equal to the initial temperature difference over which the cylinder is being quenched. For the spatially dependent h , the data were reported in terms of the Biot number, calculated using the average value of the heat transfer coefficient.

Furthermore, for convenience, the transient temperature and stresses were expressed in terms of the non-dimensional stress:

$$\sigma^* = \sigma(1-\nu)/\alpha E \Delta T \quad (3)$$

the non-dimensional temperatures:

$$T^* = (T - T_f)/(T_0 - T_f) \quad (\text{cooling}) \quad (4a)$$

and

$$T^* = (T - T_0)/(T_f - T_0) \quad (\text{heating}) \quad (4b)$$

and non-dimensional time:

$$t^* = \kappa t/R^2$$

where σ is the stress, ν is Poisson's ratio, α is the coefficient of thermal expansion, E is Young's modulus, κ is the thermal diffusivity, t is the time, T_0 is the initial specimen temperature, T_f is the temperature of the fluid medium and $\Delta T = T_0 - T_f$.

The validity of the dependence of the heat transfer coefficient on $(\Delta T_i)^{1/4}$ in natural convection was established experimentally by measuring the temperature response of an appropriate specimen consisting of a right circular cylinder 5 cm in height by 5 cm in diameter. The cylinder was composed of an industrial polycrystalline alumina for which the thermal diffusivity and conductivity were measured by the laser-flash method. The pre-heated cylinder initially at thermal equilibrium at approximately 40°C was subjected to sudden cooling by immersion into a silicon oil over a temperature range of 20°C. The temperature at the exact center of the cylinder was measured by a thermocouple inserted into a hole drilled to the center along the cylinder axis. The relatively low thermal diffusivity, the large specimen size and the low heat transfer coefficient for $\Delta T = 20^\circ\text{C}$ assured that time period of less than 1 sec required for insertion of the cylinder into the oil was very small compared to the total time period of approximately 30 min. over which the temperature was recorded. The data obtained were converted to non-dimensional temperature and plotted against the non-dimensional time calculated with the aid of the value of thermal diffusivity and cylinder dimensions.

The transient temperature response at the center of the cylinder was calculated from the analytical solutions of Fautz.²² For the ΔT -dependent heat

transfer, the latter solutions were modified to permit the calculations of the transient temperatures by iterative means. Calculations were made only for values of the Biot number near the value corresponding the dimensions and thermal conductivity of the cylinder and the heat transfer characteristics of the silicon oil for the particular conditions of the experiment.

III. RESULTS AND DISCUSSION

A. Natural Convection With ΔT -Dependent h

Figures 1a and 1b show the time-dependence of the temperatures at the surface and center of the cylinder, respectively, for both natural ($h = C(\Delta T_i)^{1/4}$) and forced ($h = \text{constant}$) convective cooling for a range of values of the Biot number. The transient temperatures for convective heating can be obtained by subtracting the data shown in Fig. 1 from unity. The values for constant h agree with the analytical solution of Schneider.²³ Comparison of the data for the two modes of heat transfer indicates that any given temperature for natural convection lags behind the corresponding value of temperature for forced convection. This is in accordance with general expectations, because h decreases with decreasing ΔT_i for natural convection, which is not the case for forced convection.

Thermal stress failure in brittle ceramic materials subjected to quenching occurs usually in tension. For this reason, the maximum values of the tensile thermal stresses are of primary interest. Figures 2a and 2b compare the tensile thermal stresses in the surface of the cylinder cooled by natural and forced convection for a range of values of the Biot number as a function of time. On the surface of the cylinder the thermal stress state is uniform biaxial, so that the data shown in Figs. 2a and 2b apply both to the axial and tangential stresses.²⁴ For forced convection ($h = \text{constant}$)

the data show excellent agreement with the solutions of Jaeger¹³. Comparison shows that for any given value of Biot number the stresses for natural convection are less than those for forced convection. The time period required for the stresses to reach their maximum value is also less for natural convection than for forced convection.

Figures 3a and 3b compare the transient tensile thermal stresses at the center of the cylinder for natural and forced convective heating. These stresses are a maximum in the axial direction and are twice the value of the stresses in the radial and tangential direction. The stresses for natural convection are less than those for forced convection, as was found for cooling. The time required for the stresses to reach their maximum value for natural convection are somewhat greater than those for forced convection.

Figure 4 summarizes the values of maximum tensile thermal stress. The relative difference in the magnitude of the stresses for natural and forced convection is greater for cooling than for heating.

Figure 5 compares the experimental data for the temperature response at the center of the finite cylinder with the calculated values for $h = \text{constant}$ and $h = C(\Delta T_i)^{1/4}$. For the latter case the calculated temperature response lags behind the corresponding data for the former case. The experimental data over most of the temperature range are parallel to the curve for natural convection. This implies that the choice of $h = C(\Delta T)^{1/4}$, also backed by extensive literature data,²⁵ appears to be appropriate to describe the heat transfer coefficient for quenching in which a specimen is held stationary in a stationary fluid.

B. Spatially Varying Heat Transfer Coefficient

Figure 6 shows the angular distribution of the relative heat transfer coefficient, temperature, axial and tangential stresses on the surface of

the cylinder at the instant of maximum tensile thermal stress for Biot number $\beta = 1.5$ and an average value of the heat transfer coefficient, $h = 0.13 \text{ cal.}^\circ\text{C}^{-1} \text{ s}^{-1} \text{ cm}^{-2}$ typical of values encountered in quenching studies.⁶ The data indicate that the angular relative variation of the temperature is less than the relative variation in heat transfer coefficient. This effect arises because heat flow within the cylinder can occur in the tangential as well as the radial direction. The axial and tangential stresses are no longer equal as is the case for the spatially invariant heat transfer coefficient. An additional contributing factor to this observation is that because of the circumferential non-uniform temperature distribution, the cylinder undergoes bending deformation with a corresponding reduction in the thermal stresses.

Figure 7 compares the time-dependence of the value of the maximum axial tensile stress for spatially uniform and non-uniform convective cooling for the values of Biot number and average heat transfer coefficient for the data shown in Fig. 6. The stresses for the non-uniform heat transfer exceeds the corresponding values for uniform h . Also, for the non-uniform heat transfer the maximum value of stress occurs at a somewhat shorter value of time than for the uniform h .

Figure 8 shows the values for the maximum tensile (axial) thermal stress as a function of Biot number for the spatially uniform and variable h . The relative difference in the stresses for the two heat transfer conditions is greater for cooling than for heating. In fact, on heating the stresses for the variable h are less than for the uniform h . Figure 9 gives the actual percentage differences for the data shown in Fig. 8.

C. Discussion

The results presented above indicate that both the spatial variation as well as the ΔT -dependence of the heat transfer coefficient have an effect on the

magnitude of the maximum tensile stresses encountered during quenching. For this reason, they should have relevance to the interpretation of test results as well as the design of quenching experiments.

It is encouraging to note that the spatial non-uniformity of the heat transfer coefficient for the specific numerical data chosen, has a relatively small effect on the magnitude of the maximum tensile thermal stress. In the case of heating, in fact, this effect to a first approximation is negligible. Even on cooling the maximum difference in stresses for the spatially uniform and non-uniform h is only about 17%, inspite of the factor of three variation in the heat transfer coefficient as pointed out earlier. At least qualitatively, the stresses are affected only slightly, possibly because of the combined effects of non-radial heat flow and the accommodation of the differential thermal strains by bending.

The numerical differences in the maximum thermal stresses due to the non-uniformity of the heat transfer coefficient are relevant to prediction or interpretation of the results of thermal quenching experiments. Such experiments involving single thermal cycles concentrate on determining the critical temperature difference (ΔT_c) required to initiate thermal stress failure. Calculations of ΔT_c from data for physical properties and spatially independent heat transfer coefficient will result in an over-estimate of ΔT_c on cooling and an under-estimate, albeit small, for heating. On the other hand, if experimental values of ΔT are used to evaluate the tensile failure stress, ignoring the spatial dependence of the heat transfer coefficient will result in an underestimate on cooling and an overestimate for heating at least for the data of the present study.

However, the statistical nature of brittle fracture is expected to reduce the above over- and underestimates. In the tensile failure of

brittle materials each stressed element makes a contribution to the failure probability. For this reason, estimates of the effect of non-uniform h on thermal stress failure should be based on statistical theories such as the Weibull theory.²⁶

It should be noted that the stress values shown in Fig. 7 and 8 are strictly valid only for the specific numerical example chosen. Different relative effects may be encountered for other geometries and/or heat transfer conditions. For this reason, each case must be examined individually.

Regardless of the numerical differences involved, the existence of an effect of non-uniform h on magnitude of thermal stress suggests care in the performance of quenching studies. In the example considered above, the tangential non-uniformity of h occurs because the relative motion of the fluid flow occurs perpendicularly to the axis of the cylinder. Such tangential non-uniformity does not exist if the fluid flow occurs parallel to the cylinder axis. For this reason, specimen orientation relative to the fluid is expected to influence the results of quenching studies. Unspecified or random orientation can handicap data comparison and contribute to data scatter. Identical specimen orientation, either perpendicular or parallel to the fluid flow is preferred. In the latter case axial variation in heat transfer coefficient may occur which may move the position of maximum tensile stress and resulting fracture (if any) towards the leading end of a cylinder of finite length. Such an effect, however, was not observed during a recent study of the heat transfer characteristics of a fluidized bed for thermal quenching purposes.²⁷

The large relative difference between the maximum tensile stresses for forced and natural convection for the same initial value of the Biot number also has significant implications for the analysis of thermal quenching experiments. The range of the applicability of the thermal stresses calculated for these two modes of heat transfer requires examination in some detail. Clearly, in

the case of a specimen moving relative to the fluid, the stress data for forced convection ($h = \text{constant}$) will apply. For specimens held stationary in a stationary fluid, the question of which set of stress data apply is more complex. Quenching into a stationary fluid requires insertion of the specimen into the fluid. During this period, because of the relative motion between the specimen and fluid, forced convective conditions will prevail. Once the specimen has reached its stationary position, after a transient during which any fluid turbulence is damped out, heat transfer will occur by natural convection. For these reasons the dominant mode of heat transfer is expected to critically depend on the time period required for specimen insertion relative to the time required for the stresses to reach their maximum value. Two limiting cases can be defined. In the first case, the time of maximum stress is less than the time period required for specimen insertion. In this case, the specimen is subjected to forced convective heat transfer with constant h only. In the second case, the time to maximum stress greatly exceeds the time period required for specimen insertion, such that the heat transferred during insertion becomes negligible compared to the total heat transfer while the specimen is held stationary. In this case, the specimen is primarily subjected to natural convection mode of heat transfer.

These two limiting cases can be illustrated by a simple numerical example. Let it be assumed that it takes 0.1 second for a quench specimen to move through the fluid to reach its stationary position. For a Biot number, $\beta=2$, the non-dimensional time, $\kappa t/R^2$ required for the maximum value of stress is of the order of 0.08. For thermal stress failure to be caused by forced convective heat transfer during insertion of the specimen into the fluid, this value of t^* should be such that the real time of maximum stress is equal or less than 0.1 sec. Taking a value for the thermal diffusivity, $\kappa=0.03 \text{ cm.}^2\text{s}^{-1}$

(typical for a polycrystalline alumina), forced convection heat transfer will prevail for a cylinder radius $R < 0.2$ cm. Similar values of specimen sizes can be calculated for other materials with ranges of thermal diffusivity and Biot number encountered for typical ceramic materials. A specimen radius of $R < 0.2$ cm is of the order common to the vast majority of laboratory studies of the quenching behavior of many ceramic materials. Obviously, then the analysis of the results of such studies should be based on the thermal stresses calculated for a constant heat transfer coefficient.

Thermal stress failure by naturally convective heat transfer will occur when the time of maximum stress greatly exceeds the time period required for specimen insertion, so that to a first approximation the heat transferred during this latter period is negligible relative to the total heat transferred by natural convection. For an estimate of the minimum specimen size required for this latter condition to prevail it may be assumed that the time of maximum stress should be greater than 10 sec. For the same values for the Biot number, time to maximum stress and thermal diffusivity considered above, this condition is met for a cylinder radius $R \geq 2$ cm. This value is equal to the radius of the alumina specimen, which as shown by the data in Fig. 5, demonstrated that natural convection was the primary mode of heat transfer. Radii larger than 2 cms are encountered in actual ceramic components for industrial or other applications subjected to thermal shock during quenching or during removal from a kiln, furnace etc., for cooling in room air. The results of thermal fracture under such conditions should be based on thermal stresses calculated from heat transfer coefficients for natural convection. Analysis of such **results** on the basis of forced convection will result in an over-estimate of the thermal stresses at which failure occurred. On the other hand, of course, the assumption of heat transfer by forced convection when in fact,

natural convection heat transfer prevails, will yield a conservative estimate of thermal stress resistance. As pointed out elsewhere²⁸, major differences in thermal fatigue life can be found between forced and natural convective heat transfer, not only due to the differences in stress values but also due to the difference in the duration of each thermal stress cycle. For specimen sizes intermediate to values below and above which heat transfer occurs primarily by forced and natural convection, resp., heat transfer will occur by both mechanisms. Thermal stress analysis, in that case, should be based on the superposition of the thermal stress by an initial pulse of forced convection, followed by natural convection thereafter.

In general, the results of this study illustrate that a quantitatively meaningful analysis of experimental results of thermal stress fracture or their prediction, requires a quantitative understanding of the heat transfer environment.

ACKNOWLEDGMENT

This study was conducted as part of a research program on the thermo-mechanical and thermal properties of brittle structural materials supported by the Office of Naval Research under Contract N00014-78-C-0431. The experimental and theoretical thermal response (for constant h) of the right circular cylinder shown in Fig. 5, were obtained at the DFVLR, Cologne, Federal Republic of Germany.

REFERENCES

1. W. D. Kingery, "Factors Affecting Thermal Stress Resistance of Ceramic Materials," J. Am. Ceram. Soc., 38 [1] 3-15 (1955).
2. D. P. H. Hasselman, "Unified Theory of Thermal Shock Fracture Initiation and Crack Propagation in Brittle Ceramics," J. Am. Ceram. Soc. 52 [11] 600-04 (1969).
3. R. W. Davidge and G. Tappin, "Thermal Shock and Fracture in Ceramics," Trans. Brit. Ceram. Soc., 66 [8] 405-22 (1967).
4. C. Y. King and W. W. Webb, "Photoelastic Observations of Transient Heat Transfer Across a Solid-Fluid Boundary," J. of Heat Transfer, 89 [1] 65-68 (1967).
5. W. B. Crandall and J. Ging, "Thermal Shock Analysis of Spherical Shapes," J. Am. Ceram. Soc., 38 [1] 44-54 (1955).
6. J. P. Singh, Y. Tree and D. P. H. Hasselman, "Effect of Bath and Specimen Temperature on the Thermal Stress Resistance of Brittle Ceramics Subjected to Thermal Quenching," J. Mat. Sc. (in press).
7. C. L. Ammann, J. E. Doherty and C. G. Nessler, "Thermal Fatigue Behavior of Hot Pressed Silicon Nitride," Materials Science and Engineering, 22, 15-22 (1976).
8. J. E. Doherty, J. G. Tschinkel and S. M. Copley, "Improvement of Thermal Shock Resistance by Surface Prestressing," Am. Ceram. Soc. Bull. 52 [9] 681-86 (1973).
9. S. S. Manson and R. W. Smith, "Quantitative Evaluation of Thermal Shock Resistance," Trans. ASME, 78 [3] 533-44 (1956).
10. P. F. Becher, D. Lewis III, K. R. Carman and A. C. Gonzales, "Thermal Shock Resistance of Ceramics: Size and Geometry Effects in Quench Tests," Amer. Ceram. Soc. Bull 59 [5] 542-545, 548 (1980).

11. G. G. Trantina, "Statistical Fracture Analysis of Brittle Materials in Thermally Stressed Components," pp. 229-244 in Thermal Stresses in Severe Environments, Ed. by D. P. H. Hasselman and R. A. Heller. Plenum Press (1980) 737 pp.
12. J. T. Callahan, "Heat Transfer Characteristics in Air Fluidized Solids up to 900°F," J. Basic Eng. 165-78 (1971).
13. J. C. Jaeger, "On Thermal Stresses in Circular Cylinders," Phil. Mag. 36 [257] 418-25 (1945).
14. M. P. Heisler, "Transient Thermal Stresses in Slabs and Circular Pressure Vessels," J. Appl. Mech. 20 [2] 261-69 (1953).
15. J. P. Holman, Heat Transfer, McGraw-Hill Book Company, New York, 1976.
16. J. P. Singh, J. R. Thomas and D. P. H. Hasselman, "Analysis of Effect of Heat-Transfer Variables on Thermal Stress Resistance of Brittle Ceramics Measured by Quenching Experiments," J. Am. Ceram. Soc. 63 [3-4] 140-44 (1980).
17. K. M. Krahl and E. R. G. Eckert, "Local Heat Transfer Around a Cylinder at Low Reynolds Number," ASME, J. Of Heat Transfer, 95 [2] 273-74 (1973).
18. D. P. H. Hasselman, R. Badalian, K. R. McKinney and C. H. Kim, "Failure Prediction of the Thermal Fatigue Resistance of a Glass," J. Mat. Sc., 11, 458-64 (1976).
19. S. P. Lin, "Transient Momentum and Heat Transfer from A Cylinder," Arch. Mech. 32 [6] 831-41 (1980).
20. K. Satyamurthy, J. P. Singh, D. P. H. Hasselman and M. P. Kamat, "Effect of Spatially Varying Thermal Conductivity on Magnitude of Thermal Stress in Brittle Ceramics Subjected to Convective Heating," J. Am. Ceram. Soc., 63 [7-8] 363-67 (1980).
21. K. Satyamurthy, J. P. Singh, D. P. H. Hasselman and M. P. Kamat, "Transient Thermal Stresses in Cylinders with a Square Cross Section Under Conditions of Convective Heat Transfer," J. Am. Ceram. Soc., 63 [11-12] 694-98 (1980).

22. H. Fautz, Waermeleitung und Temperatúrausgleich, Verlag Chemie, GmbH, Weinheim, Federal Republic of Germany (1971).
23. P. J. Schneider, Temperature Response Charts, John Wiley, New York, 1963, 158 pp.
24. B. A. Boley and J. H. Weiner, Theory of Thermal Stresses, John Wiley, New York (1960) 586 pp.
25. Alan J. Chapman, Heat Transfer, 3rd Ed., McMillan Publishing Co., Inc. New York (1974).
26. W. Weibull, "Statistical Theory of the Strength of Materials," Ing. Vetenskap. Akad., 151, 1-45 (1939).
27. K. Niihara, J. P. Singh and D. P. H. Hasselman, "Characteristics of a Fluidized Bed for the Testing of Thermal Stress Resistance of Brittle Ceramics by the Quenching Method," (in preparation).
28. J. P. Singh, K. Niihara and D. P. H. Hasselman, "Analysis of Thermal Fatigue Behavior of Brittle Structural Materials," J. Mat. Sc. (in press).

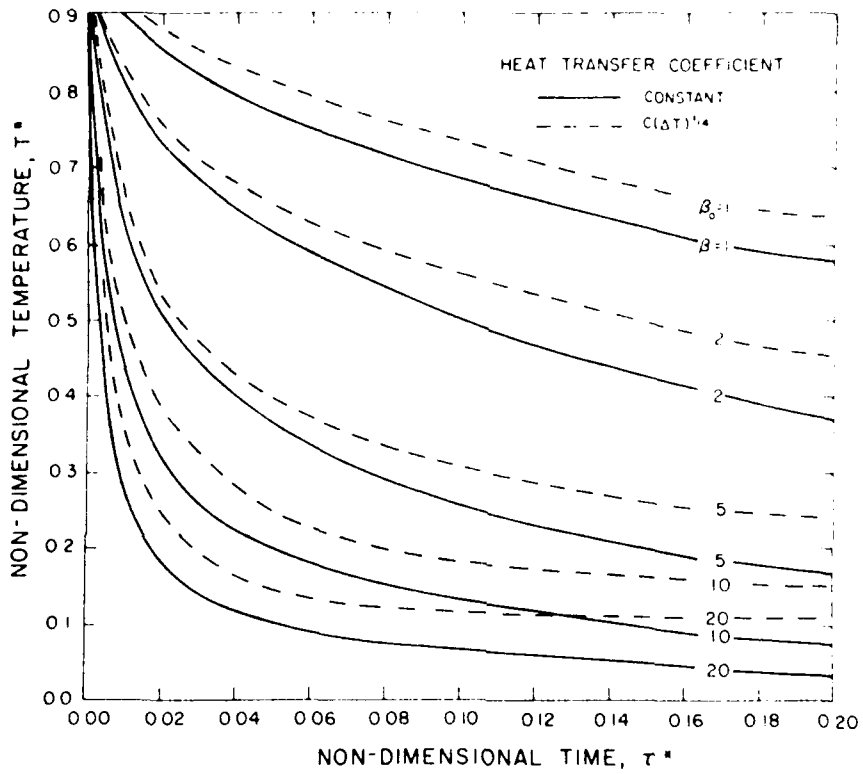


Fig. 1a. Time dependence of temperature at surface of solid circular cylinder subjected to change in ambient temperature for natural ($h = C(\Delta T)^{1/4}$) and forced ($h = \text{constant}$) convection for a range of values of Biot number.

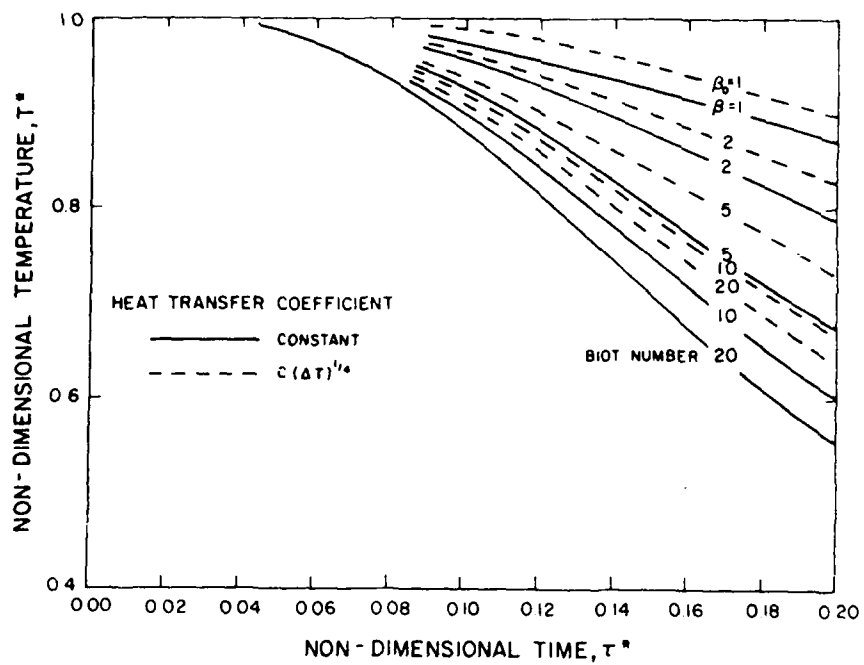
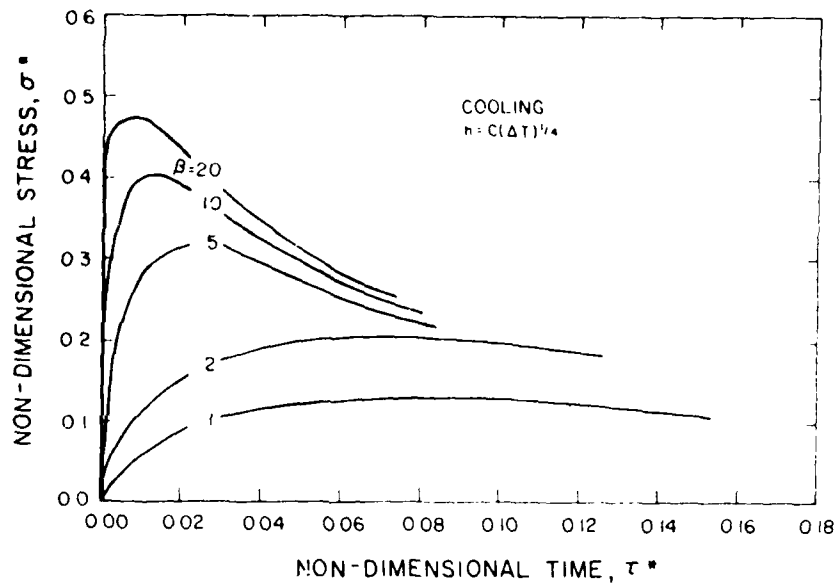
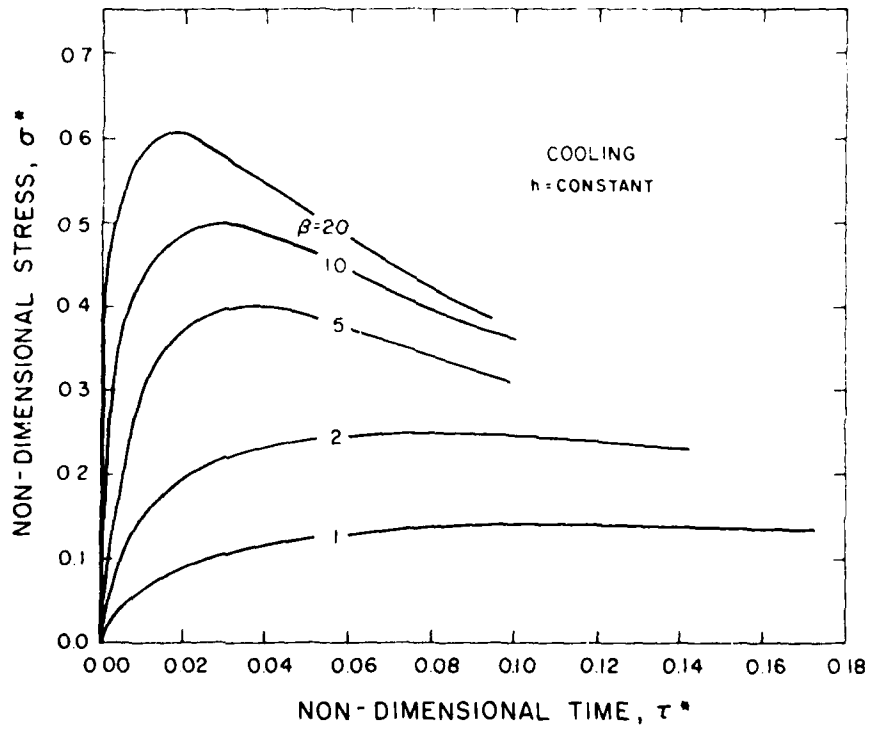


Fig. 1b. Time dependence of temperature at the center of circular cylinder subjected to change in ambient temperature for natural convection ($h = C(\Delta T)^{1/4}$) and forced convection ($h = \text{constant}$) for a range of values of the Biot number.

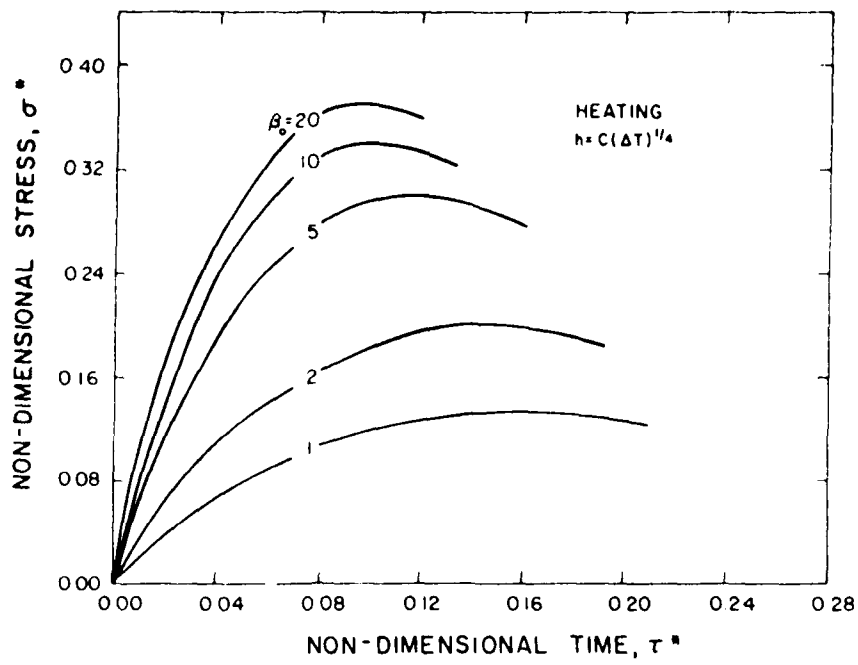


a.

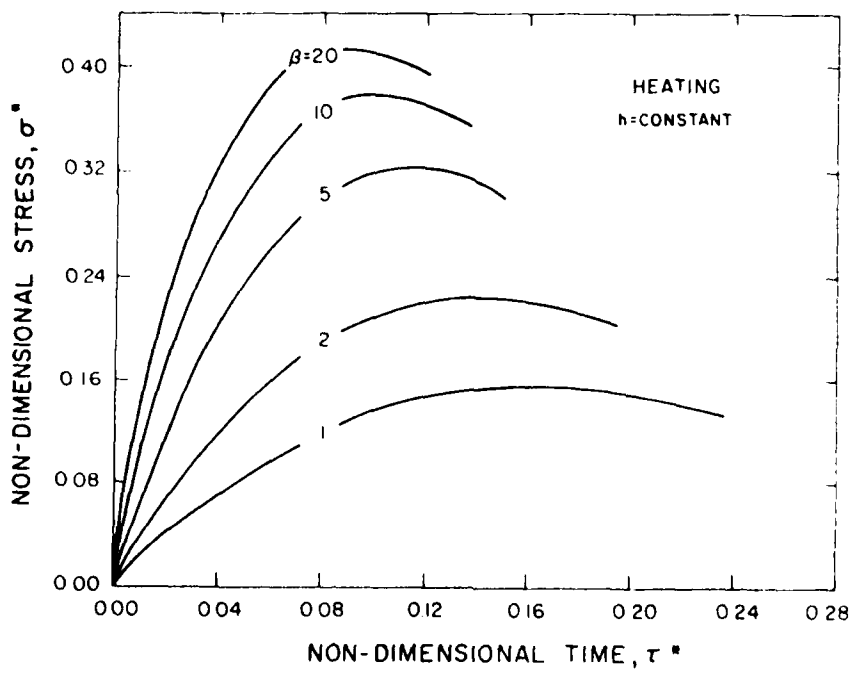


b.

Fig. 2. Transient thermal stresses in the surface of solid circular cylinder subjected to change in ambient temperature for a range of Biot number: a, natural convection and b, forced convection.



a.



b.

Fig. 3. Transient thermal stresses in the center of solid circular cylinder subjected to change in ambient temperature for a range of Biot number: a, natural convection and b, forced convection.

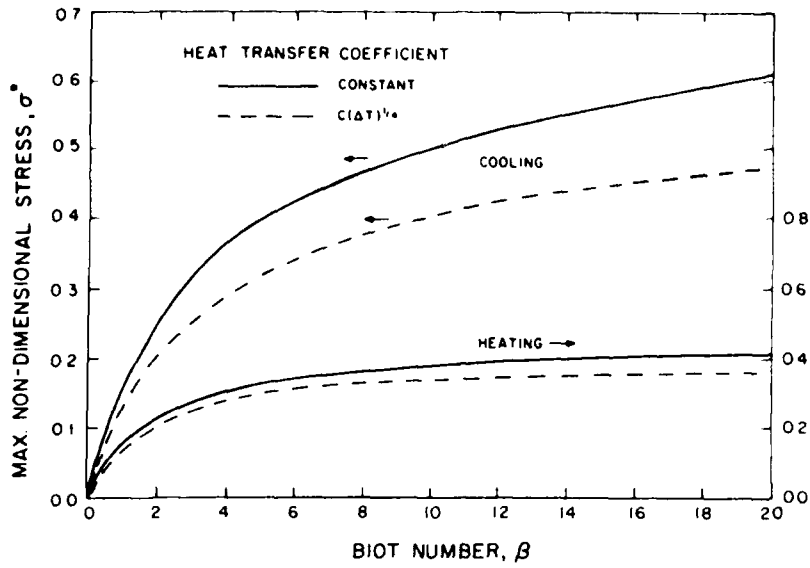


Fig. 4. Maximum value of tensile transient thermal stresses in solid circular cylinder subjected to change in ambient temperature as a function of Biot number for natural and forced convection.

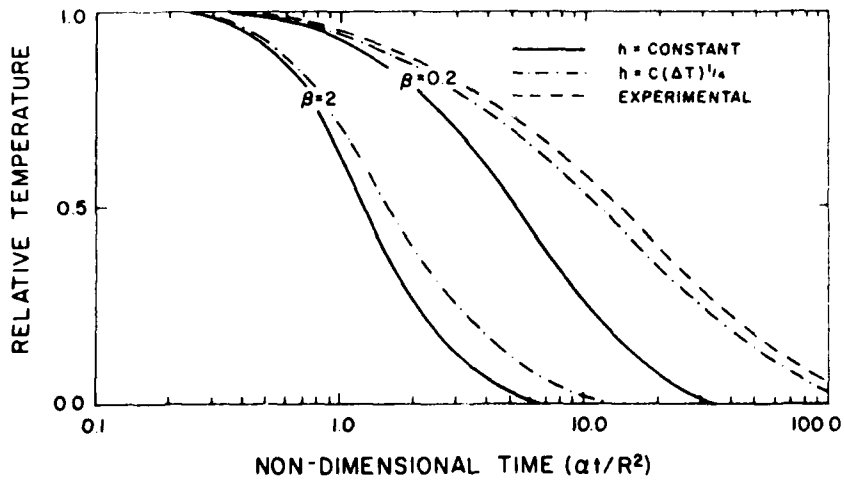


Fig. 5. Comparison between calculated and measured thermal response at the center of a solid circular cylinder of finite length.

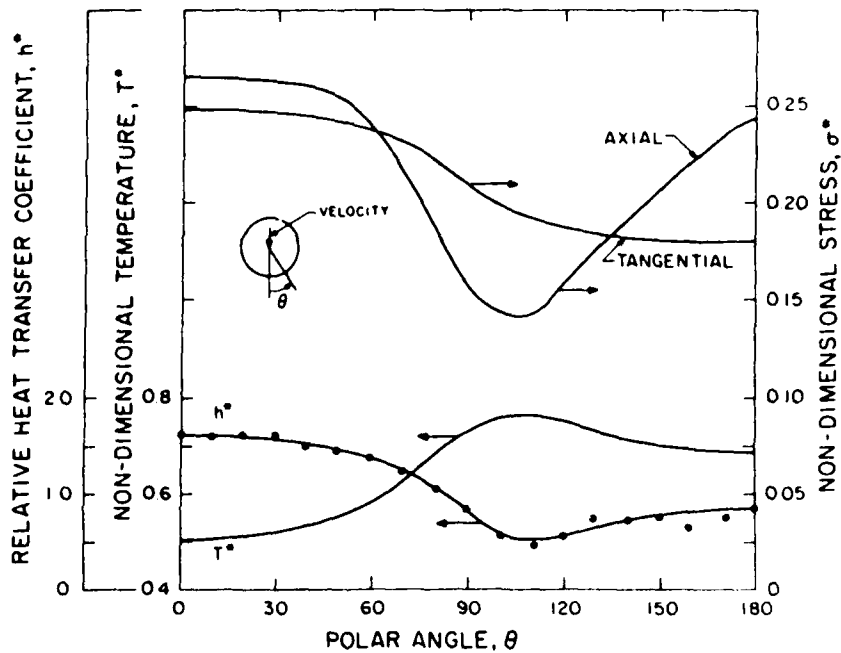


Fig. 6. Angular distribution of relative heat transfer coefficient, temperature, axial and tangential stresses on the surface of a solid circular cylinder subjected to change in ambient temperature at the instant of time of the maximum axial tensile stress: $h_{av} = 0.13 \text{ cal.} \cdot \text{c.}^{-1} \cdot \text{s.}^{-1} \cdot \text{cm}^{-2}$ and $\beta = 1.5$.

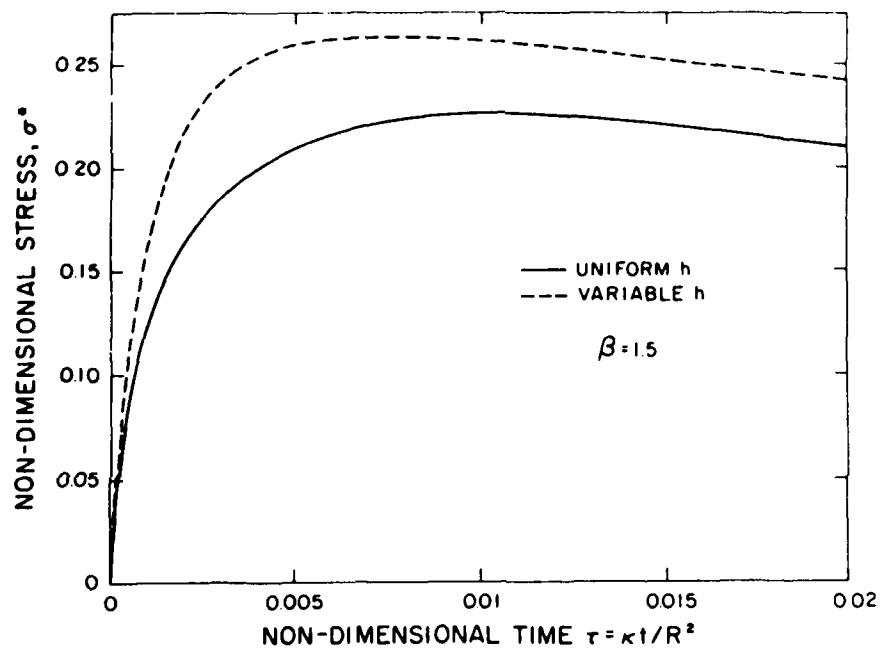


Fig. 7. Time dependence of the axial tensile stress on the surface of a solid circular cylinder subjected to sudden cooling for spatially uniform and variable heat transfer coefficient, h .

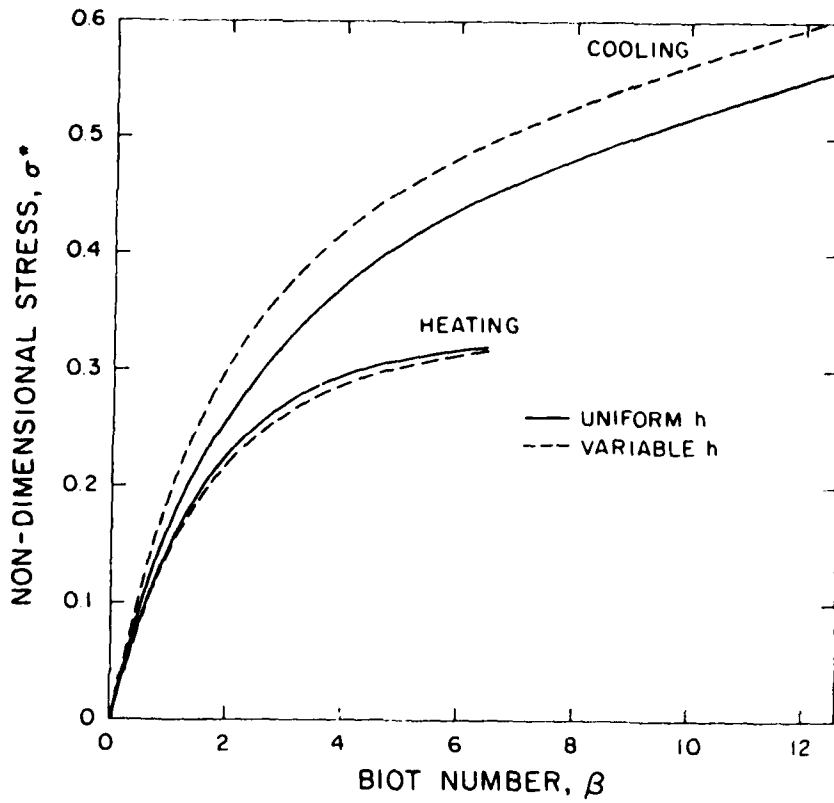


Fig. 8. Variation of the maximum axial tensile stress as a function of Biot number in a solid circular cylinder subjected to change in ambient temperature for spatially uniform and variable heat transfer coefficient, h .

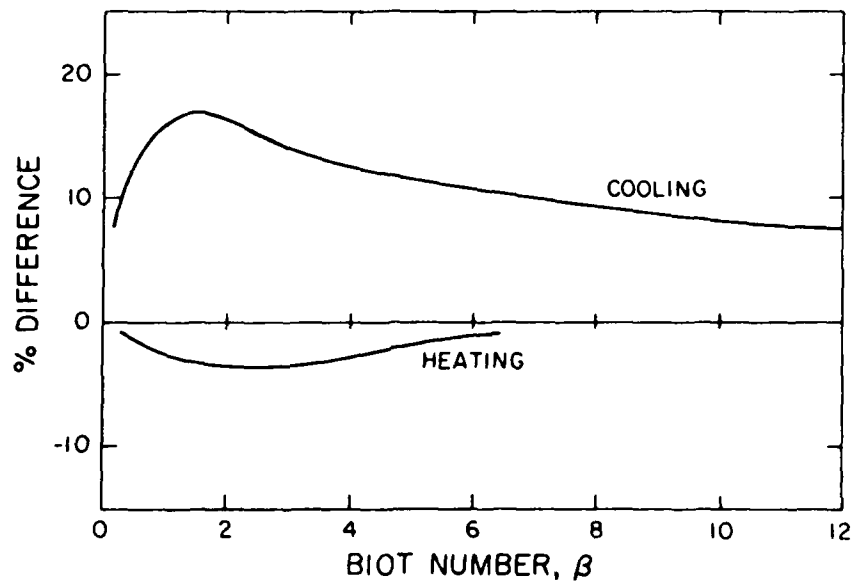


Fig. 9. Relative difference in the maximum axial tensile stresses as a function of Biot number β in a solid circular cylinder subjected to change in ambient temperature for spatially uniform and variable heat transfer coefficient, h : surface stresses for cooling and center stresses for heating.

CHAPTER III

ANALYSIS OF ROLE OF CRACK INTERACTION
ON NATURE OF STRENGTH-LOSS OF BRITTLE CERAMICS
SUBJECTED TO THERMAL SHOCK

by

J. P. Singh, C. Shih and D. P. H. Hasselman

Department of Materials Engineering
Virginia Polytechnic Institute and State University
Blacksburg, Virginia 24061 USA

ABSTRACT

A fracture mechanics analysis is presented to study the effect of collinear crack interaction on the crack stability and propagation behavior in a brittle material subjected to thermal stress failure. It is shown that collinear crack interaction may result in crack coalescence and complete failure.

I. INTRODUCTION

Brittle ceramic materials for use at high temperature are highly susceptible to failure by transient or steady-state thermal stresses.¹ The extensive crack propagation which frequently accompanies such failure can have a profound adverse effect on the structural integrity of the ceramic and corresponding load-bearing ability.^{2,3,4} For the purpose of engineering design, material selection and failure analysis, it is critical that the variables which control the nature and extent of crack propagation in thermal stress fields is qualitatively and quantitatively well understood. Previous analyses^{5,6} of crack propagation in and retained load-bearing ability of brittle materials subjected to thermal stresses, generally considered the simultaneous propagation of a number of cracks, without considering possible crack-interaction effects. As a result of this assumption, these analyses predict that for stable crack propagation, strength will decrease monotonically with increasing severity of thermal shock, above the level required to initiate crack propagation. The same effect is expected at levels of thermal shock for materials with large crack sizes which resulted from unstable crack propagation. This conclusion implies that the ceramic always should exhibit some residual load-bearing ability regardless of the severity of thermal shock and corresponding extent of crack propagation.

Experimentally, however, complete disintegration of a ceramic structure or laboratory specimen on occasion is observed. One explanation for such observation is that due to the combination of the pertinent material, geometric and environmental variables, the size of the cracks, which resulted from thermal stress failure, exceeded the dimensions of the ceramic

structure, component or specimen. Crack interaction, however, should also be considered as an explanation for complete fracture. In particular this should be the case for two or more cracks located on the same plane of propagation. Coalescence of such cracks may result in a macro-crack exceeding the dimensions of the ceramic, even when the extent of propagation of each crack can be relatively small. It is the purpose of this study to analyze the effect of co-planar crack propagation and coalescence on the nature of the corresponding retained load-bearing ability of brittle ceramics subjected to thermal stress.

II. ANALYSIS

The mechanical model and assumptions for the present study will be similar to those chosen for the two previous studies^{5,6} which did not consider crack interaction. Specifically, the mechanical model consists of a thin plate uniaxially constrained from thermal expansion on cooling over a temperature range ΔT . A plate of unit thickness contains a rectangular array of cracks of equal size oriented perpendicularly to the direction of constraint, with crack dimension and spacings shown in Fig. 1. Interaction between cracks within a column is assumed absent in order to permit an analytical assessment of the nature of crack propagation. In a previous study the effect of columnar interaction on the temperature difference (ΔT_c) required for the onset of crack propagation was assessed on the basis of the numerical results of Delameter et al.⁸ It was found that due to a decrease in stress-intensity factor with decreasing columnar crack spacing b , the value of ΔT_c increased over the value for a single crack. An estimate of the extent of crack propagation including crack coalescence would require extrapolation of the

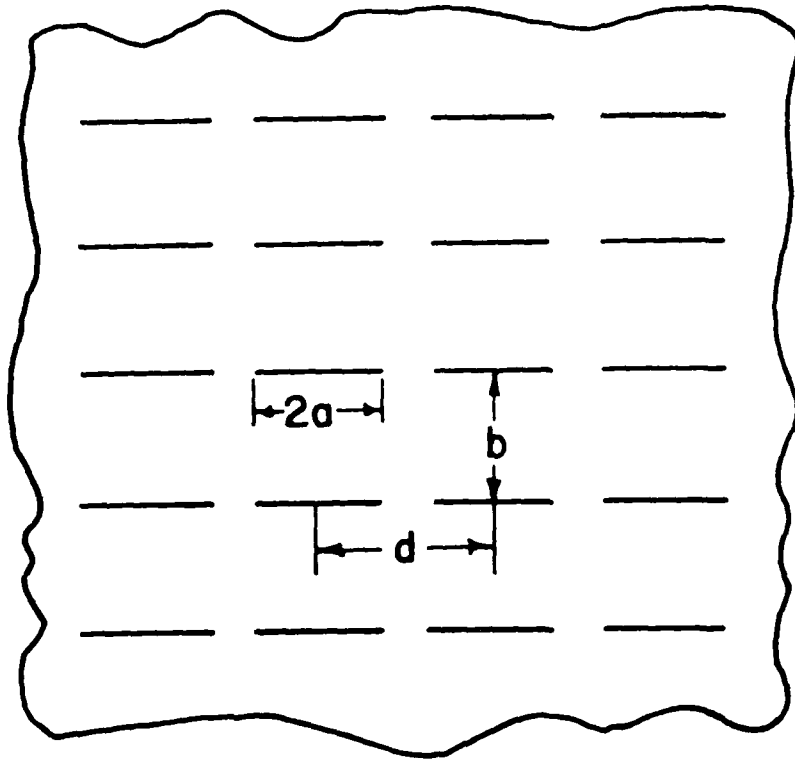


Fig. 1. Schematic of a plate with rectangular array of cracks.

numerical data of Delameter et al., with the corresponding uncertainties inherent in such a procedure. For this reason, an analytical approach is preferred. The assumption of the absence of columnar crack interaction implies that the results to be obtained in this study by analytical means for ΔT as well as the extent of unstable crack propagation represent overestimates and therefore are conservative.

The basic approach used for the present analysis is identical to the one followed in previous studies.^{5,6} From the expression for the potential energy in the plate expressed in terms of its effective elastic behavior and the fracture surface energy of the cracks, the condition for the onset of crack instability can be derived, following the energy balance of Griffith.⁹ From the total change in potential energy, the total extent of unstable crack propagation can be obtained.

An expression can be derived for the effective Young's modulus in the direction perpendicular to the plane of the cracks, from the solution of Yokobori and Ichikawa¹⁰ for the increase in potential energy (ΔW) per crack for a single row of co-planar interacting cracks (for plane strain) in a plate of unit thickness expressed by:

$$\Delta W = - \frac{2(1-\nu^2)d^2\sigma^2}{\pi E_0} \ln \cos \left(\frac{\pi a}{d} \right) \quad (1)$$

where ν is Poisson's ratio, σ is the stress and E_0 is Young's modulus of the plate in the absence of cracks.

For N cracks per unit area of the plate with $N = (bd)^{-1}$, the change in potential energy ΔW_N becomes:

$$\Delta W_N = - \frac{2(1-\nu^2)d^2\sigma^2 N}{\pi E_0} \ln \cos \left(\frac{\pi a}{d} \right) \quad (2)$$

The total elastic energy (W_p) in the plate is the elastic energy in the plate without cracks plus the change in energy due to the cracks:

$$W_p = \frac{\sigma^2}{2E_o} \left[1 - \frac{2(1-\nu^2)d^2N}{\pi} \ln \cos \left(\frac{\pi a}{d} \right) \right] \quad (3)$$

from which the effective Young's modulus, E_{eff} can be obtained:

$$E_{\text{eff}} = E_o \left[1 - \frac{4(1-\nu^2)d^2N}{\pi} \ln \cos \left(\frac{\pi a}{d} \right) \right]^{-1} \quad (4)$$

For a temperature difference ΔT over which the plate is cooled, the sum of the strain energy and the fracture surface energy per unit area of plate is:

$$W_T = \frac{\alpha^2 (\Delta T)^2 E_o}{2} \left[1 - \frac{4(1-\nu^2)d^2N}{\pi} \ln \cos \left(\frac{\pi a}{d} \right) \right]^{-1} + 4GaN \quad (5)$$

where α is the coefficient of thermal expansion (with $\alpha > 0$) and G is the energy required to create unit area of new fracture surface, which includes all forms of energy dissipation including plastic flow, viscous deformation, acoustic energy losses and others.

The cracks are unstable at a value of $\Delta T = \Delta T_c$ when:

$$\frac{d(W_T)}{da} \leq 0 \quad (6)$$

which for simultaneous crack propagation, yields:

$$\Delta T_c = \{ [2G/(1-\nu^2)\alpha^2 E d] \cot(\pi a/d) \}^{1/2} \left[1 - \frac{4(1-\nu^2)d}{\pi b} \ln \cos \left(\frac{\pi a}{d} \right) \right] \quad (7)$$

In eq. 7 when $a/d \rightarrow 0$, ΔT_c approaches the solution for the absence of crack interaction.

The extent of unstable crack propagation for crack instability at $\Delta T = \Delta T_c$ can be derived by equating the total loss in elastic energy on crack propagation from an initial value, a_o to a final value, a_f to the

required change in surface fracture energy, which yields:

$$\frac{\alpha^2 (\Delta T_c)^2 E_o}{2} \left[\frac{1}{1 - \frac{4(1-\nu^2)d^2 N}{\pi} \ln \cos \left(\frac{\pi a_o}{d} \right)} - \frac{1}{1 - \frac{4(1-\nu^2)d^2 N}{\pi} \ln \cos \left(\frac{\pi a_f}{d} \right)} \right] = 4GN(a_f - a_o) \quad (8)$$

For extensive crack propagation such that $a_f \gg a_o$ the final crack length (if arrested, to be discussed later) to a good approximation can be expressed as:

$$a_f = \frac{\alpha^2 (\Delta T_c)^2 E_o}{8GN} \left[1 - \frac{4(1-\nu^2)d^2 N}{\pi} \ln \cos \left(\frac{\pi a_o}{d} \right) \right]^{-1} \quad (9)$$

III. RESULTS AND DISCUSSION

In Fig. 2, the solid curves show the normalized values of ΔT_c as a function of the ratio a/d for a range of values of b/d . With the exception for the highest values of a/d , above $b/d \approx 1.0$, ΔT_c shows a U-shaped behavior qualitatively similar to the results found for the absence of crack interaction. At the low values of a/d and high values of b/d , ΔT_c is not affected by crack interaction due to the large inter-planar and inter-columnar crack spacings compared to the crack size. In this range of values of a/d and b/d , ΔT_c decreases with increasing crack length. The increase in ΔT_c for values of a/d larger than the value for the minimum in ΔT_c is because the effective Young's modulus of the plate decreases faster with increasing a/d than the corresponding decrease in stress required for fracture of the plate. This latter quantity is controlled by the collinear crack interaction only, whereas Young's modulus is governed by the total crack array. The value of crack length corresponding to the minimum in ΔT_c will be denoted as a_{min} .

An interesting effect occurs at the higher values of a/d . For a given value of b/d , ΔT_c exhibits a maximum at a crack length denoted as a_{\max} . For $a > a_{\max}$, ΔT_c decreases rapidly to approach zero as $a/d \rightarrow 0.5$. This latter effect corresponds to crack coalescence and the formation of a macrocrack and complete disintegration of the material. The maximum in ΔT_c at the higher values of a/d , contrasts with the findings of the previous studies which indicated that without crack interaction ΔT_c would increase monotonically with increasing crack length. (Of course, as long as the crack size did not exceed the dimensions of the material.)

As discussed earlier, for values of a/d smaller than a_{\min}/d , the strain energy release rate for crack instability at $\Delta T \geq \Delta T_c$ exceeds the fracture surface energy required to create the new fracture surfaces. This fact will cause the crack to propagate in a so-called unstable or dynamic mode. In contrast, cracks with $a_{\min}/d \leq a/d \leq a_{\max}/d$ will propagate in a stable manner for $\Delta T \geq \Delta T_c$, with the relationship between ΔT_c and a/d at any stage of crack propagation process described by eq. 7.

The dotted curves in Fig. 2 denote the maximum values of the final crack length, a_f which result from the unstable crack propagation of cracks with an initial crack length, $a_o < a_{\min}$ calculated by means of eq. 9. For purpose of clarity, Fig. 3 shows the value of ΔT_c and a_f on an expanded scale for $0.4 \leq a/d \leq 0.5$. As long as the value of a_f for a given value of b/d lies below the corresponding curve for ΔT_c , the crack will be arrested. Furthermore, it will be subcritical and for continued propagation will require a finite increase in ΔT over the value of ΔT_c originally required to initiate crack propagation at $a = a_o$. Qualitatively, a similar result was predicted for the absence of crack interaction. However, due to the co-planar

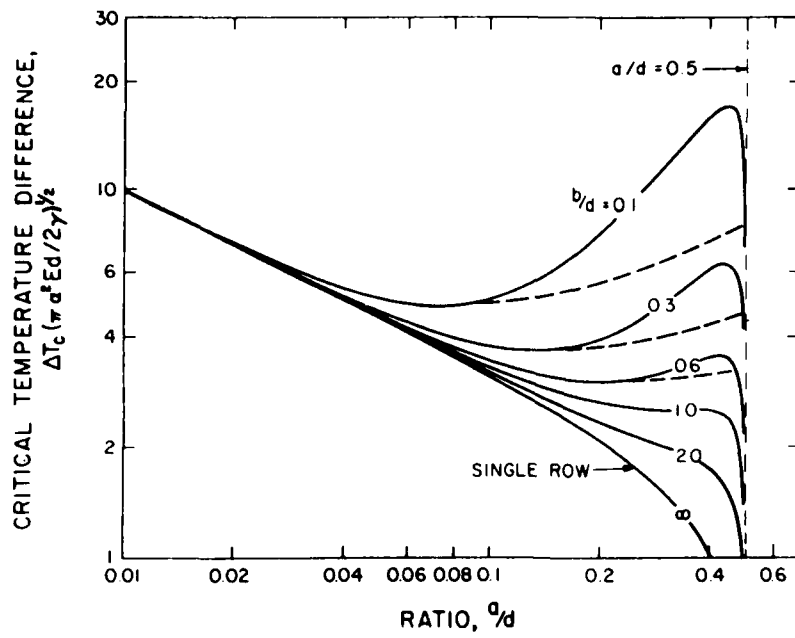


Fig. 2. Effect of collinear crack interaction on the critical temperature difference for constant collinear crack spacing.

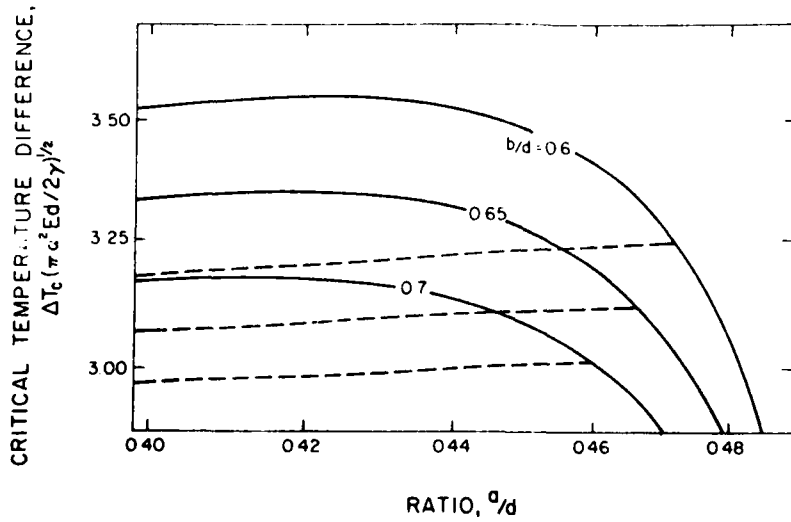


Fig. 3. Figure 2 shown on an expanded scale.

crack interaction considered in the present study, an interesting effect will occur for values of a_f of sufficient size that the corresponding value for ΔT_c for continued propagation is smaller than the value of ΔT_c which initiated the crack propagation at $a \approx a_0$. In Figs. 2 and 3, this corresponds to values of a/d equal to or greater than the critical value of a_f/d (i.e. a'_f/d) at the points of intersection between the solid curves for ΔT_c and the dotted curves for a_f . If unstable crack extension is sufficiently extensive that this effect occurs, crack arrest will not take place. Instead, the crack will continue to propagate in a stable manner until $a/d = 0.5$ when all cracks coalesce, to result in complete fracture. It is interesting to note that this result differs from that for a single crack for which under "fixed grip" conditions, the stress intensity factor, K_I is controlled by compliance effects and decreases due to stress relaxation with increasing crack length. In the present case for multiple collinear cracks, when the cracks increase in length and approach each other, the stress intensity factor K_I becomes very large due to the existence of a double singularity. This effect dominates over the effect of increasing compliance which tends to reduce K_I . The combined result of the two effects leads to crack coalescence and complete fracture. Clearly, to avoid this mode of failure, the initial crack size in the material prior to thermal stress failure should be larger than a critical initial size, a_c which would result in the critical final size, a'_f .

The lengths of cracks, a_c and a'_f as well as the length a_{\min} and a_{\max} corresponding to minimum and maximum values of ΔT_c (i.e., at $d(\Delta T_c)/da = 0$) are shown schematically in Fig. 4 for given values of planar and columnar crack spacings. Figure 4 also indicates the crack propagation behavior after ΔT_c has been reached for different values of initial crack length a_0 .

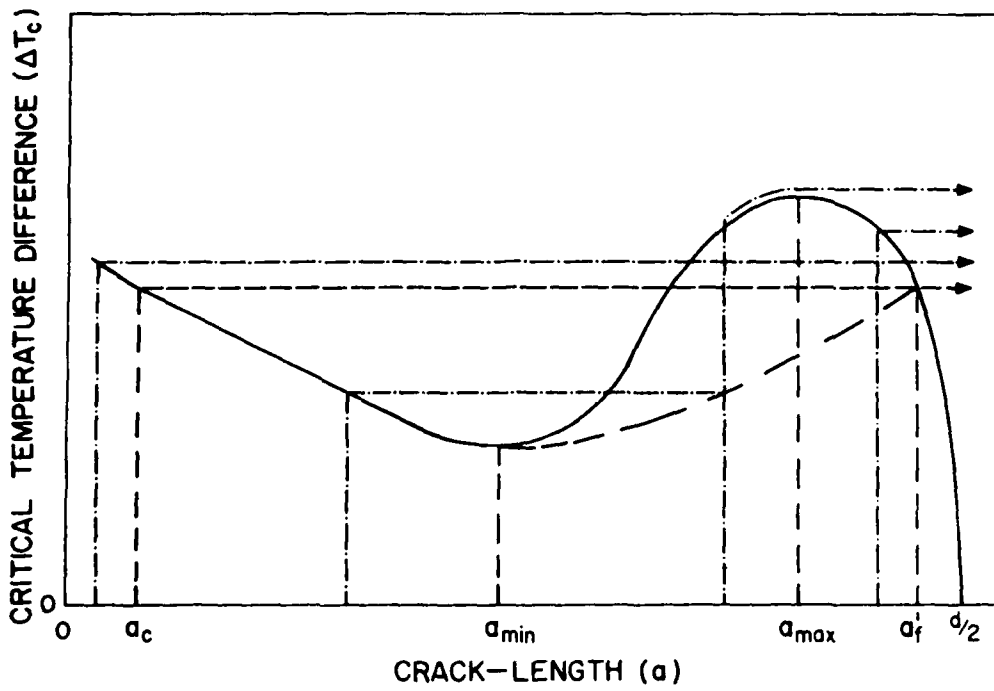


Fig. 4. Diagram for crack stability showing a_c , a_{min} , a_{max} and a_f and the crack propagation behavior for cracks of different initial lengths.

For $a_o < a_c$ and $a_o > a_{max}$, Fig. 4 shows that the crack length remains constant until ΔT equals ΔT_c when the crack becomes unstable and results in a complete fracture for reasons explained before. The paths for crack propagation are shown in chain lines. For $a_c < a_o < a_{min}$, the crack length remains constant until the critical ΔT_c is reached when the crack propagates instantaneously to a new length and becomes subcritical. At this stage, further increase in ΔT to some value ΔT_{c1} is required to re-propagate the crack. For $\Delta T > \Delta T_{c1}$, the crack propagates stably until the crack length equals a_{max} when the material fractures completely. For $a_{min} < a_o < a_{max}$, the crack length remains constant until ΔT equals ΔT_c . For $\Delta T > \Delta T_c$, the crack propagates in a stable manner until a_{max} is reached and a complete fracture occurs.

Figure 5 indicates schematically the corresponding strength loss behavior as a function of ΔT . For $a_o < a_c$ and $a_o > a_{max}$, the ceramic will exhibit a total loss in strength. For $a_c < a_o < a_{min}$ strength loss is governed by both unstable and stable crack propagation. For $a_{min} < a_o < a_{max}$, the strength loss is governed by stable crack propagation only and does not exhibit the discontinuity in strength encountered for unstable crack propagation. Comparison of the four diagrams in Fig. 5 with the nature of strength loss behavior predicted for the lack of crack interaction shows that the effect of such interaction can have pronounced effect on the strength loss behavior of a brittle ceramic subjected to severe thermal shock. It should be noted, however, that for a batch of specimens, flaw sizes and the degree of possible flaw interaction is subject to statistical variation. For this reason, the crack propagation behavior predicted by the present analysis and corresponding strength loss characteristics may be observed only for a few specimens within a given batch. In fact, an unusual data scatter in retained strength values at least in part could be attributed to varying degrees of crack interaction.

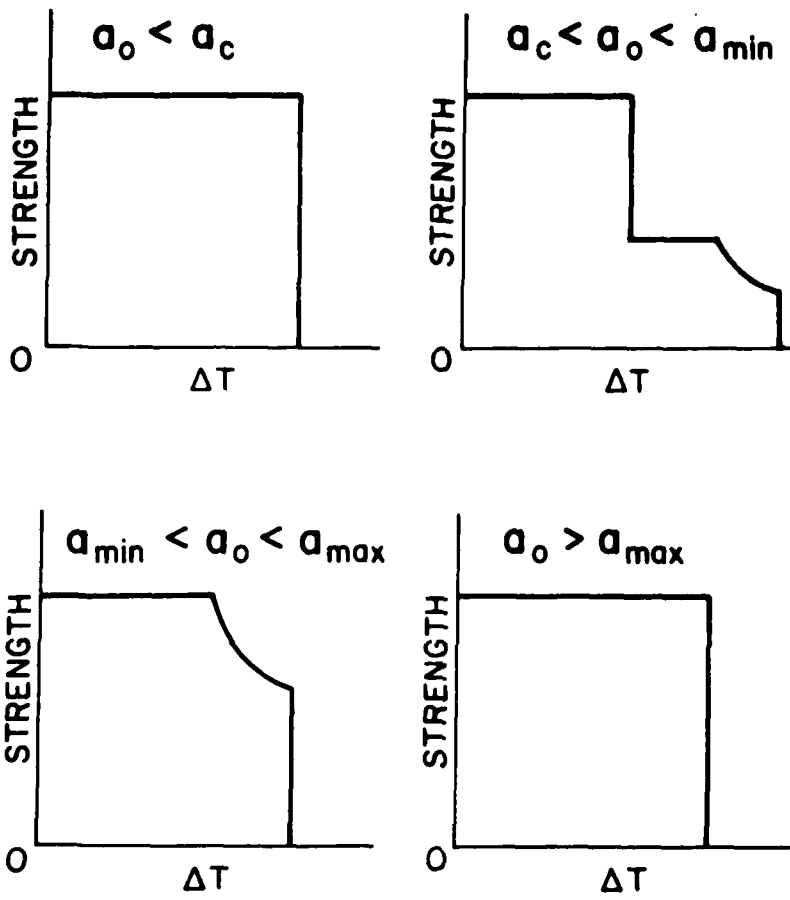


Fig. 5. Schematic for strength loss behavior for brittle ceramics with collinear interacting cracks.

For this reason, the experimenter may wish to base his data interpretation on the examination of each specimen tested rather than on comparison of averaged data.

It is suggested here that similar crack propagation behavior is expected also in the formation of microcracks due to the thermal expansion anisotropy in polycrystalline materials or composites, because the variables which affect microcrack formation and thermal stress failure in the absence of external body forces are quantitatively identical.

ACKNOWLEDGMENT

The present study was conducted as part of a research program on the thermal and thermo-mechanical behavior of structural ceramics supported by the Office of Naval Research under Contract: N00014-78-C-0431.

REFERENCES

1. W. D. Kingery, "Factors Affecting Thermal Stress Resistance of Ceramic Materials," *J. Am. Ceram. Soc.*, 38 (1) 3-15 (1955).
2. W. R. Morgan, "Thermal Shock Effect on the Transverse Strength of Clay Bodies," *J. Am. Ceram. Soc.*, 14 (2) 913-23 (1931).
3. D. P. H. Hasselman, "Strength Behavior of Polycrystalline Alumina Subjected to Thermal Shock," *J. Am. Ceram. Soc.*, 53 (9), 490-95 (1970).
4. T. K. Gupta, "Crack Healing and Strengthening of Thermally Shocked Alumina," *J. Am. Ceram. Soc.*, 59 (5-6) 259-62 (1976).
5. D. P. H. Hasselman, "Unified Theory of Thermal Shock Fracture Initiation and Crack Propagation of Brittle Ceramics," *J. Am. Ceram. Soc.*, 52 (11) 600-04 (1969).
6. D. P. H. Hasselman, "Thermal Stress Crack Stability and Propagation in Severe Thermal Environments," pp. 89-103 in *Materials Science Research, Vol. V, Ceramics in Severe Environments*, Ed. by W. W. Kriegel and Hayne Palmour III, Plenum Press, New York (1971).
7. C. Shih, J. P. Singh and D. P. H. Hasselman, "Effect of Crack Interaction on the Fracture Initiation and Crack Propagation in Brittle Ceramics Subjected to Severe Thermal Shock," *High Temperatures-High Pressures* (in press).
8. W. R. Delameter, G. Herrmann and D. M. Barnett, *J. Appl. Mech., Trans. ASME* 42, 74-80 (1975).
9. A. A. Griffith, "Theory of Rupture," pp. 55-63 in *Proceedings First International Congress of Applied Mechanics*. Ed. by J. Waltman, Jr., Delft, Holland (1924).
10. T. Yokobori and M. Ichikawa, "Elastic Solid with Infinite Row of Co-linear Cracks and the Fracture Criterion," *J. Phys. Soc. Japan*, 19, 2341-42 (1964).

CHAPTER IV

ANALYSIS OF THERMAL FATIGUE BEHAVIOR
OF
BRITTLE STRUCTURAL MATERIALS

by

J. P. Singh, K. Niihara and D. P. H. Hasselman

Department of Materials Engineering
Virginia Polytechnic Institute and State University
Blacksburg, Virginia 24061 USA

ANALYSIS OF THERMAL FATIGUE BEHAVIOR OF BRITTLE STRUCTURAL MATERIALS

J. P. Singh, K. Niihara and D. P. H. Hasselman
Department of Materials Engineering, Virginia
Polytechnic Institute and State University
Blacksburg, Virginia 24061, USA

ABSTRACT

The effect of the level of maximum temperature (T_{\max}), the temperature range (ΔT) and the mode of convective heat transfer on the thermal fatigue resistance of brittle structural materials is analyzed. Expressions are derived for the number of thermal cycles to failure in terms of the appropriate mechanical and thermal properties, crack growth parameter, ΔT and T_{\max} . For simultaneous changes in T_{\max} and ΔT commonly used in practice, the change in thermal fatigue life is governed by both the thermal stress intensity exponent (n) and the activation energy (Q) for subcritical crack growth, in contrast to the results of other studies. For constant T_{\max} but variable ΔT , thermal fatigue life is affected by n only, whereas, for constant ΔT but variable T_{\max} , the value of Q alone governs changes in fatigue-life. Heat transfer by natural or forced convection will result in differences in thermal fatigue resistance.

Recommendations are made for the design and analysis of thermal fatigue experiments. Figures-of-merit for the selection of materials with high thermal fatigue resistance are presented.

1. INTRODUCTION

Brittle structural materials can exhibit static [1,2], dynamic [3,4], cyclic [5,6] as well as thermal fatigue [7,8]. These mechanisms of fatigue result from sub-critical crack growth due to stress-corrosion at low temperatures or diffusional mechanisms at high temperatures. For the purpose of reliable design of structures or components made of brittle materials, it is imperative that the mechanisms responsible for fatigue are qualitatively as well as quantitatively well understood. An extensive literature indicates that the "failure-prediction" of brittle materials subjected to static [9,10], dynamic or cyclic fatigue [11] under isothermal conditions appears well-understood. The statistical nature of brittle fracture can also be incorporated into predictions of fatigue-behavior.

The thermal fatigue behavior of brittle materials is more complex for the principal reasons that both the stresses and temperatures change simultaneously, requiring numerical techniques for the calculations of thermal fatigue behavior. In a number of such studies [12-14], reasonable to excellent agreement was found between laboratory data and the predicted number of thermal cycles-to-failure. More recently, by analyzing experimental data for thermal fatigue behavior of a number of brittle structural material, Kamiya and Kamigaito [15] obtained quantitative information on the behavior of sub-critical crack growth during thermal fatigue.

In order to provide a basis for the objectives of the present study, it should be noted that for convective heat transfer used in most thermal fatigue studies the magnitude of the transient thermal stresses is a function of the temperature differences encountered. The rate of sub-critical crack growth, however, is a function of the thermal stresses as well as the

absolute temperatures involved. These two separate effects are critical to the design of a thermal fatigue experiment as well as to the analysis of the data obtained.

In general, the thermal fatigue behavior of a material is established by measuring the number of thermal cycles (N) required to cause failure of appropriate specimens cycled over a temperature range ΔT , between an upper temperature T_{\max} and a lower temperature, T_{\min} . Figure 1 schematically show the time-dependence of the temperatures and stresses in the surface of a thermal fatigue specimen.

A complete thermal fatigue curve is established by determining the number of thermal cycles N for a range of values of ΔT . However, critical to the results obtained is the specific way in which ΔT is varied. Commonly, ΔT is varied by lowering the upper temperature T_{\max} while the lower temperature T_{\min} is kept constant. In this case the magnitude of the stresses as well as the absolute values of temperature are varied. If ΔT were changed by raising (or lowering) T_{\min} , the stresses are varied, but the absolute temperatures at which most of the crack growth takes place are kept constant. Similarly, ΔT can be kept constant, by changing T_{\max} and T_{\min} by equal amount. Depending on the kinetics of crack growth, these three different conditions are expected to lead to differences in thermal fatigue behavior as measured by the number of cycles-to-failure. A further complexity is introduced by noting that heat transfer can occur in a forced or natural convective mode. In forced convection, heat transfer is Newtonian, i.e., the heat transfer coefficient is independent of the difference in instantaneous temperature of the surface of the specimen and the temperature of the fluid medium used for heating or cooling the specimen. In

contrast, for natural convection, the heat transfer coefficient is a non-linear function of the difference in instantaneous surface temperature and the temperature of the fluid medium [16]. Under these conditions the heat transfer coefficient changes as the specimen changes in temperature (see Fig. 1) towards thermal equilibrium. Detailed calculation of this effect by the finite element method, to be reported elsewhere [17], showed that for a given material and specimen size and identical values of the heat transfer coefficient at the beginning of the thermal cycle, the magnitude of the maximum thermal stress under conditions of natural convection, are significantly less than the corresponding values for forced convection.

It is the purpose of this study to present an analytical treatment of the temperature and heat transfer variables in the thermal fatigue resistance of brittle materials, in order to establish guidelines for the design of thermal fatigue experiments and analysis of the data in terms of crack-growth behavior.

2. ANALYSIS

2.1. General

The analysis will concentrate on thermal fatigue specimens in the shape of long cylinders with circular cross-section. For this geometry, solutions for the thermal stresses are available [17,18]. The ends of the specimens are assumed to be thermally insulated so that fracture at the ends is avoided. This assumption will permit the use of the thermal stresses calculated for circular cylinders of infinite length. It is further assumed that the thermal fatigue mechanism operates only during the cooling part of the cycle. This latter assumption is reasonable since

under those conditions the stresses exceed those during heating and are a maximum in the specimen surface most susceptible to stress-corrosion and the introduction of flaws during specimen preparation and handling. The results of the analysis can be easily extended to other specimen geometries or thermal fatigue during heating or combinations of heating and cooling. Finally it is assumed that between thermal cycles the specimen comes to thermal equilibrium so that overlapping of the transient thermal stresses of successive thermal cycles need not be considered.

2.2. Theory

The rate of sub-critical crack growth (\dot{a}) under conditions of thermal fatigue will be assumed to be identical to the expression for isothermal conditions given by:

$$\dot{a} = AK_I^n \exp(-Q/RT) \quad (1)$$

where A is a constant, n is the stress intensity exponent, K_I is the mode I stress-intensity factor, Q is the activation energy, R is the gas constant and T is the absolute temperature.

In terms of the thermal stress (σ) and crack size (a), K_I is defined by:

$$K_I = Y\sigma\sqrt{a} \quad (2)$$

where Y is a constant related to the stress distribution and the geometry of the crack. Implicit in the use of Equation 2, is the assumption that over the total range of crack growth, the crack size remains sufficiently small compared to the size of the specimen that the compliance of the specimens remains unaffected. This will permit calculation based on thermo-elastic

theory. In this manner, the complexity of the effect of the presence of the crack on the thermal stress field and thermal stress intensity factor, which would require numerical methods, is avoided.

For a given value of thermal stress, failure will occur at a critical crack size, a_c such that $K_I = K_{Ic}$, the critical stress intensity factor. The thermal fatigue life is defined by the number of thermal cycles required to propagate the crack from an initial crack size, a_0 to the critical crack size, a_c .

In direct analogy to the time-to-failure under isothermal conditions, the number of cycles-to-failure (N) in thermal fatigue can be expressed:

$$N = B \int_0^{K_{Ic}} K_I dK_I / \dot{a} \sigma^2(t) Y^2 \quad (3)$$

where B is a constant and $\sigma(t)$ is the transient thermal stress. Because of the relative complexity of the analytical expressions for the transient temperatures and stresses even for the simple geometry such as a solid circular cylinder, the integration of Equation 3 is most conveniently carried out by numerical methods, such as those employed in a number of previous investigations [12,19,20].

However, in order to obtain a convenient analytical expression for the number of cycles-to-failure, a number of simplifying, but entirely reasonable assumptions are made. Firstly, as indicated by Fig. 1 any temperature during the thermal cycle can be expressed as a fractional value of the maximum temperature, T_{max} at the beginning of the thermal cycle. For this reason, the effect of the thermally activated nature of the crack growth on thermal fatigue life can be expressed uniquely in terms of a factor $\exp(Q/RT_{max})$. Secondly and similarly, any value of the transient thermal stress during

the thermal cycle can be expressed as a function of the maximum value of thermal stress, σ_{\max} encountered during the thermal cycle. Furthermore, the analytical results for the time-to-failure [10] under isothermal, constant stress conditions, indicate that unless the total extent of crack growth is small, the time-to-failure is an inverse function of the value of the stress intensity factor at the time ($t=0$) of the application of the load. For these latter two reasons, it will be assumed that the number of cycles-to-failure, as affected by the stress-intensity factor, can be uniquely defined in terms of an inverse function of the maximum value of the thermal stress intensity factor (K_{Ii}) encountered during the first thermal cycle. In effect this changes the lower limit of the integral of Equation 3 from zero to K_{Ii} . Furthermore, it will be assumed that the number of thermal cycles-to-failure is an inverse function of the time-duration over which the transient thermal stress acts for each cycle. Analytical results [18] for the thermal stresses indicate that the magnitude of stress as a function of time can be expressed in terms of a non-dimensional time, $\tau = \kappa t/R^2$, where κ is the thermal diffusivity, t is the real time and R is the radius of the cylinder. For any material and specimen size, the time period of each thermal stress pulse is proportional to R^2/κ making the number of cycles-to-failure proportional to κ/R^2 .

Substitution of Equation 1 into Equation 3 and incorporation of the above conclusions, the number of thermal cycles-to-failure, in analogy to the time-to-failure under iso-stress and iso-thermal conditions can be written in the general form:

$$N = C_k \exp(Q/RT_{\max}) / A \sigma_{\max}^2 R^2 \gamma^2 (n-2) K_{Ii}^{(n-2)} \quad (4)$$

where C is a constant which, in principle, can be obtained by numerical integration of Equation 3 and K_{Ii} is defined by:

$$K_{Ii} = Y_{\sigma_{\max}} \sqrt{a_i} \quad (5)$$

Substitution of Equation 5 into Equation 4, results in the value of N expressed directly in terms of the maximum value of the thermal stress

$$N = C_K \exp(Q/RT_{\max}) / R^2 \sigma_{\max}^n A^{(n-2)} Y^n a_i^{\frac{n-2}{2}} \quad (6)$$

2.3. Derivation of thermal fatigue-life

2.3.1. Forced convection

Under forced convection, the heat transfer coefficient is independent of the range of temperature difference over which the specimen is being cycled. Over the range of the Biot number, $1 < \beta < 20$, the maximum value of tensile thermal stress in the surface of a circular rod to a very good approximation can be expressed [18,21]

$$\sigma_{\max}^{-1} = \frac{(1-\nu)}{\alpha E \Delta T} (1.45 + 4.95/\beta) \quad (7)$$

where α is the coefficient of thermal expansion, E is Young's modulus of elasticity, ν is Poisson's ratio, ΔT is the temperature range over which the specimen is being cycled ($\Delta T = T_{\max} - T_{\min}$, see Fig. 1) and $\beta = Rh/k$ where R is the cylinder radius, h is the heat transfer coefficient and k is the thermal conductivity.

Substitution of Equation 7 into Equation 6 yields:

$$N = \frac{C_K}{Y^n (n-2) A R^2 a_i^{(n-2)/2}} \left(\frac{1-\nu}{\alpha E \Delta T} \right)^n \left(1.45 + 4.95/\beta \right)^n \exp(Q/RT_{\max}) \quad (8)$$

In order to establish the nature (slope, etc.) of a thermal fatigue curve for a given material it is most convenient to derive expressions for the ratio of the values of N for two conditions of thermal fatigue. As discussed earlier, there are three basic ways in which a thermal fatigue experiment can be carried out: 1, ΔT can be varied by raising or lowering T_{\max} , keeping T_{\min} constant; 2, ΔT can be varied by keeping T_{\max} constant, and raising or lowering T_{\min} and 3, ΔT can be kept constant by raising or lowering T_{\max} and T_{\min} by equal amounts.

The effect of these three changes in temperature on thermal fatigue-life will be different.

For analytical purposes, it is most convenient to examine these quantitatively by deriving expressions for the ratio of the number of cycles-to-failure for small differences in T_{\max} , T_{\min} or ΔT , which yield the following results.

2.3.1.1. ΔT varied; T_{\max} constant

For this condition, the ratio of the number-of-cycles to failure N_1 and N_2 for values of ΔT_1 and ΔT_2 , respectively is:

$$N_1/N_2 = (\Delta T_1/\Delta T_2)^{-n} \quad (9)$$

2.3.1.2. ΔT constant; T_{\max} varied

For two values of $T_{1 \max}$ and $T_{2 \max}$ the ratio of the cycles-to-failure N_1 and N_2 , respectively is:

$$N_1/N_2 = \exp \left[\frac{Q}{R} \left(\frac{1}{T_{1 \max}} - \frac{1}{T_{2 \max}} \right) \right] \quad (10)$$

2.3.1.3. ΔT varied; T_{\min} constant

For this condition the ratio of the cycles-to-failure N_1 and N_2 for values of ΔT_1 and ΔT_2 , respectively, becomes:

$$\frac{N_1}{N_2} = \left(\frac{\Delta T_1}{\Delta T_2} \right)^{-n} \exp \left[\frac{Q}{R} \left(\frac{1}{T_{1 \max}} - \frac{1}{T_{2 \max}} \right) \right] \quad (11)$$

2.3.2. Natural convection

Under conditions of natural convection the heat transfer coefficient is a function of the instantaneous temperature difference (ΔT_i) between the specimen surface and the fluid medium. For values of the Grashof, Prandtl and Nusselt numbers appropriate for laboratory studies of thermal fatigue behavior, the heat transfer coefficient can be expressed [16]

$$h = C' (\Delta T_i)^{1/4} \quad (12)$$

where C' is a constant which depends on the properties of the fluid medium such as the viscosity, density, thermal expansion, specific heat and thermal conductivity as well as on the size of the structure being heated or cooled. Equation 12 indicates that the heat transfer coefficient decreases as the difference in temperature between the specimen surface and medium (ΔT_i) decreases during the transient heat transfer. In accepting the validity of Equation 12, it is implicitly assumed that during the transient heat transfer, conditions for natural free convection pertain, which essentially is a steady-state phenomenon.

The transient thermal stresses in a solid cylinder under natural heat conditions described by Equation, 12 were calculated by finite element methods to be reported in detail elsewhere. It was found that the

maximum value of the tensile thermal stresses in the surface of the cylinder over the range $0.5 < \beta < 20$, to an excellent approximation can be written [17].

$$\sigma_{\max}^{-1} = \frac{1-\nu}{\alpha E \Delta T} (1.90 + 6.0/\beta) \quad (13)$$

where the Biot number, β now is defined in terms of the maximum value of the heat transfer coefficient encountered, i.e., at the value of ΔT_i in Equation 12 equal to ΔT of the thermal fatigue environment, such that

$$\beta = RC'(\Delta T)^{1/4}/k \quad (14)$$

With β defined in this manner, a direct comparison of Equations 7 and 13, shows that for the same Biot number, the magnitude of maximum thermal stress in natural convection is considerably less than the corresponding value for forced convection.

Substitution of Equation 13 into Equation 6 results in the number of thermal cycles-to-failure under conditions of natural convection:

$$N = \frac{Ck}{Y^2(n-2)AR^2a_i^{(n-2)/2}} \left(\frac{1-\nu}{\alpha E \Delta T} \right)^n \left\{ 1.9 + \frac{6.0k}{RC'(\Delta T)^{1/4}} \right\}^n \exp(Q/RT_{\max}) \quad (15)$$

In direct analogy to the expressions derived earlier in case of forced convection for the ratio of the thermal cycles to failure, corresponding Equations for condition of natural convection can also be derived as follows:

2.3.2.1. ΔT varied; T_{\max} constant

From Equation 15, the ratio of the thermal cycles-to-failure N_1 and N_2 , corresponding to values of ΔT_1 and ΔT_2 , becomes:

$$\frac{N_1}{N_2} = \left(\frac{\Delta T_1}{\Delta T_2} \right)^{-n} \left\{ 1.90 + \frac{6.0k}{RC'(\Delta T_1)^{1/4}} \right\}^n \left\{ 1.90 + \frac{6.0k}{RC'(\Delta T_2)^{1/4}} \right\}^{-n} \quad (16)$$

Equation 16 can be presented in simplified form for the two limiting values of the Biot number:

$$\frac{N_1}{N_2} = \left(\frac{\Delta T_1}{\Delta T_2} \right)^{-n} \quad \beta \gg 1 \quad (17a)$$

$$\frac{N_1}{N_2} = \left(\frac{\Delta T_1}{\Delta T_2} \right)^{-5n/4} \quad \beta \ll 1 \quad (17b)$$

2.3.2.2. ΔT constant; T_{\max} varied

For two values of $T_{1 \max}$ and $T_{2 \max}$ the ratio of the thermal cycles-to-failure N_1 and N_2 , respectively, with the aid of Equation 15 can be derived to be:

$$\frac{N_1}{N_2} = \exp \left[\frac{Q}{R} \left(\frac{1}{T_{1 \max}} - \frac{1}{T_{2 \max}} \right) \right] \quad (18)$$

2.3.2.3. ΔT varied; T_{\min} constant

For convenience, the ratio of the thermal cycles-to-failure N_1 and N_2 corresponding to values of ΔT_1 and ΔT_2 and values of $T_{1 \max}$ and $T_{2 \max}$ will be written directly for the high ($\beta \gg 1$) and low ($\beta \ll 1$) Biot number approximations:

$$\frac{N_1}{N_2} = \left(\frac{\Delta T_1}{\Delta T_2} \right)^{-n} \exp \left[\frac{Q}{R} \left(\frac{1}{T_{1 \max}} - \frac{1}{T_{2 \max}} \right) \right] \quad \beta \gg 1 \quad (19a)$$

$$\frac{N_1}{N_2} = \left(\frac{\Delta T_1}{\Delta T_2} \right)^{-5/4n} \exp \left[\frac{Q}{R} \left(\frac{1}{T_{1 \max}} - \frac{1}{T_{2 \max}} \right) \right] \quad \beta \ll 1 \quad (19b)$$

3. DISCUSSION

The analytical results indicate that the role of the individual parameters specifically n and Q , which affect the kinetics of thermal fatigue crack growth, depends on the method by which a thermal fatigue curve is established. For simplicity, relative thermal fatigue-life will be considered only, such that the discussion can focus in detail on the crack growth variables which affect the ratios of cycles-to-failure for a given thermal environment, material, specimen and crack geometry.

As indicated by Equations 9 and 17, if thermal fatigue life is established by keeping T_{\max} constant and varying ΔT by varying T_{\min} , relative changes in thermal fatigue life are governed only by the stress intensity factor exponent, n . In contrast, as indicated by Equations 10 and 18, if a thermal fatigue curve is established by keeping ΔT constant and varying T_{\max} and T_{\min} by equal amounts, changes in thermal fatigue life are influenced only by the activation energy for sub-critical crack growth.

If, however, as is common in practice, thermal fatigue behavior is measured by keeping T_{\min} constant and varying T_{\max} and ΔT by the same amount, changes in thermal fatigue life as indicated by Equations 11 and 19, are affected by both the stress intensity exponent as well as the activation energy for crack growth. Comparing the analytical results for forced and natural convection shows that for the latter (with $\beta \ll 1$) the role of the

stress intensity factor exponent (n) is greater than in the former. In the high Biot number approximation, the role of n is identical for both forced and natural convection.

The above conclusions are critical to the design of thermal fatigue experiments and the analysis of experimental data obtained. One significant conclusion is that thermal fatigue data obtained by varying ΔT and T_{\max} simultaneously (as is the usual case), cannot be used to obtain a quantitative value for the stress intensity exponent, by obtaining the value of the slope of $\log N$ vs $\log \Delta T$. This latter conclusion is at variance with the recent results of Kamiya and Kamigaito [15], which could lead to misleading results, unless due care is exercised.

For the purposes of illustration, a numerical example will be considered on thermal fatigue for hot-pressed polycrystalline silicon nitride subjected to forced convection heat transfer by Ammann et al. [13] by cycling appropriate specimens at an initial temperature of near 1600°K into a fluidized bed at approximately 313°K. Appropriate values for the stress intensity exponent, and activation energy for sub-critical crack growth are $n = 6$ and $Q = 170$ Kcal/mole, respectively. The change in thermal fatigue life caused by a simultaneous decrease in T_{\max} and ΔT of 20°C will be considered. Substitution of the above values of n and Q into Equation 11 yields the result that due to the decrease in magnitude of thermal stress (i.e. ΔT) thermal fatigue life is increased by 15% (i.e. by a factor of 1.15). In contrast, the decrease in the value of T_{\max} increases thermal fatigue-life by a factor equal to 1.97, for a total increase in fatigue-life due to both effects equal to 2.26. These numerical results indicate that in silicon nitride the activation energy for slow crack growth plays a far more im-

portant role in establishing thermal fatigue behavior than the stress intensity exponent. For this reason, a plot of $\log N$ vs $\log \Delta T$ of the data of Ammann et al [13] cannot yield a reliable value of n in contrast with the findings of Kamiya and Kamigaito [15]. Because of the relatively small effect of the value of n on thermal fatigue life, it is more appropriate to plot $\log N$ vs $1/T_{\max}$ to yield a value of Q . Doing this with the data of Ammann et al [13] results in a value of $Q \approx 130$ Kcal/mole which is less than the value found by experiment. In fact, because the role of n is ignored in this approach, the activation energy determined from the slope of the $\ln N$ vs $1/T_{\max}$ plot should be higher than the value of Q determined by actual measurement. It is the view of these writers that the total number (seven) of data points in the set of data of Ammann et al [13] is too small to reliably establish the thermal fatigue behavior of silicon nitride. Of the seven, four show significant data scatter for nearly identical values of T_{\max} , leaving only three data points to establish the effect of ΔT or T_{\max} on fatigue-life. Three data points are not considered adequate in view of the statistical nature of brittle fracture of such materials as silicon nitride resulting from variations in crack size, geometry, orientation and other variables.

Such statistical effects were largely eliminated in the study of Hasselman et al [30] of the thermal fatigue behavior of circular rods of soda-lime-silica glass, thermally cycled from higher temperature into a water bath at constant lower temperature. The excessive scatter in thermal fatigue data was reduced by promoting failure at artificial surface flaws introduced by diamond indentation. The data obtained and the property value for the glass can be used to numerically illustrate the relative influence of n and Q on thermal fatigue life.

For the soda-lime-silica glass rods investigated, $n \approx 16$ and $Q \approx 25$ Kcal/mole. In the fatigue experiments $T_{\max} \approx 433^\circ\text{K}$ and $\Delta T \approx 130^\circ\text{C}$. The relative change in thermal fatigue life which results from a decrease in T_{\max} and ΔT of 10°C will be calculated. Assuming that heat transfer occurred by forced convection as the result of the motion of the specimen through the water, substitution of the above values of n and Q in Equation 11 yields an increase in thermal fatigue-life due to the decrease in ΔT by a factor of 3.6 whereas the decrease in T_{\max} increases thermal fatigue-life by a factor approximately equal to 1.92. In the case of soda-lime-silica glass, then, the stress intensity exponent plays a more important role in establishing fatigue-life than the activation energy. This contrasts with the previous findings for silicon nitride. Of course, such an effect is expected since for the silicon nitride the values of n and Q are lower and higher respectively than the corresponding values for the soda-lime-silica-glass.

The data for the soda-lime-silica glass rods of Hasselman et al. [20] can be used to illustrate the erroneous values of n and Q , which can be obtained unless care is taken. Figures 2a and 2b show the experimental data for the number-of-cycles to failure for the fifth specimen out of a total set of nine. Figure 2a shows $\ln N$ plotted as a function of $\ln \Delta T$, whereas Fig. 2b shows the identical data plotted as a function of $1/T_{\max}$. Except for the data for 1 cycle-to-failure ($\log N = 0$), which may be governed by failure well before the end of the first cycle, both sets of data show reasonable linear behavior. The slope of the data in Fig. 2a yields an apparent value for the stress intensity exponent of 22.7. This is significantly higher than the literature value [10] of n for this

material, as expected since a plot of $\ln N$ vs $\ln \Delta T$ does not reflect changes in the value of T_{\max} . Figure 2b results in an apparent value of $Q \approx 69$ Kcal/mole. This is far in excess of the experimental value, because a plot of $\ln N$ vs $1/T_{\max}$ does not reflect the role of the stress intensity exponent in thermal fatigue-life. Assuming the existence of natural convection during the thermal quench of the soda-lime-silica glass rods results in an only slightly lower value of n , because the value of the Biot number due to the thermal conductivity has a value of near 5 to 10.

Since the above numerical examples indicate that care needs to be exercised in the analysis of thermal fatigue data, the following recommendations are made: Values of thermal fatigue-life should be established for two basic conditions; 1. T_{\max} should be kept constant with ΔT being varied by changing T_{\min} ; 2. ΔT should be kept constant by varying T_{\max} and T_{\min} by equal amount. The data obtained for the first condition should result in an unambiguous value of n whereas the results for the second condition should give an unbiased value for Q . The data obtained in this manner should be sufficient to make predictions of thermal fatigue-life for any combination of T_{\max} , T_{\min} and ΔT . If desired, additional experimental data can be obtained for verification of such predictions.

Equation 8 and 15 indicate that even for identical specimen temperatures, the thermal fatigue life for natural and forced convection modes of heat transfer will be different. Therefore, for quantitative evaluation of thermal fatigue-life, the mode of heat transfer must be established. Typically, in a thermal fatigue experiment, the hot specimen is inserted into a quenching bath at lower temperature and held there for a specified period of time. There, for a small specimen in a quenching medium (such as water)

with a high heat transfer coefficient where the maximum stress could develop during the time period when the specimen is moving through the medium, the thermal fatigue-life will be controlled by the forced convection mode of heat transfer. On the other hand for a large specimen in a quenching medium (such as oil) with a low heat transfer coefficient where the maximum stress will develop during the hold period after insertion into the fluid, the fatigue life will be controlled by the natural convection. This suggests the need for a-priori rough estimation of the mode of heat transfer before the quantitative data analysis can be made.

Some materials may show the existence of a pronounced fatigue-limit, i.e., a value of stress intensity factor below which no slow crack growth occurs. This appears to be the case for polycrystalline mullite investigated by Kamiya and Kamigaito[15]. In case of such a pronounced fatigue-limit, the expressions presented earlier will need to be modified. A further complexity in data analysis arises for heat transfer coefficient which may indicate a strong temperature dependence. For many fluid media, this can result from the effects of nucleate boiling and film-formation. The corresponding changes in h with changes in T_{max} , T_{min} and ΔT could well play a major role in governing fatigue-life. In particular, this could be the case with water, commonly used as a quenching medium. Extra caution is recommended in analyzing data of thermal fatigue experiments obtained with water baths. For this reason, fluidized beds may be preferred over water bath. However, in the use of a fluidized bed, caution must be exercised with specimens such as glass whose thermal fatigue life may be greatly influenced by surface conditions. The surface of a glass specimen may be damaged during its motion through the fluidized bed due to particle impact and the fatigue life may be

AD-A111 575

VIRGINIA POLYTECHNIC INST AND STATE UNIV BLACKSBURG --ETC F/8 11/2
THERMO-MECHANICAL AND THERMAL BEHAVIOR OF HIGH-TEMPERATURE STRU--ETC(U)
DEC 81 D P HASSELMAN, L D BENTSEN N00014-78-C-0431

UNCLASSIFIED

NL

2 of 2

AD-A
1-82



811

111

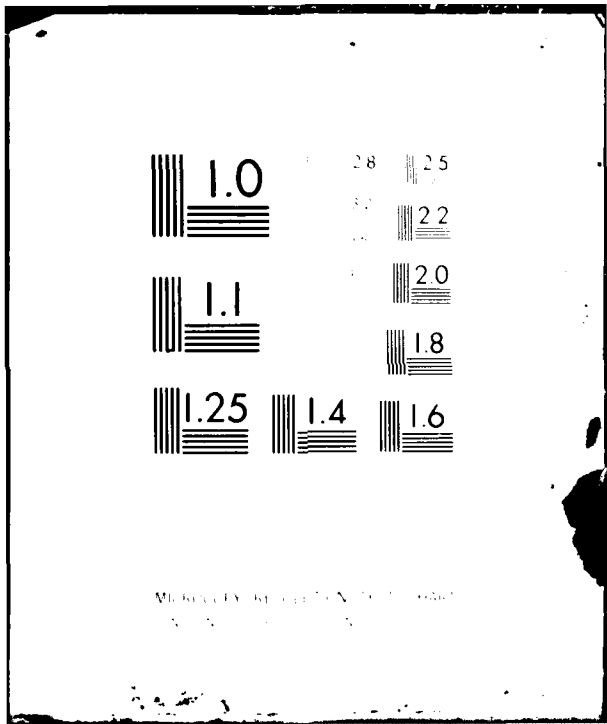
END

DATE

FORMED

13-82

DTIC



MILWAUKEE ELECTRIC TOOL COMPANY
MILWAUKEE, WISCONSIN

greatly reduced. Therefore, the effect of surface damage due to particle contact in the fluidized bed must be independently evaluated and incorporated in the quantitative evaluation and interpretation of the experimental data.

The above analyses also shed light on the effect of specimen size and material properties on thermal fatigue life. For high values of Biot number, Equations 8 and 15 indicate that thermal fatigue-life is inversely proportional to the square of the dimensions of the specimen. On dimensional grounds, this conclusion should be generally valid regardless of geometry. For low values of Biot number, frequently encountered in laboratory studies and such components as silicon nitride and silicon carbide turbine blades and valves, a very pronounced size effect exists. For both forced and natural convection, Equations 8 and 15 suggest that

$$N \propto 1/R^{n+2} \quad \beta \ll 1 \quad (20)$$

This result indicates that major improvements in thermal-fatigue life can be achieved by minor design changes in the form of even slight reduction in component size.

In practice, the materials technologist may wish to select the material with highest thermal fatigue resistance. For a specimen of given size and geometry with a given crack size and configuration and given heat transfer environment, highest thermal fatigue resistance can be obtained by optimizing the relevant material properties which govern thermal fatigue failure. Materials with optimum thermal stress resistance can be selected on the basis of thermal stress resistance parameters or figures-of-merit which are available for a wide variety of heat transfer conditions and

modes of thermal stress failure. Similar figures-of-merit can be defined for optimizing thermal fatigue resistance. For both forced and natural convection these can be obtained from Equations 8 and 15.

$$\frac{\kappa}{A(n-2)} \left\{ \frac{(1-\nu)k}{\alpha E} \right\}^n \exp(Q/RT_{\max}) \quad \beta \ll 1 \quad (21a)$$

$$\frac{\kappa}{A(n-2)} \left\{ \frac{(1-\nu)k}{\alpha E} \right\}^n \exp(Q/RT_{\max}) \quad \beta \gg 1 \quad (21b)$$

These figures-of-merit indicate that thermal fatigue-life is governed by as many as seven material properties. Without quantitative information on these properties, estimates of thermal fatigue-life are not feasible. Of interest to note is that high thermal fatigue resistance requires high values of the thermal diffusivity κ , thermal conductivity k , stress intensity factor exponent n and activation energy Q with low values of constant A , Young's modulus E and coefficient of thermal expansion α .

In this respect, for basic studies of thermal fatigue life, materials with low thermal diffusivity and conductivity may be most useful since thermal fatigue curves can be established with minimum number of cycles. Glassy materials, for this reason, appear most useful.

ACKNOWLEDGMENTS

The present study was conducted as part of a research program on the thermo-mechanical and thermo-physical properties of high-temperature structural materials supported by the Office of Naval Research under Contract: N00014-78-C-0431.

REFERENCES

1. L. S. WILLIAMS, Trans. Br. Ceram. Soc. 55 (1956) 287.
2. S. M. WIEDERHORN and L. H. BOLZ, J. Am. Ceram. Soc. 53 (1970) 543.
3. J. E. RITTER, JR. and M. S. CAVANAGH, J. Am. Ceram. Soc. 59 (1976) 57.
4. J. E. RITTER, JR. and C. L. SHEROURNE, J. Am. Ceram. Soc. 54 (1971) 601.
5. C. GURNEY and S. PEARSON, Proc. Phys. Soc. London Sect. B62 (1958) 537.
6. RAM KOSSOWSKY, J. Amer. Ceram. Soc. 56 (1973) 531.
7. B. K. SARKAR and T. G. J. GLINN, Trans. Brit. Ceram. Soc. 69 (1970) 199.
8. V. I. TUMANOV, Z. A. GOLDBERG, V. V. CHERNYSHEV and A. I. PAVLOVA, Poroshkovaya Metallurgiya 10 (1966) 71.
9. R. C. BRADT, D. P. H. HASSELMAN and F. F. LANGE, eds. "Fracture Mechanics of Ceramics, Vol. 2 Microstructure, Materials and Applications," (Plenum Press, New York, 1974).
10. A. G. EVANS, J. Mat. Sc. 7 (1972) 1137.
11. A. G. EVANS and E. R. FULLER, Met. Tran. 5 (1974) 27.
12. D. P. H. HASSELMAN, R. BADALIANCE, K. R. MCKINNEY and C. H. KIM, J. Mat. Sc. 11 (1976) 458.
13. C. L. AMMANN, J. E. DOHERTY and C. G. NESSLER, Mat. Sc. Eng. 22 (1976) 15.
14. D. P. H. HASSELMAN, E. P. CHEN, C. L. AMMANN, J. E. DOHERTY AND C. G. NESSLER, J. Am. Ceram. Soc. 58 (1973) 513.
15. N. KAMIYA and O. KAMIGAITO, J. Mat. Sc. 14 (1979) 573.
16. A. C. CHAPMAN, "Heat Transfer", Third Edition. (MacMilan Publishing Co., Inc., New York, 1967).
17. K. SATYAMURTHY, G. ZIEGLER, J. P. SINGH and D. P. H. HASSELMAN (in preparation).
18. J. C. JAEGER, Philos. Mag. 36 (1945) 418.
19. R. BADALIANCE, D. A. KROHN and D. P. H. HASSELMAN, J. Am. Ceram. Soc. 57 (1974) 432.
20. D. P. H. HASSELMAN, E. P. CHEN and P. A. URICK, Bull Am. Ceram. Soc. 57 (1978) 190.
21. J. P. SINGH, J. R. THOMAS JR., and D. P. H. HASSELMAN, J. Am. Ceram. Soc. 63 (1980) 140.

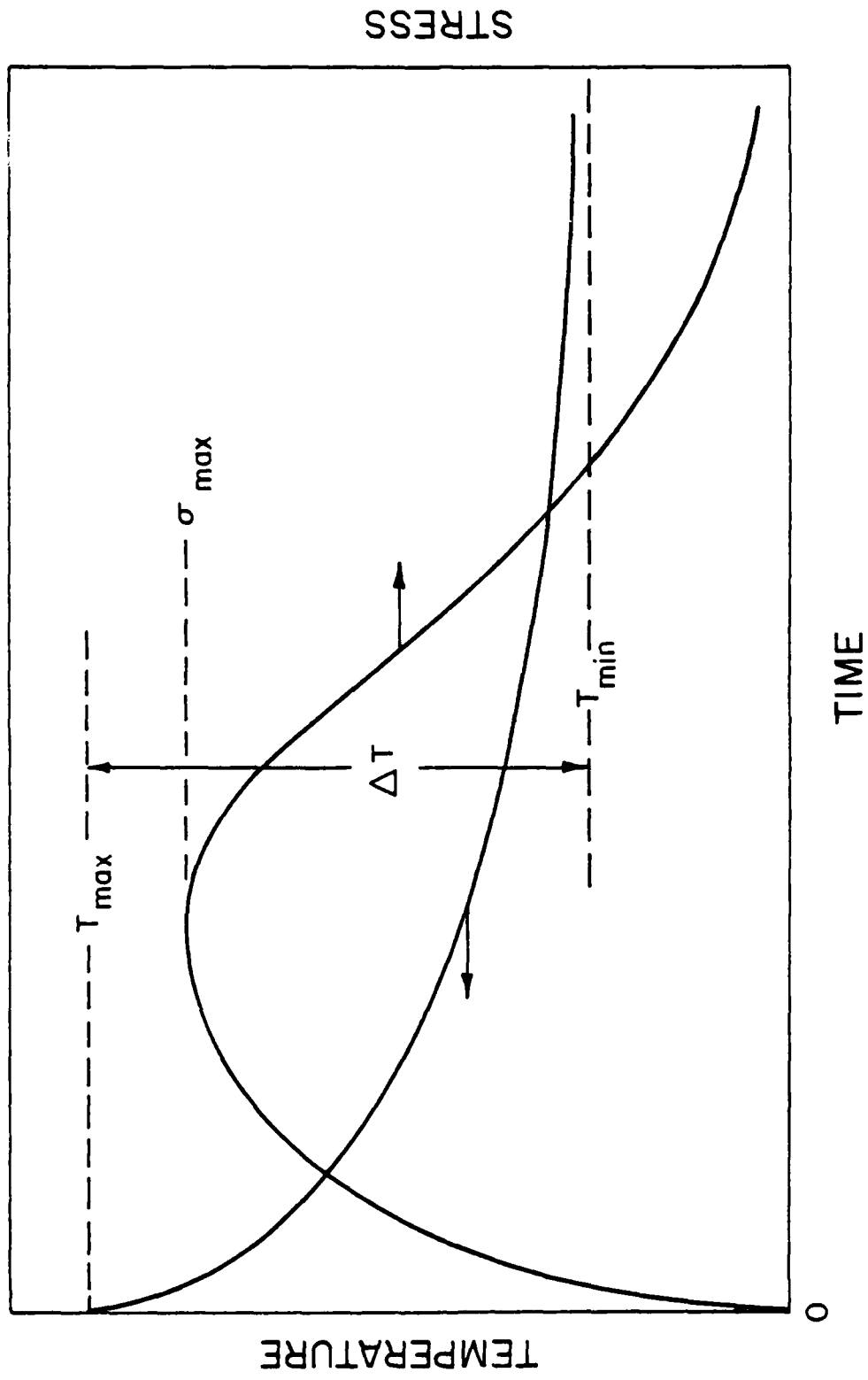


Fig. 1. Schematic representation of the time-dependence of the temperature and stress in the surface of a thermal fatigue specimen.

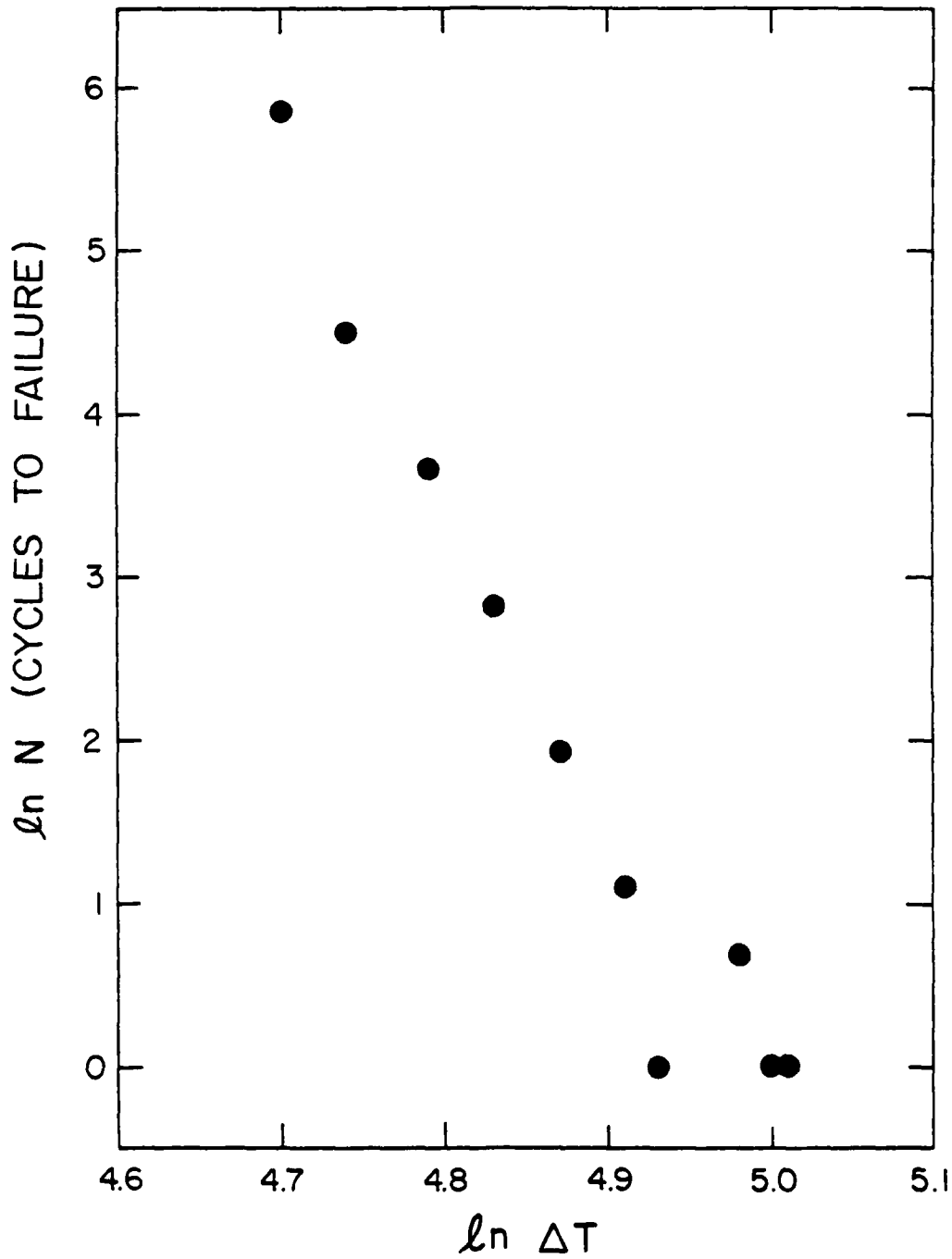


Fig. 2a. Thermal fatigue life of soda-lime-silica glass specimen subjected to repeated water quench (after ref. [20]).
 a; as a function of the initial temperature difference,
 b; as a function of the maximum temperature.

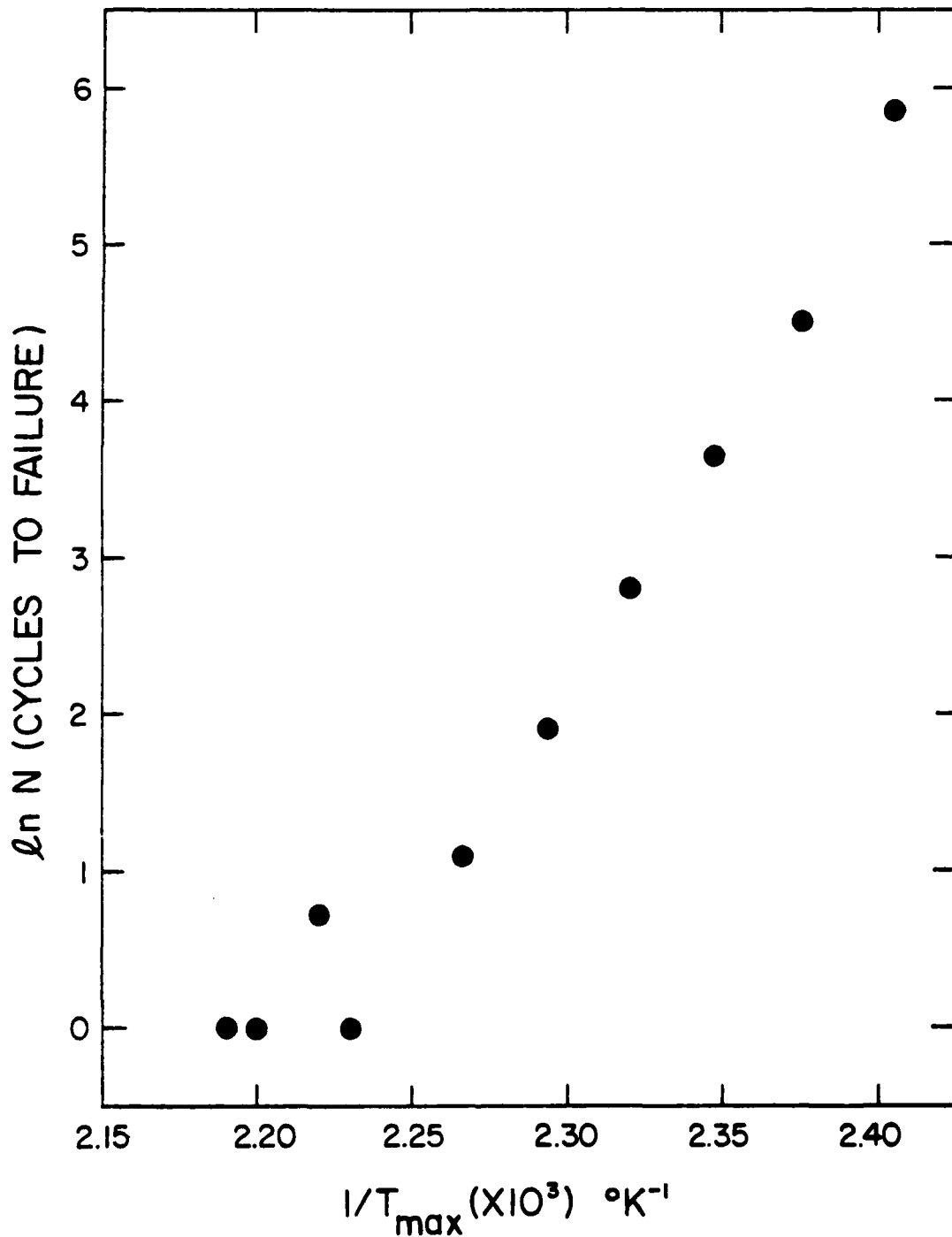


Fig. 2b. Thermal fatigue life of soda-lime-silica glass specimen subjected to repeated water quench (after ref. [20]).
 a; as a function of the initial temperature difference,
 b; as a function of the maximum temperature.

CHAPTER V

THERMAL STRESSES IN A PARTIALLY ABSORBING
FLAT PLATE ASYMMETRICALLY HEATED BY CYCLIC THERMAL
RADIATION AND COOLED BY CONVECTION

J. R. Thomas, Jr., J. P. Singh and D. P. H. Hasselman

Departments of Mechanical and Materials Engineering
Virginia Polytechnic Institute and State University
Blacksburg, VA 24061, USA

ABSTRACT

An analysis is presented for the temperatures and thermal stresses in a partially absorbing flat plate subjected to normally incident cyclic thermal radiation on the front face, and cooled by convection on the rear face.

The resulting temperature and stress responses are cyclic in nature with the temperatures and stresses in the center and the back face lagging behind those in the front face. The amplitude of the temperature fluctuation is found to be maximum in the front face. During the initial thermal cycles the maximum stress in the plate is compressive. In contrast, when the plate approaches thermal equilibrium after many cycles, the maximum stress is tensile. The values of the maximum tensile and compressive stresses were found to depend on the frequency of the incident cyclic radiation.

INTRODUCTION

Radiation heat transfer can result in transient and steady-state thermal stresses. This problem is particularly severe in components and structures such as lenses, windows, heat exchangers, etc., subjected to intense radiation from lasers, solar energy concentrators and other sources.

Solutions for the thermal stresses due to suddenly applied constant flux black-body radiation were presented earlier for materials totally opaque to the incoming radiation [1]. This solution was extended to include materials opaque above a given wavelength and totally transparent below this wavelength of black-body radiation [2]. More recently, for a variety of boundary conditions, solutions were obtained for the thermal stresses in materials suddenly subjected to a constant radiative heat flux, absorbed internally as described by the absorption coefficient [3-6].

In practice, radiative heat fluxes can be constant or vary with time. This latter condition is encountered for pulsed lasers or solar-energy concentrators under conditions of intermittent cloud cover. Such rapid changes in radiation intensity are expected to give rise to transient thermal stresses. The purpose of this paper is to present an analysis of the thermal stresses in a partially transparent flat plate subjected to thermal radiation with an intensity which varies sinusoidally in time.

ANALYSIS

Boundary and Initial Conditions

The flat plate, infinite in extent, is located in the yz plane, and $-a < x < a$. At the front face ($x = -a$) the plate is subjected at time

$t = 0$ to normally incident, spatially uniform radiation which oscillates in time with angular frequency ω .

At the back face ($x = a$), the plate is cooled by Newtonian convection with a heat transfer coefficient h . As for the previous analysis [3-6] the optical properties of the plate are assumed to be "grey," i.e., independent of wavelength. The reflectivity of the plate is assumed sufficiently low so that the effect of multiple reflections within the plate can be neglected. The material properties that affect the temperature distribution and thermal stresses, such as the emissivity (absorptivity), absorption coefficient, thermal conductivity and thermal diffusivity, coefficient of thermal expansion, Young's modulus and Poisson's ratio are assumed to be independent of temperature. It is also assumed that the temperatures in the plate remain sufficiently low so that the intensity of any re-emitted radiation, to a first approximation, is negligible in comparison to the intensity of the incident radiation.

The intensity $q(t)$ of the radiation as it approaches the plate is assumed to be of the form

$$q(t) = q_0 [1 + \delta \sin(\omega t)] \quad (1)$$

where $0 \leq \delta \leq 1$ and t is the time. For this study, δ will be taken as 1, so that the magnitude of incident radiation heat flux varies between the values $2q_0$ and 0.

The intensity of the heat flux q at x within the plate due to the thermal radiation entering at $x = -a$ is

$$q(x,t) = \epsilon q_0 e^{-\mu(a+x)} [1 + \delta \sin(\omega t)] \quad (2)$$

where $\epsilon = 1-r$ with r being the reflectivity and μ is the absorption coefficient. The rate of internal heat absorption per unit volume g''' within the plate at x is thus

$$g'''(x,t) = \mu \epsilon q_0 e^{-\mu(a+x)} [1 + \delta \sin(\omega t)] \quad (3)$$

Solutions for the transient temperature $T(x,t)$ are obtained by solving the heat conduction equation [7]

$$\frac{\partial^2 T}{\partial x^2} + \frac{g'''(x,t)}{k} = \frac{1}{\kappa} \frac{\partial T}{\partial x} \quad (4)$$

where k is the thermal conductivity and κ is the thermal diffusivity.

For the given heating and cooling conditions the initial and boundary conditions are

$$T(x,0) = T_0 \quad (5)$$

$$\frac{\partial T}{\partial x}(-a,t) = 0 \quad (6)$$

$$\frac{\partial T}{\partial x}(a,t) = -\frac{h}{k}[T(a,t) - T_0] \quad (7)$$

where h is the heat transfer coefficient.

Solutions for the transient temperatures were obtained using standard techniques [7]

$$T(x,t) = T_0 + \sum_{n=1}^{\infty} B_n(t) \cos(\lambda_n x) \quad (8)$$

where λ_n are the roots of the transcendental equation

$$\lambda_n \tan(2\lambda_n a) = \frac{h}{k} \quad (9)$$

and

$$B_n(t) = \frac{G_n \omega \delta}{\omega^2 + (\kappa \lambda_n^2)^2} [e^{-\kappa \lambda_n^2 t} - \cos \omega t + \frac{\kappa \lambda_n^2}{\omega} \sin \omega t] + \frac{G_n}{\kappa \lambda_n^2} (1 - e^{-\kappa \lambda_n^2 t}) \quad (10)$$

with

$$G_n = \frac{\kappa q_0 \epsilon \mu}{N_n k} \left[\frac{\mu + e^{-2\mu a} \{ \lambda_n \sin(2\lambda_n a) - \mu \cos(2\lambda_n a) \}}{\mu^2 + \lambda_n^2} \right] \quad (11)$$

and
$$N_n = \frac{1}{2\lambda_n} [\sin(2\lambda_n a) \cos(2\lambda_n a) + 2\lambda_n a] \quad (12)$$

THERMAL STRESSES

Expressions for the thermal stresses $\sigma_{y,z}(x,t)$ are obtained [8] by substitution of eq. (8) for T into

$$\sigma_{y,z} = \frac{\alpha E}{1-\nu} \left[-T + \frac{1}{2a} \int_{-a}^a T dx + \frac{3x}{2a^3} \int_{-a}^a T x dx \right] \quad (13)$$

which yields

$$\begin{aligned} \sigma_{y,z} = & -\frac{\alpha E}{1-\nu} \sum_{n=1}^{\infty} B_n(t) \cos[\lambda_n(x+a)] \\ & + \frac{\alpha E}{2a(1-\nu)} \sum_{n=1}^{\infty} \frac{B_n(t)}{\lambda_n} \sin(2\lambda_n a) \\ & + \frac{3\alpha E}{2a(1-\nu)} \sum_{n=1}^{\infty} B_n(t) \left[\frac{\sin(2\lambda_n a)}{a\lambda_n} + \frac{1}{a^2 \lambda_n^2} \cos(2\lambda_n a) - \frac{1}{a^2 \lambda_n^2} \right] \end{aligned} \quad (14)$$

For convenience, the numerical results are reported in terms of the non-dimensional temperature

$$T^* = \frac{(T-T_0)k}{\epsilon q_0 a}$$

the non-dimensional stress

$$\sigma^* = \frac{\sigma(1-\nu)k}{\alpha E q_0 \epsilon a}$$

the non-dimensional time, $t^* = \kappa t/a^2$ and the non-dimensional distance, x/a .

RESULTS AND DISCUSSION

The analytical results for the temperatures and stresses obtained above are most easily illustrated and discussed by means of a numerical example. In order to keep the amount of data to be presented within reasonable bounds, emphasis will be placed on the effect of the cyclic nature of the incident radiation for single values of the other parameters ($k, h, \kappa, a, \mu a$). These latter quantities were taken as $k = 0.3 \text{ watts.cm}^{-1}\text{°C}^{-1}$, $h = 6 \times 10^{-3} \text{ watts.cm}^{-2}\text{°C}^{-1}$, $\kappa = 0.1 \text{ cm.}^2\text{s}^{-1}$ and $a = 1 \text{ cm.}$ The value of optical thickness μa was chosen as 3, which is near the value which resulted in the maximum magnitude of stresses under steady-state conditions for a flat plate asymmetrically heated by a constant radiative heat flux and cooled by convection on either the back or front face [5,6].

Figure 1 for an arbitrarily selected value of $\omega = 0.21 \text{ s}^{-1}$ illustrates the magnitude of the temperature as a function of t^* for three different time intervals and three positions within the plate, $x = -a, 0,$ and a . Figure 1a shows the temperature response during the first few cycles. Figure 1c corresponds to the magnitude of temperature at large values of time for which the temperatures in the plate approach the values encountered at $t = \infty$. This condition corresponds to a time-averaged back-face temperature $T^* = 49.9$ at which the average convective heat flux equals the time-averaged radiative heat flux absorbed within the plate. For $\mu a = 3$ for this numerical example, this corresponds to 99.8% of the radiant flux which enters the plate at $x = -a$. As shown in Fig. 1 for all three time intervals, as expected, the cyclic temperature response at the center and back-face lags behind the corresponding value for the front face. Also the rate of rise of average temperature decreases with

increasing time as the rate of heat removal by convection increases with increasing back-face temperature.

Figure 2 shows the spatial distribution and amplitude of the temperature oscillation for the time-interval in Fig. 1c. The amplitude of the temperature oscillation is greatest at the front-face and decreases with increasing distance towards the back-face. The temperature distribution exhibits a pronounced downward concavity. This results from the asymmetric distribution of the rate of internal heat generation.

Figure 3 shows the thermal stresses at $x = -a, 0$ and a for the time intervals shown in Fig. 1. In Fig. 3c the cycle-to-cycle variation in the magnitude of thermal stress is less than 0.02%. Of interest is the general reversal of stress as time proceeds. The stresses in the center of the plate, which are primarily tensile during the first few cycles of the radiation become primarily compressive at the higher values of time as the plate approaches its final maximum temperature. The opposite effect occurs for the stresses at the back face. At the front of the plate the stresses initially cycle between tension and compression, to become entirely tensile at large values of time. Such tensile stresses occur in the front face, which is at the highest temperature, because of the downward concavity of the temperature distribution [9]. The stress values shown in Fig. 3 were calculated for a given value of heat transfer coefficient ($h = 0.006 \text{ watts.cm}^{-2} \text{ } ^\circ\text{C}^{-1}$). However, as indicated by the results of earlier studies of time-invariant radiation [5,6], the magnitude of the stresses are not expected to depend strongly on the heat transfer coefficient values encountered in practice. During the first few cycles, the back face temperature is not sufficiently high that the temperature distribution is affected strongly by the convective heat losses. Similarly, at the large values of time, although the absolute

values of temperature encountered are an inverse function of the heat transfer coefficient, the temperature profile, which controls the magnitude of thermal stresses, is governed by the distribution of internal heat generation rather than the heat transfer coefficient.

Figure 4 shows the maximum values of the tensile and compressive stresses encountered during each cycle with increasing total number of cycles of incident radiation. During approximately the first 25 cycles, plate failure most likely will occur in compression unless the plate is composed of a highly brittle material with high ratio of compressive to tensile strength. After more than about twenty-five cycles, however, failure is expected in a tensile mode regardless of whether the plate is composed of brittle or ductile material.

The magnitude of the thermal stresses are expected to be a function of the frequency of incident radiation in view of the expected coupling between the time period of a thermal cycle and the transit time of a thermal wave through the plate. This latter quantity is a function of the plate dimensions and the thermal diffusivity. Evidence for the validity of this hypothesis is shown in Figures 5a and 5b. Figure 5a shows the dependence of the maximum tensile and compressive stresses during the first cycle in the center and the back face of the plate, respectively as a function of angular frequency, ω . Figure 5b shows the corresponding stresses at steady state conditions in the front face and the center of the plate respectively. It can be noted that for this numerical example at steady state, a maximum in tensile stress value is obtained at an angular frequency of $\omega \approx 0.6$ (a period of approx. 10 sec.) whereas a peak in compressive stress value occurs at an angular frequency of $\omega \approx 0.1$. At $\omega = 0$ and ∞ , the plate in effect is subjected to a constant heat flux, q_0 , with a corresponding value of $\sigma^* = 0.167$ in agreement with earlier results [5].

The results of Fig. 5 clearly indicate that for the same time averaged radiative heat flux, the stresses for cyclic conditions can exceed those for a constant heat flux by a considerable margin.

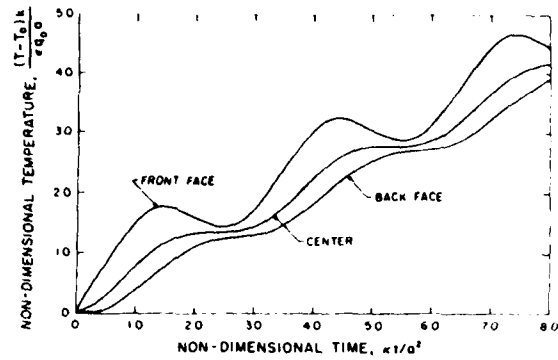
ACKNOWLEDGMENT

This study was conducted as part of a research program on the thermomechanical and thermal properties of brittle structural materials, supported by the Office of Naval Research under Contract No. N00014-78-C-0431.

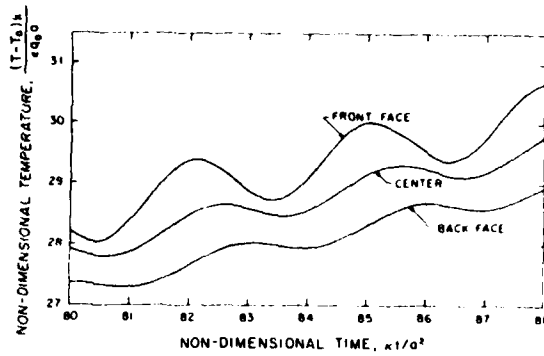
REFERENCES

1. D. P. H. Hasselman, Thermal Shock by Radiation Heating, J. Am. Ceram. Soc. Vol. 46, pp. 229-234, 1963.
2. D. P. H. Hasselman, Theory of Thermal Stress Resistance of Semi-Transparent Ceramics Under Radiation Heating, J. Am. Ceram. Soc., Vol. 49, pp. 103-104, 1966.
3. D. P. H. Hasselman, J. R. Thomas, Jr., M. P. Kamat and K. Satyamurthy, Thermal Stress Analysis of Partially Absorbing Brittle Ceramics Subjected to Symmetric Radiation Heating, J. Am. Ceram. Soc., Vol. 63, pp. 21-25, 1980.
4. J. P. Singh, J. R. Thomas, Jr., and D. P. H. Hasselman, Thermal Stresses in a Partially Absorbing Flat Plate Symmetrically Heated by Thermal Radiation and Cooled by Convection. J. Thermal Stresses, Vol. 3, pp. 341-349, 1980.
5. J. R. Thomas, Jr., J. P. Singh and D. P. H. Hasselman, Analysis of Thermal Stress Resistance of Partially Absorbing Ceramic Plate Subjected to Asymmetric Radiation, I: Convective Cooling at Rear Surface, J. Am. Ceram. Soc., Vol. 64, pp. 163-169, 1981.

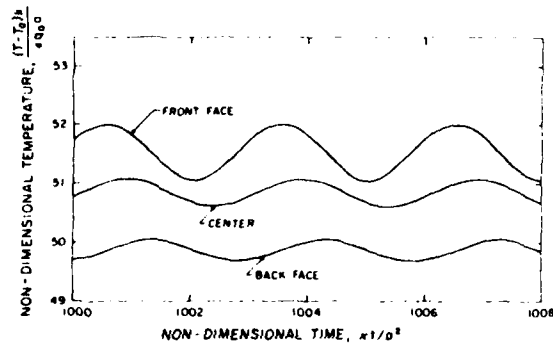
6. J. P. Singh, K. Satyamurthy, J. R. Thomas, Jr., and D. P. H. Hasselman, Analysis of Thermal Stress Resistance of Partially Absorbing Ceramic Plate Subjected to Asymmetric Radiation, II: Convective Cooling at Front Surface, J. Am. Ceram. Soc., Vol. 64, pp. 169-173, 1981.
7. H. S. Carslaw and J. C. Jaeger, Conduction of Heat in Solids, 2nd ed., Clarendon Press, Oxford, 1960.
8. B. A. Boley and J. H. Wiener, Theory of Thermal Stresses, Wiley, New York, 1960.
9. K. Satyamurthy, D. P. H. Hasselman and J. P. Singh, Effect of Nature of Concavity of Temperature Distribution on Position and Sign of Maximum Thermal Stress: A Short Note, J. Thermal Stresses, Vol. 3, pp. 551-553, 1980.



a.



b.



c.

Fig. 1. Transient temperature in a partially absorbing flat plate heated in front by normally incident cyclic thermal radiation and cooled at the rear surface by convection for three different time intervals: $h = 0.006 \text{ W.cm.}^{-2}\text{C}^{-1}$, $k = 0.3 \text{ W.cm.}^{-1}\text{C}^{-1}$, $\kappa = 0.1 \text{ cm.}^2\text{s}^{-1}$, $\omega = 0.21 \text{ s}^{-1}$, $\mu a = 3$ and $a = 1 \text{ cm}$.

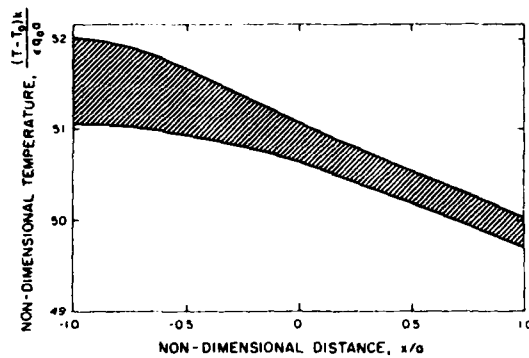
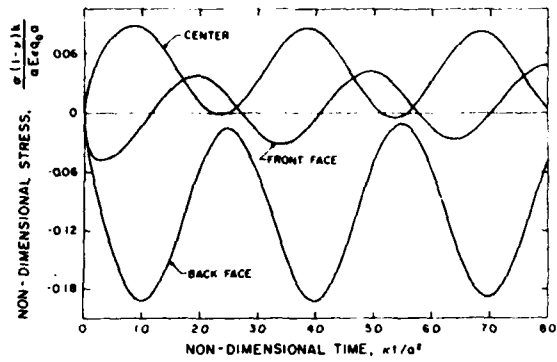
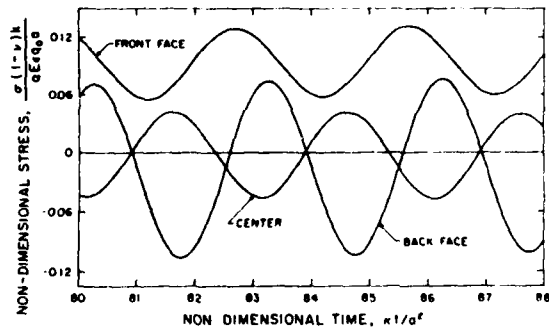


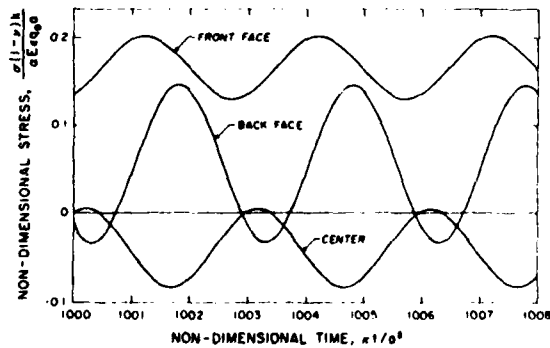
Fig. 2. Envelope of the temperature oscillation in a partially absorbing flat plate heated in front by normally incident cyclic radiation and cooled at the rear surface by convection corresponding to the time interval in figure 1c: $h = 0.006 \text{ W.cm.}^{-2}\text{C}^{-1}$, $k = 0.3 \text{ W.cm.}^{-1}\text{C}^{-1}$, $\kappa = 0.1 \text{ cm.}^2\text{s.}^{-1}$, $\omega = 0.21 \text{ s.}^{-1}$, $\mu a = 3$ and $a = 1 \text{ cm.}$



a.



b.



c.

Fig. 3. Transient thermal stresses in a partially absorbing flat plate heated in front by normally incident cyclic thermal radiation and cooled at the rear surface by convection for three different time intervals: $h = 0.006 \text{ W.cm.}^{-2}$ $^{\circ}\text{C.}^{-1}$, $k = 0.3 \text{ W.cm.}^{-1}\text{^{\circ}\text{C.}^{-1}}$, $\kappa = 0.1 \text{ cm.}^2\text{s.}^{-1}$, $\omega = 0.21 \text{ s.}^{-1}$, $\mu_a = 3$ and $a = 1 \text{ cm.}$

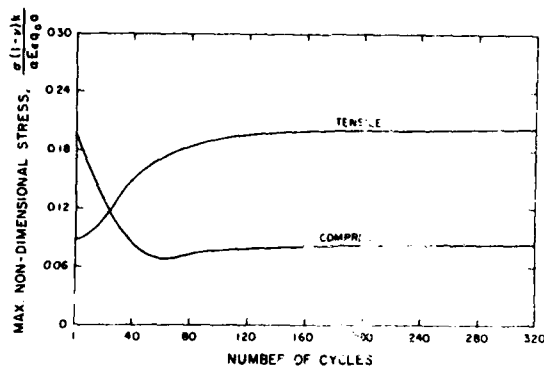
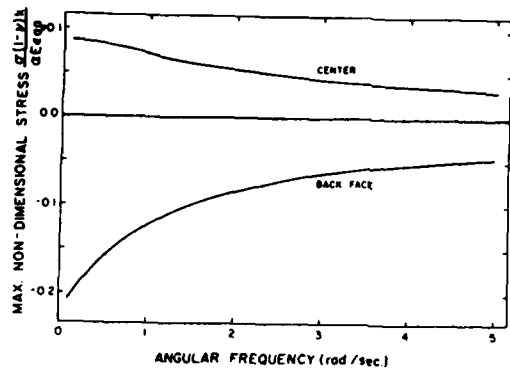
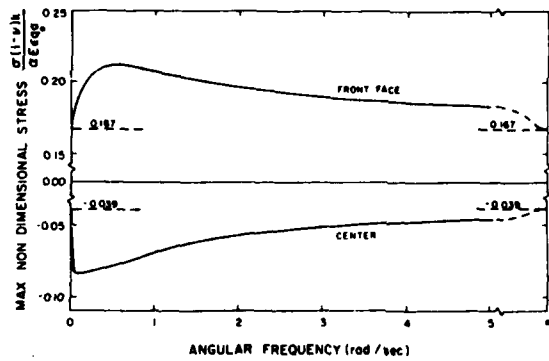


Fig. 4. Maximum tensile and compressive stresses in a partially absorbing flat plate heated in front by normally incident cyclic thermal radiation and cooled at the rear surface by convection: $h = 0.006 \text{ W.cm.}^{-2}\text{C.}^{-1}$, $k = 0.3 \text{ W.cm.}^{-1}\text{C.}^{-1}$, $\kappa = 0.1 \text{ cm.}^2\text{s.}^{-1}$, $\omega = 0.21\text{s.}^{-1}$, $\mu a = 3$ and $a = 1 \text{ cm.}$



a.



b.

Fig. 5. Variation of the maximum tensile and compressive stresses with the frequency of the incident cyclic thermal radiation in a partially absorbing flat plate heated in front and cooled at the rear surface by convection: $h = 0.006 \text{ W.cm.}^{-2}\text{C.}^{-1}$, $k = 0.3 \text{ W.cm.}^{-1}\text{C.}^{-1}$, $\kappa = 0.1 \text{ cm.}^2\text{s.}^{-1}$, $\mu a = 3$ and $a = 1 \text{ cm.}$ (a) for first cycle, (b) for steady state.

CHAPTER VI

ANISOTROPY OF THE THERMAL DIFFUSIVITY

OF Si_3N_4 -BN COMPOSITES

K. Niihara, L. D. Bentsen, D. P. H. Hasselman
Department of Materials Engineering
Virginia Polytechnic Institute and State University

K. Mazdidasni
Air Force-Wright Aeronautical Laboratory
Wright-Patterson Air Force Base, Ohio 45433

The thermal diffusivity of silicon nitride-boron nitride composites is shown to exhibit considerable anisotropy with respect to the hot-pressing direction due to the preferred orientation of the boron nitride inclusions.

During the powder-metallurgical processing of composites involving mechanical compaction, the particles of one or both components can take on a preferred crystallographic orientation with respect to the direction of compaction. Materials such as mica [1], graphite [2], or boron nitride, frequently exhibit a pronounced anisotropy of many of their properties such as elastic moduli [3], thermal expansion [4], thermal conductivity and diffusivity [5,6,7]. For this reason, it is expected that the bulk properties of composites, in which such particles take on a preferred orientation, also will be anisotropic. Evidence for this effect in the form of experimental data for the thermal diffusivity of the silicon nitride containing a dispersed phase of boron nitride is presented.

The composites were made by hot-pressing mixtures of silicon nitride* powder of 99.9% purity and average particle size of 0.5 μm and boron nitride** of 1 μm particle size. The silicon nitride powder contained 6 wt.% of an alkoxy-derived CeO_2 as hot-pressing aid. The powder mixtures were dry-milled in polyethylene jars with alumina balls for a period of 4 hours. Discs 5.1 to 7.6 cm in diameter by 0.6 cm thick were uniaxially hot-pressed in graphite dies coated with BN and lined with graphite foil[§] in a nitrogen atmosphere. The hot-pressing schedule consisted of slow heating to 1200°C at a pressure of about 3 MPa followed by rapid heating to 1700-1750°C and holding for a period of 30 to 60 minutes at about 30 MPa. The hot-pressed discs were allowed to cool slowly under pressure within the hot-press.

The preferred orientations of the boron nitride and silicon nitride were established by x-ray analysis of surfaces cut parallel and perpendicular to the hot-pressing direction. For all five compositions studied, Figs. 1a and 1b show the ratios of the relative summed intensities normal and parallel to the hot-pressing direction for the boron nitride and silicon nitride, respectively. The boron nitride inclusions are highly oriented with the c-axis parallel to the direction of hot-pressing. The silicon nitride also has a preferred orientation which has been observed by other investigators [8,9]. However, the degree of preferred orientation is reduced by the presence of the boron nitride particles, probably because they interfere with the direction of growth

*SN 402, GTE Laboratories, Towanda, PA.

**Cerac Inc., Menomonee Falls, WI.

§Grafoil, Union Carbide Corp., Chicago, IL.

of the β - Si_3N_4 grains perpendicular to the hot-pressing direction. Transmission electron microscopy combined with electron-beam diffraction of ion-thinned sections confirmed the preferred orientation of the BN particles. Also, the aspect ratio of the BN particles was found to have a value near three. It is postulated that this particle shape contributed to the preferred orientation achieved due to particle rearrangement during hot-pressing.

Specimens for the measurement of the thermal diffusivity in the form of disks approximately 10-12 mm in diameter by 2 mm thick were cut from each of the hot-pressed blanks. For all compositions, three specimens were cut for heat flow parallel and perpendicular to the hot-pressing direction. The thermal diffusivity at room temperature was measured by the laser-flash technique [10] using equipment described elsewhere [11,12].

Figure 2 shows the experimental data, which represent the average of the three specimens for each composition and orientation. Specimen-to-specimen variation was less than 5%. In agreement with previous findings [12], the silicon nitride without BN exhibits anisotropic thermal diffusivity. This is due to the preferred orientation of the β -grains, confirmed by the x-ray data given in Fig. 1. Upon addition of BN the anisotropy of the thermal diffusivity increases to be most pronounced at 30 wt.% BN. At low BN content the thermal diffusivity perpendicular as well as parallel to the hot-pressing direction shows a decrease with increasing BN content. This is thought to be due to the combination of two separate effects. The first effect results from the reduction in the degree of preferred orientation of the silicon nitride. The second effect results from the absolute values and anisotropy of the thermal diffusivity of the BN particles. As judged by data [6] for pyrolytic BN, the thermal diffusivity in the basal plane exceeds the value for silicon nitride by about a

factor of 5. On the other hand, the thermal diffusivity of BN perpendicular to the basal plane is only about one twentieth of that of silicon nitride. For the present samples then it would be expected that parallel to the hot-pressing direction the BN particles would cause a decrease in thermal diffusivity of the composite, as observed.

Perpendicular to the hot-pressing direction, however, an increase in the thermal diffusivity would be expected as observed at the higher value of BN content. The observed decrease at the lower volume fraction of BN, is due to the combined effects of the decrease in degree of preferred orientation of both the silicon nitride and boron nitride.

Attempts to calculate the thermal diffusivity from the thermal conductivity, specific heat and density for silicon nitride and pyrolytic BN, by using composite theory did not give good quantitative agreement with the observed data. This suggests that a third effect may also be operative such as an interfacial effect resulting from less than perfect adhesion between the silicon nitride and boron nitride. Most likely the lack of agreement between theory and experiment occurs because the BN particles in the present composites and pyrolytic BN may have different degrees of structural perfection.

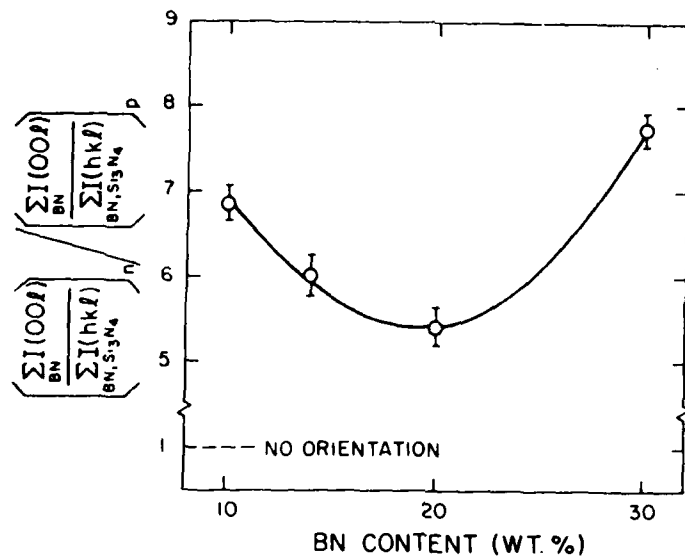
The anisotropy in thermal diffusivity observed for the present composites possibly could be used to advantage for structural components which should show good thermal insulating behavior in one direction and high thermal conductivity in a perpendicular direction, for the purpose of improving thermal stress resistance depending on the direction of heat flow.

Acknowledgment

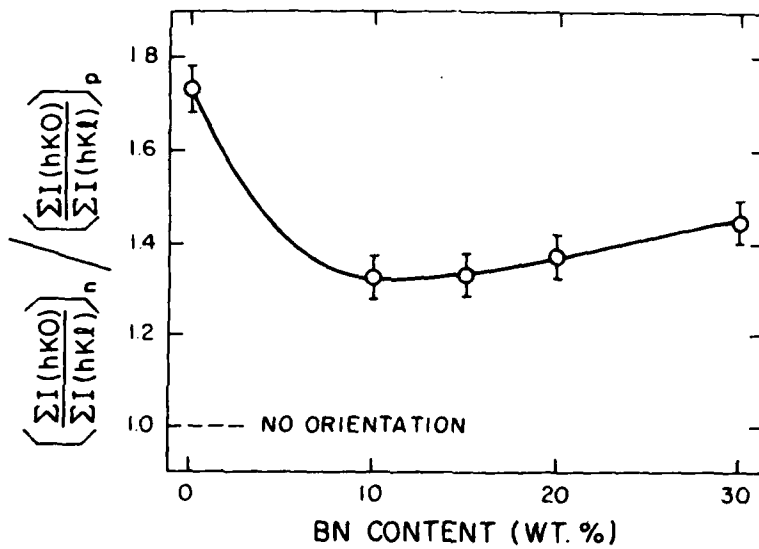
Measurements of the thermal diffusivity and x-ray analysis were conducted as part of a research program on the thermal and thermo-mechanical behavior of high-temperature structural materials supported by the Office of Naval Research under Contract N00014-78-C-0431. The specimens were fabricated at the Materials Research Laboratory of the Wright-Patterson Air Force Base.

References

1. G. E. Youngblood, L. D. Bentsen, J. W. McCauley and D. P. H. Hasselman, *Ceramic Bulletin*, 58 (1979) 620.
2. D. P. H. Hasselman and P. T. B. Shaffer, "Fractors Affecting Thermal Shock Resistance of Polyphase Ceramic Bodies," Technical Documentary Report No. WADD-TR-60-749, Part II (1962).
3. G. B. Spence; p. 351 in *Proceedings of the Fifth Conference on Carbon*, Vol. 2. Ed. by S. Mrozowski, P. K. Walker and M. L. Studebaker, Pergamon Press Inc., New York (1963).
4. *Thermal Expansion: Nonmetallic Solids*, Ed. by Y. S. Touloukian, R. K. Kirby, R. E. Taylor, and T. Y. R. Lee, *Thermophysical Properties of Matter*, Vol. 13, IFI/Plenum (New York - Washington, 1977).
5. T. Tanaka and H. Suzuki, *Carbon*, 10 (1972) 253.
6. A. Simpson and A. D. Stuckes, *J. Phys. C*, 4 (1971) 1710.
7. E. K. Sichel and R. E. Miller, pp. 11-17 in *Thermal Conductivity 14*. Ed. by P. G. Klemens and T. K. Chen, Plenum, New York, 1974.
8. F. F. Lange, *J. Am. Ceram. Soc.*, 56 (1973) 518.
9. K. Nuttall and D. P. Thompson, *J. Mat. Sci.*, 9 (1974) 850.
10. W. J. Parker, R. J. Jenkins, C. P. Butler and G. L. Abbott, *J. Appl. Phys.*, 32 (1961) 1679.
11. H. J. Siebeneck, J. J. Cleveland, D. P. H. Hasselman and R. C. Bradt, *J. Amer. Ceram. Soc.*, 59 (1976) 241.
12. G. Ziegler, L. D. Bentsen and D. P. H. Hasselman, *Communications to the American Ceramic Society* (in press).



a.



b.

Fig. 1. Ratios of integrated x-ray intensities normal and parallel to the hot-pressing direction of silicon nitride-boron nitride composites: a, BN; b, Si_3N_4

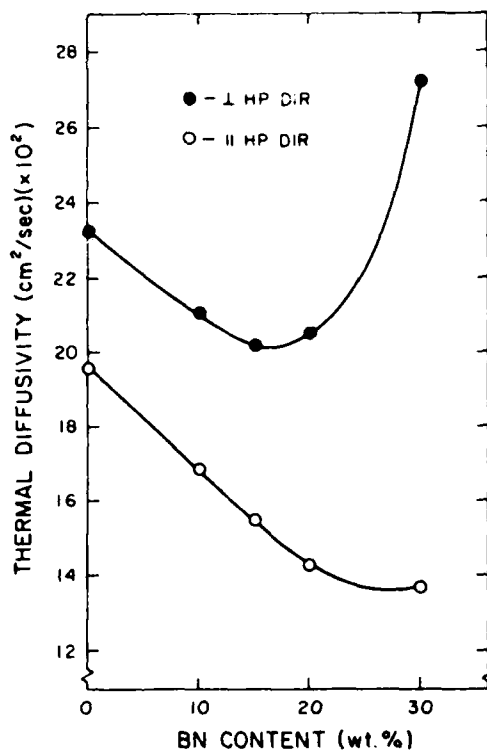


Fig. 2. Room temperature thermal diffusivity of Si_3N_4 -BN composites for two orientation relative to the hot-pressing direction.

THERMAL DIFFUSIVITY OF SILICON CARBIDE-SILICON COMPOSITES

M. Srinivasan, L. D. Bentsen, D. P. H. Hasselman

Carborundum Company, Niagara Falls, NY 14302 USA and
Virginia Polytechnic Institute and State University
Blacksburg, Virginia 24061, USA

ABSTRACT

The room temperature thermal diffusivity of silicon carbide-silicon composites was measured by the laser-flash method. The experimental results indicate that the thermal diffusivity and conductivity of these composites decreases strongly with increasing level of impurity content in both the silicon and the silicon carbide. This suggests that the heat transfer properties of these composites can be tailored by control over impurity levels.

INTRODUCTION

Increased efficiency of energy-conversion systems can be achieved by increasing their operating temperature levels. For this reason a demand has been created for engineering materials with mechanical properties and corrosion and oxidation resistance well in excess of those exhibited by super-alloys. Materials such as the refractory nitrides and carbides, in view of their chemical and structural stability at high temperature, appear to be excellent candidate materials for such applications as the all-ceramic turbine engine or internal combustion engine with retro-fitted ceramic components.

The in-service performance of these materials depends not only on their chemical and mechanical properties, but also on their thermal properties as well. These latter include the coefficient of thermal expansion and the thermal conductivity and diffusivity. Low values of the thermal conductivity lead to improved energy-conversion efficiencies since heat losses are kept to a minimum.

Due to their brittle nature, however, the above materials are highly susceptible to catastrophic failure due to thermal stresses of high magnitude which result from non-linear transient or steady-state temperature distributions. In order to minimize the possibility of this mode of failure, the optimum candidate materials should have values of the coefficient of thermal expansion as low as possible in combination with values of the thermal conductivity and thermal diffusivity as high as possible. This latter requirement is incompatible with the requirement of low thermal conductivity for high operating efficiency. Clearly, appropriate trade-offs must be made. The ability to make such trade-offs, in turn, requires quantitative information for the values of the thermal conductivity and thermal diffusivity and a detailed understanding of the materials and intrinsic variables which affect their values. In particular, such effects at higher levels of temperature are of considerable technical significance.

Heat transport through a material occurs primarily by phonon, photon or electron transport. The heat flux which results from these mechanisms depends strongly on the associated specific heat, the temperature, and the existence of structural and chemical imperfections such as vacancies, dislocations, grain boundaries, foreign atoms, optical discontinuities and any other factors which contribute to phonon, photon and electron scattering [1,2]. At the microstructural level, the conduction of heat is affected by the presence of pores, inclusions and cracks, grain boundary phases and preferred crystallographic orientation [2,3-9].

Many of the variables which affect the conduction of heat depend on processing history, which suggests that a measure of control can be exerted over the value of the thermal conductivity or thermal diffusivity of a material required for a given application. The purpose of this paper is to present experimental data for some of the variables that affect the heat conduction properties of silicon carbide-silicon composites which have demonstrated potential for ceramic turbine applications.

MATERIALS AND EXPERIMENTAL PROCEDURES

The SiC-Si composites were made by a warm molding process using an industrial grade silicon and silicon carbide powder made by the Acheson process. For two different series of samples, 400 and 1000 mesh size silicon carbide powders were used. A single sample was also prepared from 1200 mesh SiC powder. The silicon content of the composites was calculated from the measured density of the composites and values of the densities of silicon and silicon carbide of 2.33 and 3.21 g/cm³, respectively. For the composites made with the silicon carbide particle size of 400, 1000 and 1200 mesh, the final size of the silicon inclusions within the SiC

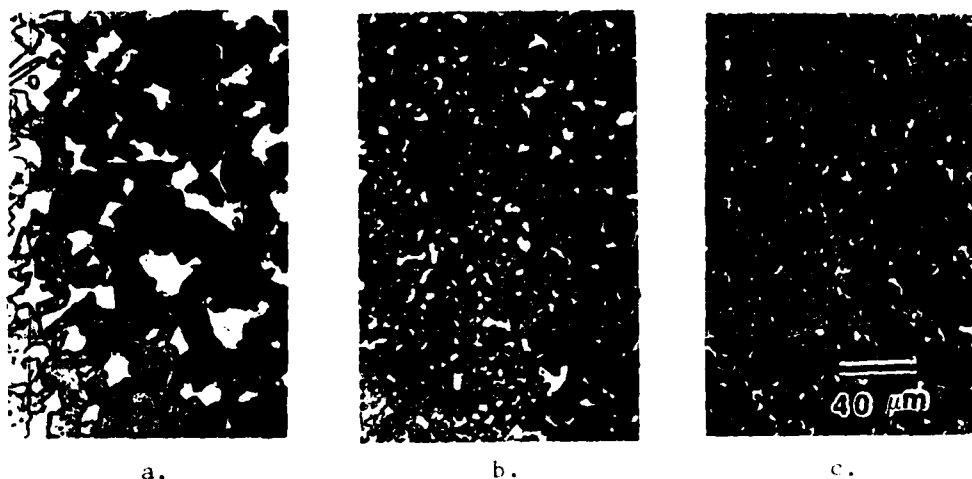


Fig. 1. Optical micrographs of silicon carbide-silicon composites with average Si particle size of a: 15 μm ; b: 5 μm and c: 4 μm .

matrix was approximately 15, 5 and 4 μm , respectively. Typical photo-micrographs are shown in Fig. 1.

For purposes of interpretation of the data additional samples included in the study consisted of dense sintered α -SiC, and a representative sample of the silicon metal used for the preparation of the SiC-Si composites. The principal impurities in this silicon metal as determined by spectro-chemical means are listed in Table 1. An additional sample consisted of zone-refined silicon of at least 99.99% purity.

TABLE 1. Principal Impurities in Industrial Grade Silicon Used For Preparation of Silicon Carbide-Silicon Composites

<u>ELEMENT</u>	<u>PERCENT</u>	<u>ELEMENT</u>	<u>PERCENT</u>
Boron	0.6	Titanium	0.004
Magnesium	0.001	Vanadium	0.001
Manganese	0.01	Copper	0.1
Iron	0.1	Chromium	0.002
Nickel	0.004	Calcium	0.06
Aluminum	0.01		

The heat conduction properties of the SiC-Si composites were determined by measurements of the thermal diffusivity by the laser-flash method [10], using a glass-Nd laser. The specimens of appropriate size and geometry were carbon-coated to prevent direct

transmission of the laser-beam. For measurements of the thermal diffusivity above room temperature, the specimens were held in a graphite resistance furnace containing a nitrogen atmosphere. At room temperature and up to about 500°C the transient temperature of the specimen was monitored with a liquid N₂ cooled InSb infrared detector. Above 500°C the specimen temperature was monitored with a Si-photodiode.

EXPERIMENTAL RESULTS AND DISCUSSION

Figures 2 and 3 show the dependence of the thermal diffusivity at room temperature on silicon content for the two series of silicon carbide-silicon composites with Si inclusion sizes of 15 and 5 μm , respectively. Table 2 lists the data for the thermal diffusivity at room temperature for the single specimens of single-phase α -SiC, the silicon used for the preparation of the specimens, the zone-refined silicon and the SiC-Si specimen with the 4 μm Si inclusions, which contained 20.82 vol.% Si. For the latter material, the thermal diffusivity was found to be independent of orientation.

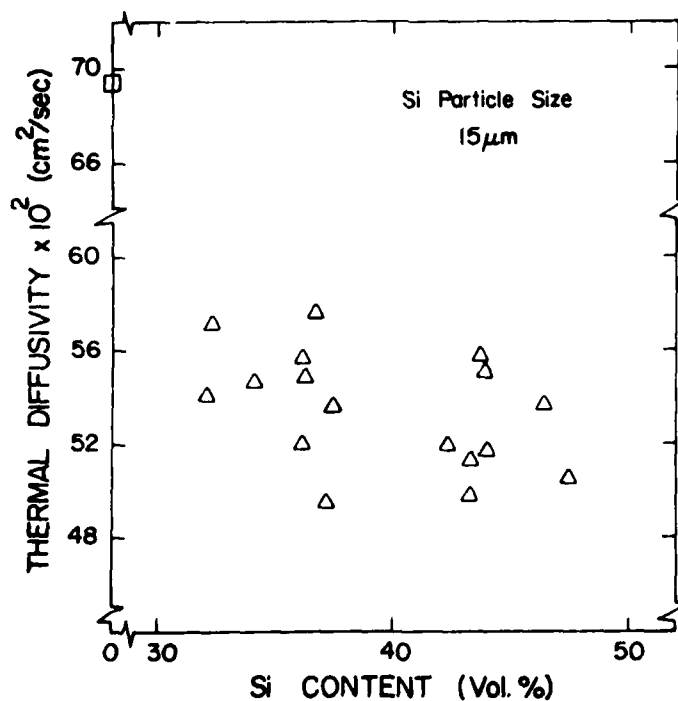


Fig. 2. Thermal diffusivity at room temperature of silicon carbide with 15 μm Si inclusions as a function of silicon content.

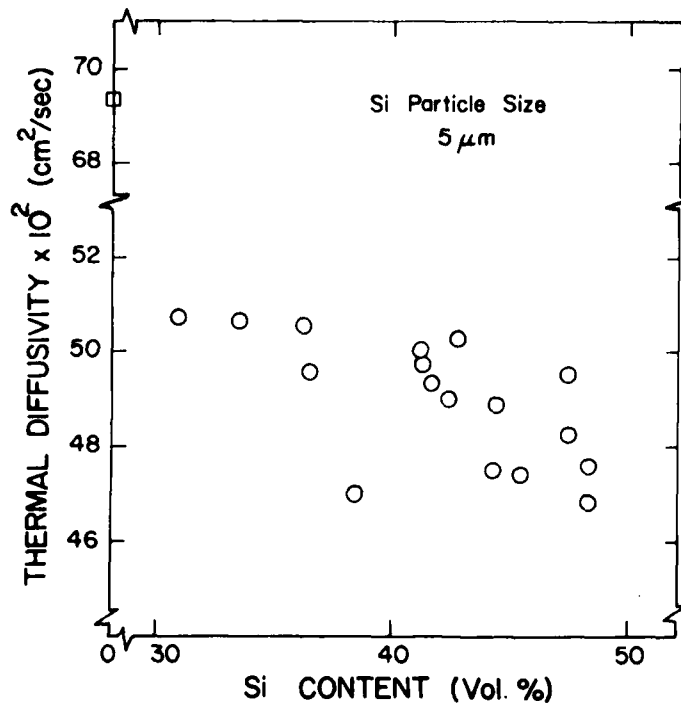


Fig. 3. Thermal diffusivity at room temperature of silicon carbide with 5 μm Si inclusions as a function of silicon content.

TABLE 2. Values for the Thermal Diffusivity at Room Temperature for Individual Samples of Silicon, SiC and SiC-Si Composites

<u>MATERIALS</u>	<u>THERMAL DIFFUSIVITY (cm²s⁻¹)</u>
Single Phase Silicon Carbide	0.694
Industrial Silicon	0.181
Zone-refined Silicon	0.668
SiC-Si composites (8 specimens)	0.774 ± 8%*

* Coefficient of variation.

Upon comparison with the value for the thermal diffusivity of the single-phase α-SiC and the inverse dependence of the thermal diffusivity on silicon content, the data shown in Figs. 2 and 3 indicate that the addition of the silicon dispersed phase to the

silicon carbide matrix results in a significant decrease in the thermal diffusivity. This is expected from the general theory of the thermal conductivity of composites, which shows that a dispersed phase with low thermal conductivity within a matrix of higher thermal conductivity will lead to a decrease in overall thermal diffusivity of the composite, regardless of the nature of the distribution of the dispersed phase [3-6]. The same conclusion applies to the thermal diffusivity of composites for components with comparable values of the specific heat per unit volume. This latter condition holds for the present samples with values for the thermal diffusivity of the silicon and silicon carbide of 0.181 and 0.694 cm^2s^{-1} , respectively. For this reason, the effect of silicon content on the thermal diffusivity shown in Figs. 2 and 3 is in general agreement with composite theory.

Comparison of the data shown in Figs. 2 and 3 shows that for a given silicon content, the thermal diffusivity is a function of the silicon particle size. Such an effect of inclusion size is not predicted by the theory of the thermal conductivity of composites, unless such a change in inclusion size is accompanied also by a corresponding change in the geometry or orientation of the inclusions. The photo-micrographs in Fig. 1 show no conclusive evidence for such a change in geometry or orientation. Also, such an effect of orientation should result in an anisotropy of the thermal diffusivity, which was not observed. If, however, the hypothesis that a change in Si inclusion size is accompanied by a change in particle geometry or orientation is correct, such differences at least qualitatively should be observed in the elastic properties of the composites as well. As shown in Fig. 4, no such effect is indicated by the data for Young's modulus [11] for all the specimens with values of thermal diffusivity shown in Figs. 2 and 3. This represents positive evidence that the apparent effect of the Si inclusion size on thermal diffusivity cannot be attributed to corresponding changes in inclusion geometry and/or orientation.

For an alternative explanation for this apparent effect of inclusion size it should be noted that generally, theories for the thermal conductivity of composites do not consider the effect of an interfacial resistance to heat flow. One possible source of such an interfacial barrier to heat flow is the difference in Young's modulus of the silicon and silicon carbide of a factor of three. The interface between the Si and SiC in these composites represents an elastic discontinuity which could contribute to increased phonon scattering. At room temperature such a discontinuity may affect the contribution to heat flow by low frequency phonons primarily. Such an effect is expected to be more pronounced for the smaller Si inclusions than for the larger ones, and may decrease the thermal diffusivity at room temperature by perhaps a fraction of a percent, but does not explain the average of 5 to 6 percent difference between the two sets of data shown in Figs. 2

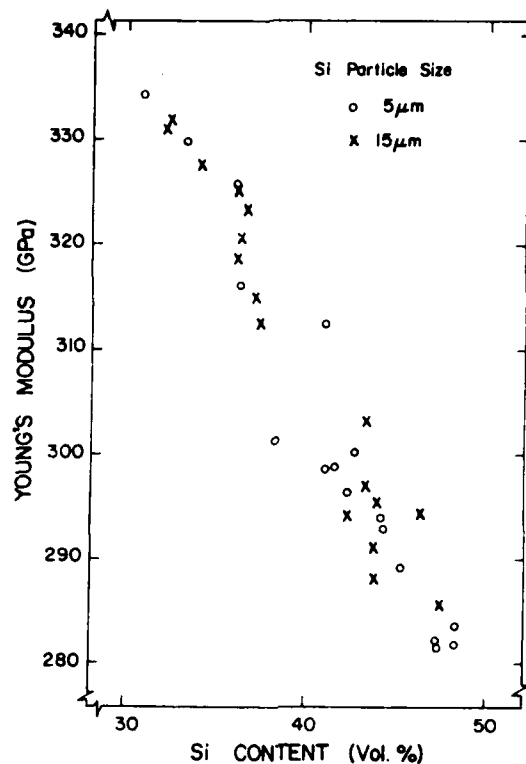


Fig. 4. Young's modulus of elasticity at room temperature for specimens of Figs. 2 and 3.

and 3.

The most likely explanation, albeit qualitative only at this time, is that the changes in Si inclusion size are accompanied by corresponding changes in the thermal diffusivity of the silicon and possibly the silicon carbide as well. Such changes in the thermal diffusivity can result from changes in impurity content. Proof for the validity of this hypothesis is offered by the large difference in the value of the thermal diffusivity of $0.668 \text{ cm}^2\text{s}^{-1}$ for the zone-refined Si and the corresponding value of $0.181 \text{ cm}^2\text{s}^{-1}$ for the silicon used for preparation of the composite specimens.

The value of $0.774 \text{ cm}^2\text{s}^{-1}$ for the thermal diffusivity of the sample with 20.82 vol.% Si with a particle size of $4 \mu\text{m}$ also is relevant to the above discussion. This value of thermal diffusivity is higher than the corresponding values of the sintered single-phase $\alpha\text{-SiC}$ as well as the zone-refined and industrial grade Si in the composites. This result contradicts composite theory, which

states that the highest value of the thermal conductivity of a composite is governed by the law of mixtures. The same holds for the thermal diffusivity of composites with components of comparable values for the specific heat per unit volume. If it is assumed that the thermal diffusivity of the silicon carbide in this sample is identical to the value for the single-phase silicon carbide, then the value for the thermal diffusivity of the Si, inferred from composite theory, would be far in excess of the value for the zone-refined Si. This does not seem likely. A more plausible explanation is that the thermal diffusivity of the SiC in this SiC-Si sample exceeds the value for the single phase silicon carbide. This latter material contains a higher level of foreign elements introduced as a sintering aid, which are absent in SiC-Si composites. It is speculated here that for high-purity silicon carbide, the value of the thermal diffusivity at room temperature may well approach $1 \text{ cm}^2\text{s}^{-1}$. Regardless of the actual value, it seems likely that impurities or added elements in both the silicon and silicon carbide can affect the heat conduction behavior of SiC-Si composites significantly.

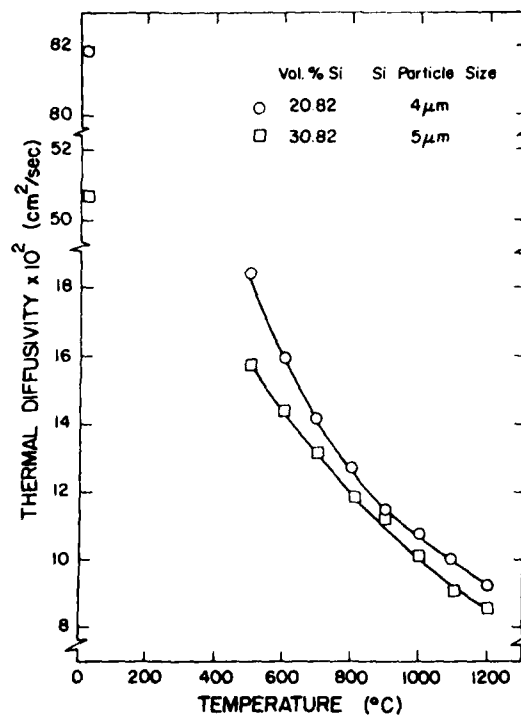


Fig. 5. Temperature dependence of the thermal diffusivity of two silicon carbide-silicon composites for two values of silicon content.

Figure 5 shows the temperature dependence of the thermal diffusivity of the sample with 20.82 vol.% of 4 μm Si inclusions and for one of the samples of Fig. 3. These data indicate that the relative difference in the thermal diffusivity decreases with increasing temperature.

Figure 6 compares the temperature dependence of the thermal diffusivity of two of the samples of Figs. 2 and 3 with comparable silicon content. These data are of interest in that they indicate that above 700°C the values for the thermal diffusivity are almost identical. It is suggested here that this effect may constitute evidence for an electronic contribution to the heat transfer by thermally activated holes and electrons, intrinsic as well as extrinsic due to the presence of the various impurities. In parti-

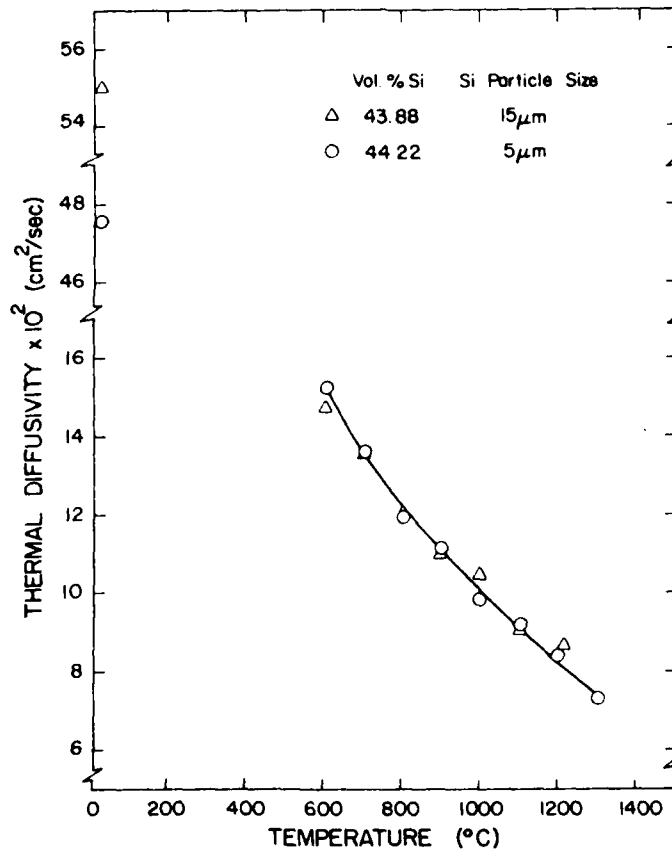


Fig. 6. Temperature dependence of thermal diffusivity of silicon carbide-silicon composites with comparable silicon contents and two different particle sizes.

cular, this would be the case for the sample with the lower value of the thermal diffusivity at room temperature, presumably because of its higher impurity content. Indeed if this hypothesis is correct, impurities in silicon or silicon carbide will lower the thermal diffusivity at low temperature, but may increase it again at higher temperatures if these impurities are of the type which affect the electrical conductivity. The higher boron content in the silicon in the present samples could especially be very effective in this respect.

Figure 7 shows the temperature dependence of the thermal diffusivity of the samples of zone-refined and industrial silicon. For these samples also, the relative difference in thermal diffusivity decreases with increasing temperature. Of interest is the irreversible increase in the thermal diffusivity of the industrial silicon following heating and cooling. This effect could arise from the formation of precipitates of impurities originally

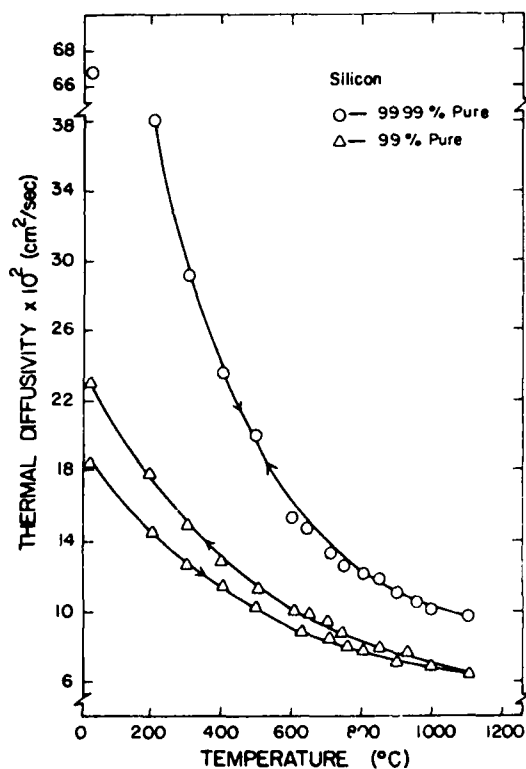


Fig. 7. Temperature dependence of the thermal diffusivity of an industrial grade and purified silicon.

in solid solution. No evidence was obtained in support of this hypothesis.

11

The experimental results obtained in this study indicate that the heat conduction properties of SiC-Si composites can be affected by a number of variables. The evidence presented indicates that impurities are particularly effective in this respect. Of particular significance is that such an effect would allow some degree of control over the desired thermal conductivity or thermal diffusivity of such composites. High impurity contents (in the absence of other adverse effects, of course) would be desirable to maximize thermal insulating properties. On the other hand, components or structures subject to thermal stress failure should be as pure as possible in order to obtain high thermal conductivity.

ACKNOWLEDGEMENT

The SiC-Si specimens investigated in this study were made by Carborundum Company, Niagara Falls, New York. The measurement of the thermal diffusivity and manuscript preparation were carried out at Virginia Polytechnic Institute and State University as part of a research program supported by the Office of Naval Research under contract: N00014-78-C-0431.

REFERENCES

1. R. Berman, Thermal Conductivity in Solids, Clarendon Press (1976).
2. W. D. Kingery, H. K. Bowen and D. R. Uhlman, Introduction to Ceramics, 2nd Ed., John Wiley, N.Y. (1975).
3. A. E. Powers, Conductivity in Aggregates, Knolls Atomic Power Laboratory, Report KAPL-2145, March 1961.
4. H. Fricke, Phys. Rev. 24 (1924) 575.
5. L. Raleigh, Phil. Mag. 34 (1892) 48.
6. J. C. Maxwell, A Treatise on Electricity and Magnetism, 3rd Ed., Oxford Univ. Press (1904).
7. D. P. H. Hasselman, J. Comp. Mat. 12 (1978) 403.
8. G. Ziegler and D. P. H. Hasselman, J. Mat. Sc. (in press).
9. G. Ziegler, L. D. Bentsen, D. P. H. Hasselman, Comm. Amer. Ceram. Soc. (in press).
10. W. J. Parker, R. J. Jenkins, C. P. Butler and G. L. Abbott, J. Appl. Phys., 32 (1961) 1679.
11. M. Srinivasan, M. Kasprzyk, Ceramic Bull. 58 (1979) 887.
12. D. P. H. Hasselman, J. Gebauer and J. A. Manson, J. Amer. Ceram. Soc., 55 (12) 588-91 (1972).

EFFECT OF MICROCRACKING ON THE CONDUCTION OF HEAT IN BRITTLE COMPOSITES

L. D. Bentsen and D. P. H. Hasselman
Virginia Polytechnic Institute and State University
Blacksburg, Virginia 24061 USA

and

N. Claussen
Max-Planck Institute
Stuttgart, Federal Republic of Germany

Abstract

The variables which affect the formation of micro-cracks due to thermal expansion mismatch in brittle composites and their effect on heat conduction properties are discussed. Experimental data for metal oxide-silicon carbide composites are presented which show that microcrack formation can lower the thermal diffusivity and conductivity significantly. Sub-critical growth and healing of the microcracks during thermal cycling are also shown to have an effect on heat transport. Evidence is presented that microcrack formation in brittle composites requires the presence of a residual pore phase.

Introduction

The conduction of heat through solids occurs primarily by phonon, electron or photon transport. Fundamentally, the heat flux by any of these transport mechanisms is governed by wave- and quantum-mechanical principles [Kittel (1962); Berman (1976); Kingery et al. (1976)]. The heat flux is affected also by any factor which contributes to phonon, electron or photon scattering. At the macro-structural level such scattering can occur at surfaces and interfaces. At the atomic level, the presence of vacancies, foreign atoms, dislocations, radiation damage, other phonons and/or electrons, absorption centers, any other structural or chemical imperfections, and elastic or optical discontinuities which promote phonon, electron or photon scattering tends to decrease the heat flux significantly.

At the microstructural level, heat conduction can be affected by grain boundaries, intergranular phases and the existence of texture.

Inclusions with heat conduction properties which differ from those of the matrix, coupled with the corresponding effect of their geometry and orientation, also can have a profound effect on the magnitude of heat flux.

Microcracks represent a particular type of microstructural imperfection. For purposes of this paper, microcracks are defined as cracks which are very small compared to the size of the sample or components in which they are contained. The effect of such microcracks on heat conduction properties will be the subject of the present paper, with special emphasis on microcracked brittle composites. Such materials are of current practical interest because of their excellent thermal shock resistance, improved fracture toughness, and machinability coupled with major decreases in elastic moduli. Most importantly, the presence of the microcracks changes the highly unstable failure mode typical for brittle materials to the far more desirable stable mode of crack propagation. These improvements in properties are critical for structural materials intended for use at high temperatures.

Microcracks represent barriers to phonon and electron transport and should have a significant effect on the heat conduction properties at levels of temperature at which radiation across the cracks is insignificant. The specific purpose of this paper is to discuss the variables which affect microcracking and their corresponding effect on thermal transport properties of brittle composites. Experimental data are presented in support of the findings obtained.

Analysis

Effect of Cracks on Thermal Conductivity

Equations for the effect of cracks on thermal conductivity were derived by Hasselman (1978) from the solutions of Fricke (1924) and Powers (1961) for the thermal conductivity of composites consisting of a continuous matrix with dilute dispersions in the shape of oblate ellipsoids of revolution as follows:

1. Randomly oriented cracks:

$$K = K_0 (1 + 8N\ell^3/9)^{-1} \quad (1)$$

where K and K_0 are the thermal conductivity of the microcracked and crack-free solids, respectively, N is the number of cracks per unit volume and ℓ is the crack radius.

2. Cracks oriented perpendicularly to the direction of heat flow:

$$K = K_0 (1 + 8N\ell^3/3)^{-1} \quad (2)$$

3. Cracks parallel to the heat flow:

$$K = K_0 \quad (3)$$

Comparison of eqs. 1, 2 and 3 shows that cracks oriented perpendicular to the heat flow are most effective in decreasing the thermal conductivity, followed by randomly oriented cracks and with no effect for cracks oriented parallel to the direction of heat flow.

Variables Which Affect Microcracking in Brittle Composites

A mismatch in the coefficients of thermal expansion of the individual components is the principal cause of microcrack formation in brittle composites. A thermal expansion mismatch results in the generation of internal stresses whenever the temperature of the composite is changed from the value at which such internal stresses are zero. This latter value normally corresponds to the manufacturing temperature. In brittle composites, such internal stresses can reach high magnitude because internal stress relief by plastic (i.e. dislocation) flow cannot occur. Stress relief could occur by diffusional processes, but only at high temperatures. For practical purposes, brittle composites exhibit elastic behavior with an internal stress magnitude directly proportional to the range of temperature over which the composite is cooled.

The internal stresses can lead to the generation of microcracks whenever their magnitude exceeds the fracture stress of either component or the cohesive strength of the interface between the components. It is generally recognized that microcracks are initiated from pre-existing flaws in the form of small pores or other crack-like defects within any of the components or at the interface. For this reason, an analysis of microcrack formation should be based on fracture-mechanical principles. In view of the generally non-uniform distribution of internal stresses which results from a thermal expansion mismatch, numerical techniques based on finite element methods are required (Evans and Clark, 1980). An exception to this is a spherical inclusion contained within an infinite matrix. For such an inclusion, the state of internal stress due to thermal expansion mismatch is uniform. By permitting microcrack formation within the inclusion only and treating the relevant properties affected by the microcracks as pseudo-continuum properties, analytical solutions, as shown by Niihara (1980), are easily obtained. From such solutions, the relevant variables which affect microcracking are easily assessed, as follows:

For a spherical inclusion, the total elastic energy (W_E) of the residual stress field in both the inclusion and matrix due to the mismatch in the coefficients of thermal expansion can be obtained from the solution of Davidge and Green (1968).

$$W_E = 2\pi(\Delta\alpha\Delta T)^2 R^3 / [(1-2\nu_p)/E_p + (1+\nu_m)/2E_m] \quad (4)$$

where $\Delta\alpha$ is the mismatch in the coefficients of thermal expansion of the inclusion and the matrix, ΔT is the temperature difference over which the composite is cooled from the value at which the internal stresses are zero (assuming linearly elastic behavior throughout), R is the radius

of the inclusion, ν is Poisson's ratio, E is Young's modulus and p and m refer to the inclusion and matrix, respectively.

For randomly oriented penny-shaped microcracks of equal size, Young's modulus of the inclusion can be expressed (Salganik, 1973):

$$E_p = E_o [1 + 16(1 - \nu_p^2)N\ell^3 / 9(1 - 2\nu_p)]^{-1} \quad (5)$$

where N is the number of microcracks per unit volume of inclusion and E_o is Young's modulus of the crack-free inclusion.

The creation of the microcracks within the inclusion, requires an expenditure of fracture energy (W_F):

$$W_F = 4\pi R^3 N \gamma_f \pi \ell^2 / 3 \quad (6)$$

where γ_f is the total energy dissipated in creating unit area of fracture surface.

Following the approach of Griffith (1924), crack instability occurs when:

$$d/d\ell(W_E - W_F) \geq 0 \quad (7)$$

which yields the critical value of temperature (ΔT_c) required for microcrack instability:

$$\Delta T_c = \left[\frac{\pi \gamma_f (1 - 2\nu_p)}{(\Delta \alpha)^2 E_o (1 - \nu_p^2)^2} \right]^{1/2} \ell^{-1/2} \left[\frac{E_o (1 + \nu_m)}{2E_m (1 - 2\nu_p)} + 1 + \frac{16(1 - \nu_p^2)N\ell^3}{9(1 - 2\nu_p)} \right] \quad (8)$$

Alternatively, eq. 1 can be rewritten in terms of the minimum size of precursor microcrack required for microcrack formation for a given value of ΔT .

Cracks can also propagate in a subcritical mode for $\gamma_s < \gamma < \gamma_f$, where γ_s is the thermodynamic surface free energy. The minimum value of ΔT required for subcritical crack propagation (ΔT_{sc}) can be obtained from eq. 8 by substitution of γ_s for γ_f . For values of $\Delta T < \Delta T_{sc}$ crack healing will occur. Of course, such subcritical crack growth and healing will take place only under environmental conditions and levels of temperature at which the appropriate reaction rates of diffusional processes are high enough.

Eq. 8 shows that the microcrack is unstable between a lower and upper value of crack length. This implies that once a microcrack is formed by propagation of a precursor flaw, it will arrest at the higher value of crack length. It should be recognized, however, that for small precursor

microcracks, at instability at $\Delta T = \Delta T_C$, the strain energy release rate exceeds the fracture surface energy. This causes the crack to propagate in an unstable mode. The crack will have maximum kinetic energy when it achieves the upper value of crack length for stable crack propagation. This will result in an "overshoot", with crack arrest following only at a value of crack length (l_f) when all the released potential energy is transformed into fracture surface energy which can be derived to be:

$$l_f = [3E_o(1+\nu_m)/16 E_m(1-\nu_p)N\ell_o]^{1/2} \quad (9)$$

Because of the "overshoot", a crack with length l_f will be subcritical with respect to the value of ΔT_C at which it formed from the precursor microcrack. Because of their subcritical nature, such microcracks may exhibit crack-healing, unless the temperature difference was raised to a value well in excess of ΔT_C .

Equations 8 and 9 for ΔT_C , ΔT_{SC} and l_f can be illustrated graphically. Unfortunately, because of the form of these equations this cannot be done in a convenient non-dimensional form, but requires the choice of a specific combination of inclusion and matrix.

For a MgO inclusion within a SiC matrix, Fig. 1 shows ΔT_C , ΔT_{SC} and l_f for an arbitrary value of crack density $N = 10^8 \text{cm}^{-3}$ and γ_f and γ_{sc} equal to 2 and 0.5J.m^{-2} , respectively. The other pertinent property data are listed in Table 1 given in the following chapter devoted to experimental data. In Fig. 1, the upper and lower solid curves correspond to ΔT_C and ΔT_{SC} for critical and subcritical crack propagation, respectively. The dotted curve represents the crack length (l_f) which results from unstable crack propagation given by eq. 9. The regions marked A, B and C represent regimes of values of ΔT and crack length in which

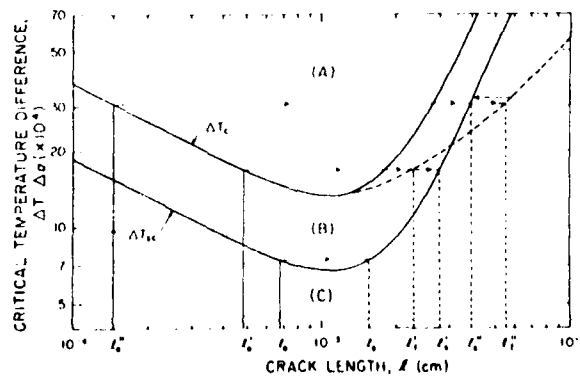


Fig. 1. Stability diagram of microcracks in MgO inclusion within SiC matrix.

the microcracks exhibit critical crack propagation, subcritical crack propagation, and crack healing, respectively. Included in Fig. 1 are paths of propagation of microcracks with three different initial sizes. The microcrack with initial size l_0 propagates entirely in a subcritical mode. For the initial size l_0' , the crack propagates in an unstable mode followed by subcritical crack growth. For a very short initial crack length, l_0'' the crack propagates in an unstable mode followed by crack healing. More complex paths, which combine both subcritical and critical crack propagation can occur as well, depending on the rate of temperature change and the presence or absence of a mechanism for subcritical crack growth.

It is important to conclude from the above derivation and discussion that a unique value of crack length is associated with each value of ΔT . For this reason any changes in ΔT will require a corresponding change in crack length. For this reason, it is expected that microcracked composites under non-isothermal conditions will exhibit time-dependent behavior of all properties affected by the presence of the microcracks.

As a final remark, it should be noted, as mentioned earlier, that a precursor such as a pore at a triple-point or grain boundary is required for microcrack formation. For this reason, it is anticipated that the amount of residual pore phase due to lack of complete densification may play a vital role in affecting the microcrack density and resulting heat conduction properties. Experimental evidence for this effect will be presented.

In summary then the above discussion indicates that the extent of microcracking in brittle composites is governed by the thermal expansion mismatch and the elastic properties of the components, the amount of pore phase, the level of temperature, and any time-dependent subcritical crack growth and healing.

The Thermal Conductivity of Microcracked Composites

Many expressions are available from the literature for the thermal conductivity of composites for many types of distributions of the individual components within the composites.

For a matrix with dilute concentrations of spherical dispersions the thermal conductivity (K_c) can be expressed, (Raleigh, 1892; Maxwell, 1904):

$$K_c = K_m \left[\frac{2K_m + K_p - 2V_p(K_m - K_p)}{2K_m + K_p + V_p(K_m - K_p)} \right] \quad (10)$$

where K is the thermal conductivity, V_p is the volume fraction of dispersed phase and the subscripts m and p refer to the matrix and dispersed phase, respectively.

The effect of microcracking in either the matrix or dispersed phase or both on the thermal conductivity of the composite can be accounted for by the appropriate substitution of eq. 1 in the case of randomly oriented microcracks for K_m and K_p in eq. 10.

In general, as decided by the direction of the thermal expansion mismatch, microcrack formation will occur in either the matrix or the dispersed phase. For this reason, the composite thermal conductivity as expressed by eq. 10 will be governed by changes in K_p or K_m only. An expression for the thermal conductivity of a dispersed phase with randomly oriented microcracks can be obtained readily by substitution of the value of Nb^3 obtained from eqs. 8 or 9 into eq. 1, which in turn, upon substitution into eq. 10 yields the value for the thermal conductivity of the composite. This should result in a reasonably reliable estimate.

Microcracking in the matrix occurs in the immediate vicinity of the inclusions. For this reason, the simultaneous effect of the inclusions on the thermal conductivity of the composite and the associated microcracking in the matrix are expected to be coupled. Therefore, a simple substitution of the value of the thermal conductivity of the microcracked matrix phase for K_m in eq. 10, possibly may not yield quantitatively reliable results. An analysis of such a coupling effect could be of interest to the reader of this paper.

In general, the above analysis and discussion shows that the thermal conductivity of microcracked brittle composites is expected to be a function of the volume fraction, thermal expansion, and elastic behavior of the individual components as well as their crack propagation characteristics including critical and time-dependent subcritical propagation as well as crack healing. The purpose of this paper is to present experimental data which illustrate a number of these effects.

Materials and Experimental Procedures

The composite materials for this study consisted of continuous matrices of aluminum oxide, beryllium oxide and magnesium oxide containing a range of volume fractions of a dispersed phase of silicon carbide. The SiC particle size was of the order of a few microns. These composites were prepared by vacuum-hot-pressing mixtures of the appropriate powders at temperatures and over time periods required to achieve nearly full densification. Samples for the BeO-SiC and MgO-SiC composites were obtained from a commercial source.* The Al₂O₃-SiC composites were made in the laboratory of one of the present writers.[§] Table 1 lists the approximate values for the coefficients of thermal expansion and elastic properties of the four individual components. The direction of the mismatch in the coefficients of expansion of the matrix and dispersed SiC

*Ceradyne Corporation, Santa Ana, California.

§Max-Planck Institute, Stuttgart, FRG.

phase is such that on cooling from the hot-pressing temperature, microcrack formation is expected to occur within the oxide matrix. Scanning electron micrography revealed that such microcracking occurred primarily by inter-granular fracture.

Table 1 Approximate Property Values for Components of Silicon Carbide-Metal Oxide Composites

Property	SiC	Al ₂ O ₃	BeO	MgO
Coefficient of thermal expansion °C ⁻¹ (x10 ⁶)	5	7	10	13
Young's modulus (10 ⁵ MPa)	4.5	4.1	3.0	3.0
Poisson's ratio	0.18	0.26	0.34	0.30

The heat conduction behavior of the composites was established by measuring their thermal diffusivity by the laser-flash method [Parker, et al., 1961] using specimens cut to the appropriate geometry and dimensions. Details of the equipment were described earlier [Siebeneck, et al., 1976]. Since microcracking has a negligible effect on the heat capacity per unit volume, the data for the thermal diffusivity closely reflect the corresponding behavior of the thermal conductivity.

Experimental Results and Discussion

Figure 2 shows the experimental data for the thermal diffusivity at room temperature for the Al₂O₃-SiC composites. All samples for these data were in the as-received condition and were subjected to cooling from the hot-pressing temperature only, without any additional heating or cooling. Included in Fig. 2 is the dependence of the thermal diffusivity on silicon carbide content for the crack-free composites calculated from the theory for the thermal conductivity of composites given by eq. 10 and the corresponding changes in density and specific heat. It can be noted that the experimental data fall far below those calculated for the crack-free material. The relative deviation increases with increasing SiC content, as expected, since the microcrack density is expected to be proportional to the number of SiC particles per unit volume. The data also indicate that for this composite system, microcracking reduces the thermal diffusivity (and therefore the thermal conductivity) by as much as a factor of two.

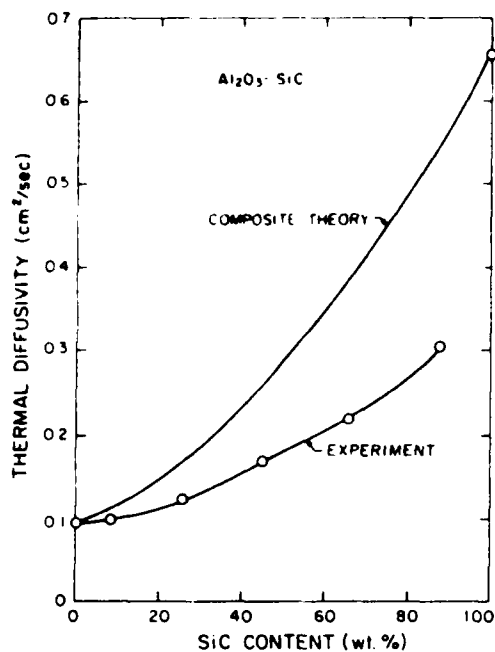


Fig. 2. Thermal diffusivity of Al₂O₃-SiC composites.

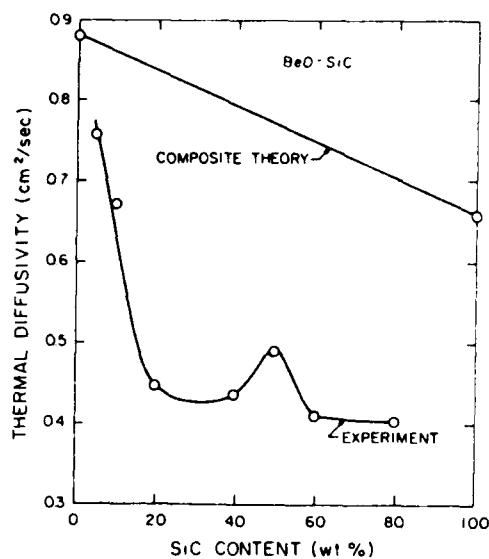


Fig. 3. Thermal diffusivity of BeO-SiC composites.

Figure 3 shows the data for the thermal diffusivity of the BeO-SiC samples. The specimens for these measurements as for the Al₂O₃-SiC data, were in the as-received condition. These data indicate that the thermal diffusivity does not decrease linearly with SiC content, as indicated by an increase in the thermal diffusivity at 50 wt.% SiC. A similar but much greater increase was observed also in a previous study [Singh, et al, 1981] which suggested a near complete suppression of micro-crack formation near 50 wt.% SiC. It is of interest to point out that experimental data for the fracture toughness and strength of BeO-SiC composites, obtained by others [Rubin, 1979], show a similar suppression of micro-cracking near 50% SiC. Near 20 and 80% SiC, toughness and strength exhibit maxima due to microcrack toughening, whereas no such toughening appears to exist near 50% SiC. These independent observations indicate that they are not spurious and confirm that the decrease in the thermal diffusivity observed in the present study indeed are caused by micro-cracking.

The observations on the MgO-SiC composites also were informative in this respect. Figure 4 shows the thermal diffusivity as a function of SiC content for a set of samples, designated Set I, investigated earlier. Figure 5 shows the thermal diffusivity of MgO-SiC composites, designated Set II, obtained more recently. For this latter set the data shown represent the average for 5 samples at a given SiC content.

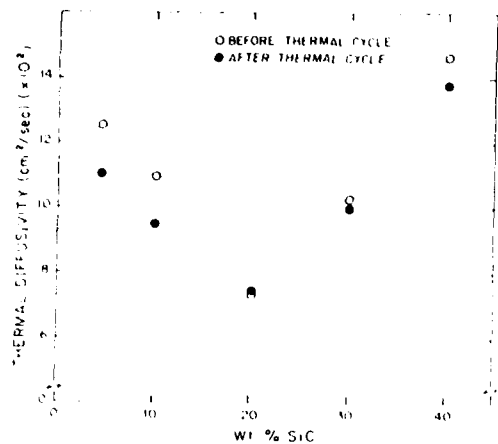


Fig. 4. Thermal diffusivity of set I of MgO-SiC composites.

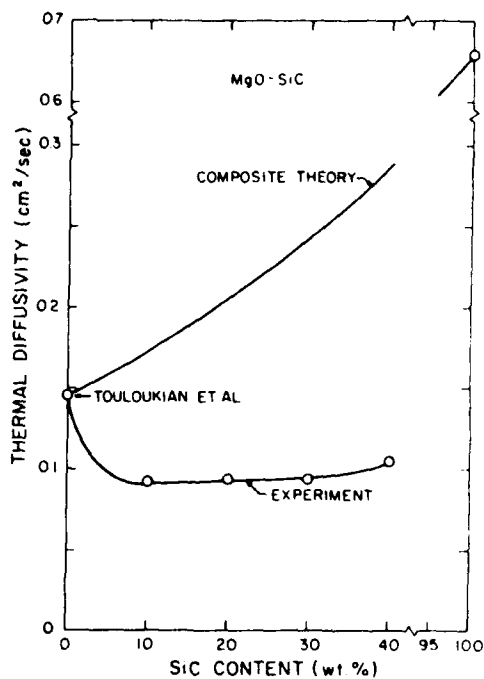


Fig. 5. Thermal diffusivity of set II of MgO-SiC composites.

Comparison of the data in Fig. 4 labelled "before thermal cycle" (i. e. immediately after cooling from the processing temperature) with those in Fig. 5, indicates that for the MgO-SiC samples considerable differences in thermal diffusivity can exist even at the same SiC content. Comparing the data for all three types of composites shows that the largest relative reductions are observed for the MgO-SiC series. This is expected, since for this composite system, the mismatch in coefficients of thermal expansion is higher than for the other two series. Comparison of all four sets of data shows that the dependence of the thermal diffusivity on silicon carbide content differs not only quantitatively but also qualitatively from composite series to series. The suppression of microcracking at the intermediate values of SiC content was attributed previously to differences in the nature of the distribution of the components within the composite at low, high and intermediate contents of silicon carbide [Singh, 1981]. Such differences not only give rise to differences in the magnitude of the internal stress, but also affect the probability of microcrack formation.

Such effects undoubtedly are still operative. However, with the accumulation of additional data for the other composite series an additional explanation can be given, based on differences in residual pore content from sample to sample, which also accounts for the qualitative differences between the different composite and sample series.

Evidence for the validity of this hypothesis is presented in Figs.

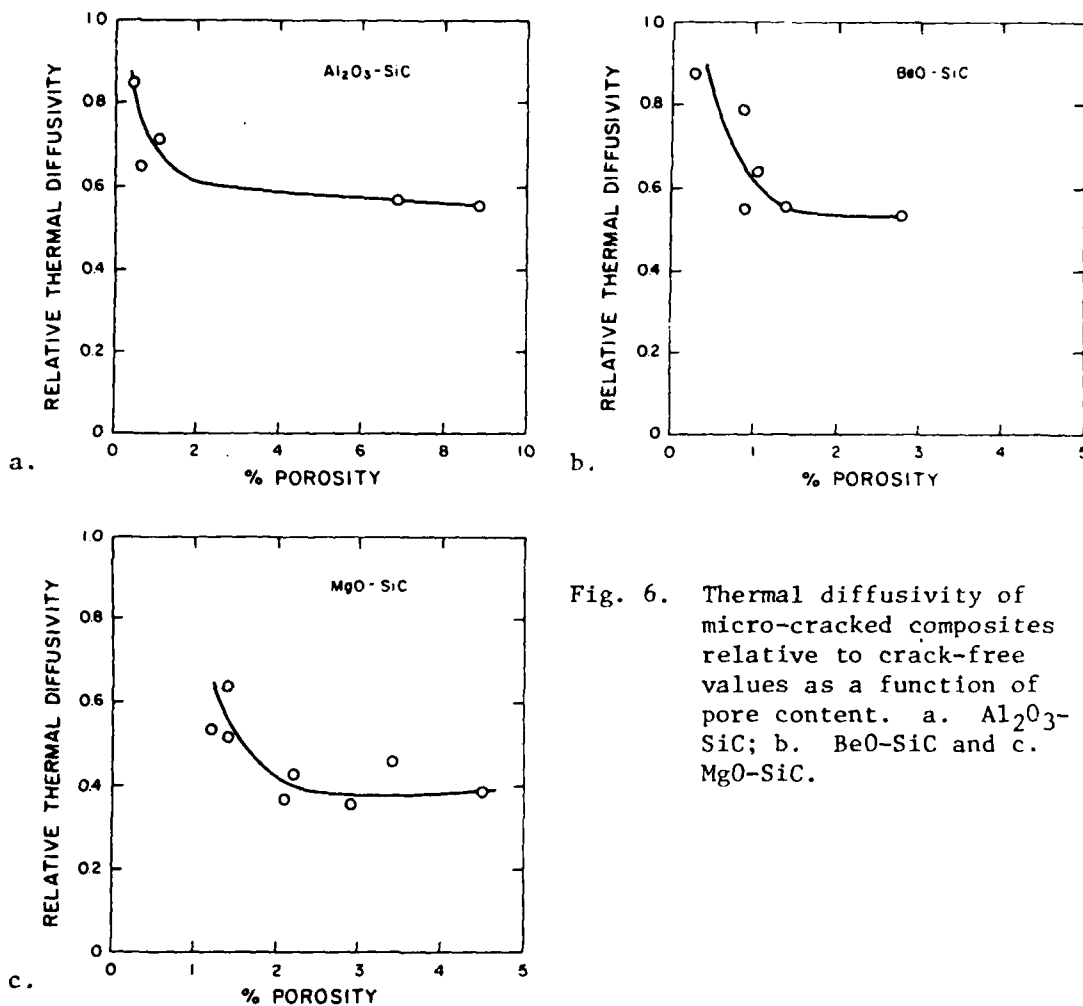


Fig. 6. Thermal diffusivity of micro-cracked composites relative to crack-free values as a function of pore content. a. $\text{Al}_2\text{O}_3\text{-SiC}$; b. BeO-SiC and c. MgO-SiC .

6a, b and c which show the value of the thermal diffusivity of the Al_2O_3 , BeO and MgO -based composites, respectively, relative to the crack-free value plotted as a function of pore content. It can be noted that for all three series the relative thermal diffusivity, albeit with some scatter, decreases very rapidly with increasing pore content. In interpreting this effect, it should be noted that this inverse correlation between thermal diffusivity and pore content cannot be regarded as a direct cause and effect. Any decrease in density due to the presence of the microcracks is less than a fraction of one percent. For this reason the values of pore content shown in Fig. 6 reflect the lack of complete densification during the hot-pressing operation. The resulting residual pore phase can be regarded as a special case of spherical inclusions with zero thermal conductivity. For such a dispersed phase, eq. 10 shows that at low volume fractions, each percent of pore content reduces the thermal conductivity by about 1.5%. The specific heat per unit volume also is reduced by a fractional amount equal to the fractional pore volume. These two effects combined result in a net decrease in the

thermal diffusivity of 0.5% for each percent of pore phase. This value is less than the observed decreases shown in Figs. 6a, b and c by well in excess of an order of magnitude.

It is suggested that the data shown in Fig. 6 constitute evidence for the existence for pore-assisted microcrack formation. As discussed earlier, for microcrack precursors in the form of pores at triple points or grain-boundaries which are too small, microcracks will not form regardless of the magnitude of internal stress. For such small pores, the corresponding composites will exhibit near theoretical density and values of thermal diffusivity near the value for the crack-free material. For a given number of pores per unit volume, an increase in pore content is accompanied by an increase in pore size. This in turn, would promote microcrack formation and a corresponding decrease in thermal diffusivity, as observed. It is expected that for a given number of pores per unit volume, some minimum ("threshold") value of pore content would be required before microcracks can be generated. Unfortunately, the number of data points shown in Fig. 6 is insufficient to unequivocally demonstrate the existence of such "threshold" pore content. The finding of such a "threshold" value also is expected to be complicated by the usual existence of a pore-size distribution. It should be noted also that the effect of pore phase on the microcracking and the thermal diffusivity for these composites is coupled with the content of silicon carbide, which itself may lead to an increase in pore content due to the increasing degree of difficulty of densification. The role of the pore phase on microcracking can be ascertained in more quantitative detail for specimens of constant SiC content. These specimens are being obtained with results to be presented in a future report.

Regardless of the quantitative details, the data in Fig. 6 indicate that by careful control over pore content achieved by corresponding control over processing conditions, the properties of composites affected by the presence of microcracks may be tailored to specific values required for specific engineering applications.

Heat treatments, in addition to the cooling from the hot-pressing temperature, also have a significant effect on the thermal diffusivity. Experimental evidence for this effect is shown in Fig. 4 which shows data for the thermal diffusivity before and after a thermal cycle to 1400°C over a time period of approximately 8 hours. Comparison of the data shows that this thermal cycle resulted in a general decrease in the thermal diffusivity. Previously, samples of MgO + 20 wt.% SiC held at 1300°C for 0, 3 and 10 hours showed decreases in the thermal diffusivity on return to room temperature of 8.1, 11.3 and 15.4%, respectively. These observations are thought to constitute evidence of the subcritical growth of microcrack precursors which were not of sufficient size to result in microcracks during the initial cooling from the hot-pressing temperature. The additional decrease in the thermal diffusivity following thermal cycles is the result of additional microcrack formation. The above also clearly indicated, as discussed earlier, that microcracked materials are non-equilibrium materials. In fact, it can be said that microcracks can be super-cooled.

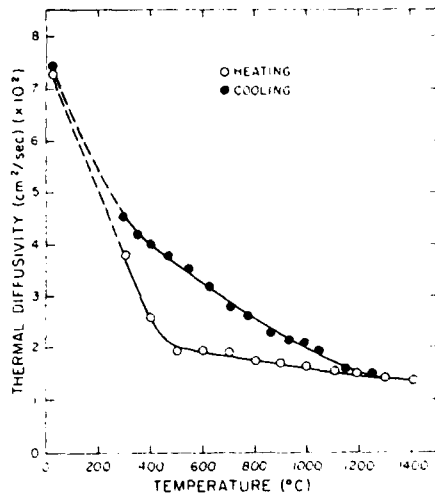


Fig. 7. Effect of thermal cycling on thermal diffusivity of MgO + 20 wt.% SiC.

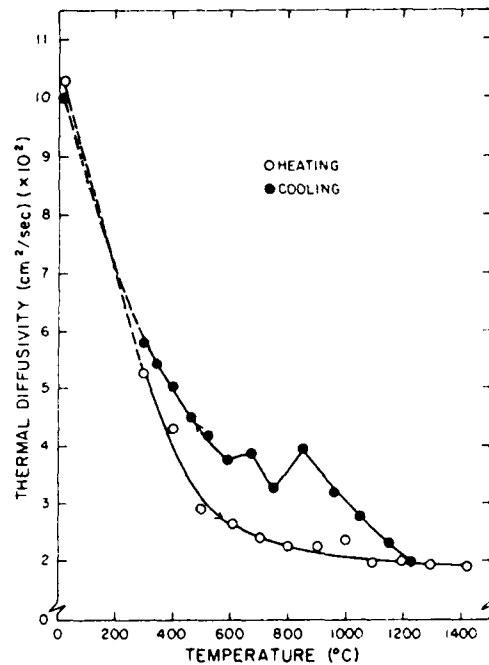


Fig. 8. Effect of thermal cycling on thermal diffusivity of MgO + 30 wt.% SiC.

Evidence for crack healing was also found. Figure 7 shows the experimental data for the thermal diffusivity of a specimen of MgO + 20% SiC during heating and cooling and holding for 3 hours at 1300°C. It may be noted that at the higher temperatures on cooling, the values for the thermal diffusivity are in excess of those observed during heat-up. It is thought that this effect arises from the healing of microcracks which formed during the initial cooling. On return to room temperature however the thermal diffusivity after the thermal cycle and hold is now less than before. This, as discussed earlier, is evidence for additional microcrack formation due to growth of precursors initially too small. It appears then that the changes in the thermal diffusivity on thermal cycling can be affected by the simultaneous healing of microcracks and growth of their precursors.

Figure 8 shows additional evidence for this effect occurring in a sample of MgO + 30% SiC cycled to 1400°C over a period of some 8 hrs. These data show clear evidence of pop-in of microcracks once the composite is cooled over a temperature range such that the stresses become sufficiently large that either healed microcracks can regenerate or that precursor cracks have reached sufficient size to form new microcracks.

Regardless of the underlying details, the data presented in this paper clearly indicate that the properties of microcracked materials are

not "hand-book values", but are strong functions of past processing and thermal history. The existence of such variations must be recognized in the applications of such materials for engineering purposes.

Acknowledgments

The present study was conducted as a cooperative research effort funded by the Office of Naval Research under contract N00014-78-C-0431 and by the Deutsche Forschungs Gemeinschaft.

References

- Berman, R. (1976), Thermal Conduction in Solids, Clarendon Press, Oxford.
- Evans, A. G. and Clarke, D. R. (1980) in Thermal Stresses in Severe Environments, Plenum Press, N.Y., pp. 629-48.
- Fricke, H. (1924), Phys. Rev. 24, 575.
- Green, T. J. (1978), J. Mat. Sc., 3, p. 629.
- Griffith, A. A. (1924), Proc. First Int. Congr. Appl. Mech., Delft, The Netherlands, pp. 55-63.
- Hasselmann, D. P. H. (1978), J. Comp. Mat. 12, pp. 403-07.
- Kingery, D. W., Bowen, H. K., Uhlmann, D. R. (1976), Introduction to Ceramics, 2nd Ed. John Wiley, N.Y., p. 613-14.
- Kittel, C. (1962), Introduction to Solid State Physics, John Wiley, N.Y.
- Maxwell, J. C. (1904), A Treatise on Electricity and Magnetism, 3rd Ed. Oxford Univ. Press.
- Niihara, K., Singh, J. P., Bentsen, L. D., Hasselman, D. P. H. (1981), Proc. of Conf. on Interfaces in Ceramic and Metal-Ceramic Systems, Berkeley, Calif., in press.
- Parker, W. J., Jenkins, R. J. Butler, C. P., Abbott, G. L. (1961), J. Appl. Phys., 32, pp. 1679-84.
- Powers, A. E. (1961), Conductivity in Aggregates, Knolls Atomic Power Laboratory, Report KAPL -2145, Schenectady, N.Y.
- Rayleigh, L. (1892), Phil. Mag. 35, p. 48.
- Salganik, R. L. (1973), Izv. Akad. Nauk SSR Mekh. Tverd. Tela 8, pp. 149-58.
- Siebeneck, H. J., Cleveland, J. J., Hasselman, D. P. H., Bradt, R. C. (1976), J. Amer. Ceram. Soc., 59, pp. 241-44.
- Singh, J. P., Hasselman, D. P. H., Su, W. M., Rubin, J. A. and Palicka, R. (1981), J. Mat. Sc., 16, pp. 141-150.

CHAPTER IX

DETERMINATION OF THE THERMAL CONDUCTIVITY
AND DIFFUSIVITY OF THIN FIBERS BY
THE COMPOSITE METHOD

J. J. Brennan,^{*} L. D. Bentsen[†] and D. P. H. Hasselman[†]

^{*}United Technologies Research Center
East-Hartford, Conn. 06108

[†]Department of Materials Engineering
Virginia Polytechnic Institute and State University
Blacksburg, Va. 24061

DETERMINATION OF THE THERMAL CONDUCTIVITY AND
DIFFUSIVITY OF THIN FIBERS BY THE COMPOSITE METHOD

J. J. BRENNAN, L. D. BENTSEN, D. P. H. HASSELMAN

United Technologies Research Center
East-Hartford, CT 06108 USA

Department of Materials Engineering
Virginia Polytechnic Institute and
State University
Blacksburg, VA 24061

ABSTRACT

It is suggested that the thermal conductivity of very fine fibers can be evaluated indirectly with the aid of composite theory using the experimental data for the heat transport properties of an appropriate composite which contains the fibers. The feasibility of this approach was investigated by determining the thermal conductivity and diffusivity of fibers of amorphous silicon carbide from 25°C to 1000°C contained within a lithium aluminosilicate glass-ceramic using the laser-flash technique for measurement of the thermal diffusivity of the composite. Due to the amorphous nature of the fibers, their values for the thermal conductivity and diffusivity were found to be far less than the corresponding data for crystalline silicon carbide. The positive temperature dependence of the thermal conductivity coupled with the independent observation of an increase in thermal conductivity with specimen thickness suggests that radiative heat transfer makes a significant contribution to the total heat transferred. A number of advantages and limitations of the composite method for the evaluation of thermal transport properties of fibers are discussed.

1. INTRODUCTION

The technical and scientific need for quantitative data for the heat conduction properties of solids has led to the development of nearly innumerable methods for the measurement of these properties [1]. For a given material the choice of the most appropriate method depends on a number of variables such as the temperature range over which the data are required and the configuration of the material to be measured. In this respect, micron-sized fibers present special difficulties.

Materials in fiber form are used extensively in the development of mechanically reinforced composites. One such composite developed during the last few years consists of a glass or glass-ceramic reinforced with fibers of silicon carbide [2]. The mechanical properties of these composites indicate excellent service performance at elevated temperature. For a micro-mechanical analysis of these composites under conditions of transient heat flow, experimental data for the thermal conductivity and diffusivity were required as a function of temperature. The choice of the method for the measurement of these properties presented a number of difficulties. Firstly, their method of preparation precluded the synthesis of larger samples with properties identical to those of the fibers. For this reason, only the fibers themselves had to be used. Secondly, the silicon carbide fibers were not electrical conductors. This eliminated the resistive heating method [3] for measuring the thermal conductivity. Although, in principle, a number of techniques could be devised, it was decided to measure the thermal conductivity and diffusivity of these fibers by an indirect method. This method consisted of measuring the thermal diffusivity of the composite as well as the matrix (without fibers), followed by calculation of the required data by means of the theory for the thermal conductivity of composites. It is the purpose of

this paper to report the data obtained.

2. EXPERIMENTAL

2.1 Materials

The silicon carbide fibers made from an organometallic polymer by the method of Yajima [4] were obtained from a commercial source.* Chemical analysis showed the fibers to consist of approximately 65% SiC, 25% SiO₂ and about 10% C. The fibers were in the form of tows of yarn containing ~500 fibers per tow. The average fiber diameter was approximately 10 μm and the density was approximately 2.55 g/cm³. X-ray analysis showed the fibers to be amorphous with a crystallite size of 25-30 Å determined from peak broadening.

The matrix material with density of 2.52 g/cm³ consisted of a lithium aluminosilicate glass-ceramic essentially identical to that of a commercial glass-ceramic[†] except that the ~3 wt.% TiO₂ nucleating agent was replaced by ~2 wt.% ZrO₂ due to reactivity between the TiO₂ and the SiC fibers.

The composite was manufactured by passing the SiC yarn through a slurry of powder of the uncrystallized glass and isopropyl alcohol. Following drying, the coated yarn was cut to fit the graphite die for hot-pressing in vacuum for times of 5 min. to 1 hr. at 1400 to 1500°C and a pressure of 14 MPa. Following hot-pressing, crystallization of the glass was carried out by heat treating for 1 to 2 hr at a temperature ranging from 880 to 1100°C. Composite samples were made in which the fibers were all parallel or with alternate layers oriented at 90°. Figure 1 shows a photomicrograph of such a 0/90 cross-ply composite. A sample of the matrix phase without fibers was also prepared as well.

* Nippon Carbon Company, Japan

† C-9608, Corning Glass Works

2.2 Measurement of the Thermal Properties

The thermal diffusivity of the composite and matrix samples was measured by the laser flash method [5] using a Nd-glass laser. The specimens used for these measurements were cut from the hot-pressed blanks, and were in the form of square plates 9-12 mm on the side by about 2 mm thick. Direct transmission of the laser beam was prevented by coating the specimen surfaces with carbon. The transient temperature response of the specimen rear surface was monitored by optical means. For measurements above room temperature the specimens were held in an appropriate holder contained within a carbon resistance furnace with nitrogen atmosphere. In the evaluation of the thermal diffusivity from the transient temperature response, the corrections for heat loss were taken into account using the analysis given by Heckman [6]. Changes in specimen thickness with temperature due to thermal expansion were taken into account as well.

The specific heat of the fibers and the glass-ceramic matrix was determined by differential scanning calorimetry using appropriate equipment.*

2.3 Evaluation of the Thermal Conductivity and Diffusivity of the Fibers From Composite Theory

For heat flow parallel to uniaxially aligned fibers, the thermal conductivity (K_c) of a composite is:

$$K_c = K_m V_m + K_p V_p \quad (1)$$

where K is the thermal conductivity, V is the volume fraction and the subscripts c , m and p , refer to the composite, matrix and fibers, respectively.

* Dupont 990 Thermal Analyzer.

For heat flow perpendicular to the fiber direction, the thermal conductivity as derived by Bruggeman [7] can be written:

$$\left(\frac{K_m - K_c}{K_m + K_c} \right) V_m = \left(\frac{K_c - K_p}{K_c + K_p} \right) V_p \quad (2)$$

From the measured value of the thermal diffusivity, the corresponding value of the thermal conductivity (K) can be calculated from:

$$K = \kappa \rho c \quad (3)$$

where κ is the thermal diffusivity, ρ is density and c is the specific heat. The specific heat of the composite can be calculated from the measured values for the specific heat of the fibers and the matrix by means of the rule of mixtures. Substitution of the values for the thermal conductivity of the matrix and the composite into Eqs. 1 or 2 permits calculations of the thermal conductivity of the fibers. The thermal diffusivity may then be determined using Eq. 3.

3. EXPERIMENTAL RESULTS

Figure 2 shows the experimental data for the specific heat as a function of temperature for the glass-ceramic matrix and the silicon carbide fibers. The data for the glass-ceramic agree very well with those obtained by the manufacture of a glass-ceramic of similar composition [8]. The specific heat of the silicon carbide fibers significantly exceeds the corresponding values for crystalline silicon carbide [9]. This difference most likely can be attributed to the non-crystalline nature of the fibers, since large relative differences in the specific heat of amorphous and crystalline polymers are also observed [10].

Table 1 lists the experimental data for the thermal diffusivity at room temperature for a number of composite samples of different thickness with a range of volume fractions and both fiber orientations. Also included in Table 1 are the values for the room temperature thermal conductivity and thermal diffusivity of the fibers calculated from the data for the specific heat, density and thermal diffusivity.

Figure 3 shows the experimental data for the temperature dependence of the thermal diffusivity of the glass-ceramic matrix and two composite samples containing 49 vol.% SiC with heat flow parallel and perpendicular to the fibers. The data for the LAS matrix show reasonable agreement with data obtained earlier [11] for a sample of a similar glass-ceramic (C9608) supplied by the manufacturer.

Figure 4 shows the values for the thermal conductivity and thermal diffusivity of the silicon carbide fibers parallel and perpendicular to the fiber axis calculated from the experimental data given in Figs. 2 and 3.

4. DISCUSSION

The values of the thermal conductivity and thermal diffusivity of the silicon carbide fibers are far below the corresponding values of crystalline silicon carbide [12,13]. The low values for the present fibers are most likely the result of their amorphous nature which limits the contribution of the phonon conductivity.

The relatively small negative temperature dependence of the thermal diffusivity and the positive temperature dependence of the thermal conductivity of the fibers is an indication that a significant fraction of the total heat conducted occurs by radiative heat transfer. Additional independent support for the latter conclusion is also provided by the observations shown in Table 1, that the thermal diffusivity of the composite samples with the SiC fibers increases with increasing specimen thickness in accordance with theoretical expectations [14]. Assuming that at room temperature the radiation contribution

is negligible, the data shown in Fig. 4 suggest that at 1000°C the radiation contribution is in excess of half of the total heat transferred. This suggests that although no supporting experimental data appear to be available, these SiC fibers possibly are excellent transmitters of infra-red radiation of relatively long wavelength.

The thermal diffusivity and conductivity perpendicular to the fiber axis is somewhat less than parallel to the fiber axis. Possibly, this could be attributed in part to a structural anisotropy within the fiber resulting from its original organic structure. No such preferred orientation, however, was detected by Yajima et al [4]. Possibly also, an interfacial contact resistance due to a lack of perfect adhesion or the factor 2-3 thermal expansion mismatch between the glass-ceramic matrix and fibers could be responsible for this effect. This would manifest itself as an apparent decrease of the thermal conductivity perpendicular to the fiber axis, because Eq. 3 does not take such an interfacial resistance into account. Such an interfacial resistance would have a much smaller (if any) effect for heat flow parallel to the fiber axes. For this reason the evaluation of fiber conductivity by the composite method preferably should rely on experimental data using uniaxially aligned composite samples with heat flow parallel to the fiber length.

Some general remarks are in order on the general feasibility of the "composite method" for obtaining heat conduction data for fibers. It is critical to note that this method relies on the theory for the thermal conductivity of composites. Generally, such theory is exact only for dilute concentrations of the second phase. At higher volume fractions, at which the local temperature fields around the dispersions will interact, composite theory must be considered to be an approximation only. Any deviations between

composite values calculated from such approximations and actual values increase with the relative difference in the values of the thermal conductivity of the individual phases. For this reason, increased accuracy of the value for the thermal conductivity of fibers obtained by the "composite method" can be achieved by choosing a matrix material with a value of the thermal conductivity as close as possible to that of the fibers. This condition is met for the composites of this study. For the same reason, the choice of the composite equation used to calculate the thermal conductivity of the SiC fibers is not critical.

Furthermore, for the "composite method" to yield reliable data for the heat transport properties of the fibers, it is essential that the scale of the microstructure and the size of the sample of the composite is such that, in its transient response, the sample, in effect, behaves as a continuum. Criteria for this condition were examined by Kerrisk [15,16], Lee and Taylor [17], and Nomura and Chou [18]. For the samples used in the present study, these criteria were met.

In summary, it is proposed that the thermal conductivity of fibers can be obtained from the corresponding data for composites by means of the theory for the thermal conductivity of composites. The data presented indicate the feasibility of this method.

ACKNOWLEDGMENTS

The present study was supported by the Office of Naval Research under contracts N00014-78-C-0431 and N00014-78-C-0503.

REFERENCES

1. Y. S. Touloukian, R. W. Powell, C. Y. Ho, and P. G. Klemens, Thermal Conductivity - Nonmetallic Solids (IFI/Plenum, New York - Washington, 1970), pp. 13a-25a.
2. K. M. Prewo and J. J. Brennan, *J. Mat. Sci.* 15, 463 (1980).
3. Y. S. Touloukian, R. W. Powell, C. Y. Ho, and P. G. Klemens, Thermal Conductivity - Nonmetallic Solids (IFI/Plenum, New York - Washington, 1970), pp. 19a-22a.
4. S. Yajima, K. Okamura, J. Hayashi, and M. Omori, *J. Am. Ceram. Soc.* 59, 324 (1976).
5. W. J. Parker, R. J. Jenkins, C. P. Butler, and G. L. Abbott, *J. Appl. Phys.* 32, 1679 (1961).
6. R. C. Heckman, *J. Appl. Phys.* 44, 1455 (1973).
7. D. A. G. Bruggeman, *Annalen Physik*, 24 636 (1935).
8. Materials Handbook, Corning Glass Works, 1961.
9. Y. S. Touloukian and E. H. Buyco, Specific Heat-Nonmetallic Solids (IFI/Plenum, New York - Washington, 1970), pp. 448-450.
10. R. A. V. Raff and K. W. Doak, Ed., Crystalline Olefin Polymers, Part II (Wiley, New York, 1964), p. 216.
11. D. P. H. Hasselman, unpublished data.
12. Y. S. Touloukian, R. W. Powell, C. Y. Ho, and P. G. Klemens, Thermal Conductivity - Nonmetallic Solids (IFI/Plenum, New York - Washington, 1970), pp. 585-588.
13. Y. S. Touloukian, R. W. Powell, C. Y. Ho, and M. C. Nicolaou, Thermal Diffusivity (IFI/Plenum, New York - Washington, 1973) pp. 447-478.
14. W. D. Kingery, H. K. Bowen and D. R. Uhlmann, Introduction to Ceramics, 2nd Ed., (Wiley, New York, 1976), pp. 627-634.

15. J. F. Kerrisk, J. Appl. Phys. 42, 267 (1971).
16. J. F. Kerrisk, J. Appl. Phys. 43, 112 (1972).
17. T. Y. R. Lee and R. E. Taylor, J. Heat Trans. 100, 720 (1978).
18. S. Nomura and T. W. Chou, J. Composite Materials 14, 120 (1980).

TABLE 1. Thermal Diffusivity at Room Temperature of LAS-SiC Composites With
A Range of Sample Thickness and SiC Content and Calculated Values For The

Thermal Diffusivity and Conductivity of the SiC Fibers

SiC Content (Vol. %)	Measured Values for Composites		Calculated Values for SiC Fibers		
	Orientation of Fibers w.r.t Direction of Heat Flow	Thickness (mm)	Thermal Diffusivity ($\times 10^{-5}$ cm ² /sec)	Thermal Diffusivity ($\times 10^{-5}$ cm ² /sec)	Thermal Conductivity (W/m.K)
48	⊥	1.020	722	642	1.10
48	⊥	1.520	824	845	1.44
48	⊥	2.250	837	873	1.49
48	//	1.050	744	669	1.14
48	//	1.540	818	831	1.42
48	//	2.130	828	854	1.46
48	//	2.690	826	848	1.45
48	//	2.785	849	899	1.53
45	⊥	0.975	735	653	1.12
45	⊥	1.485	806	803	1.37
45	⊥	2.275	855	915	1.56
38	⊥	1.235	710	587	1.17
38	⊥	1.245	753	685	1.00
32	⊥	1.305	739	624	1.07

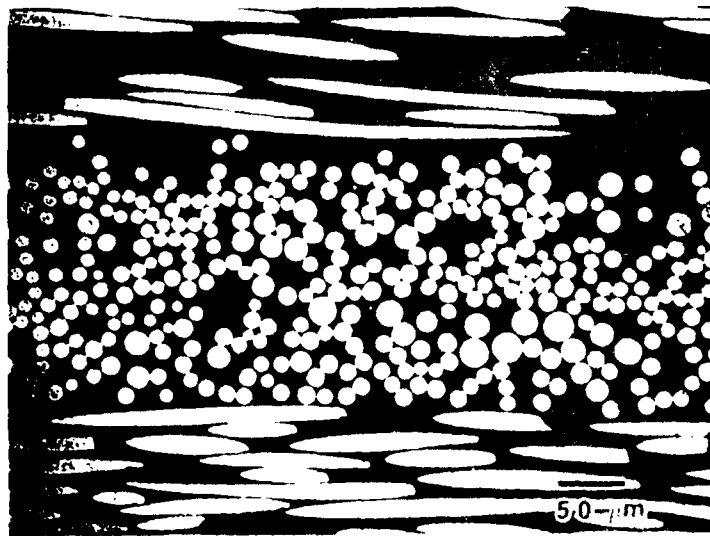


Fig. 1. Optical micrograph of 0.90° composite of lithium-alumino-silicate glass ceramic with 50 vol. % amorphous silicon carbide fibers.

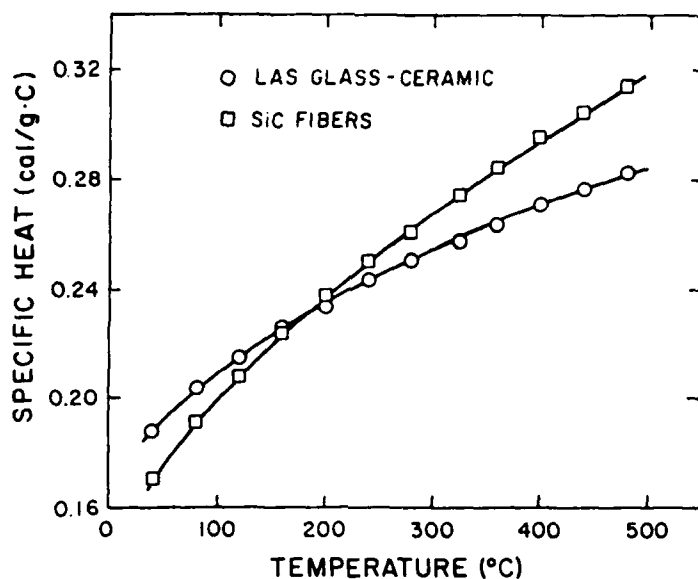


Fig. 2. Specific heat of lithium-alumino-silicate glass-ceramic and of amorphous silicon carbide fibers.

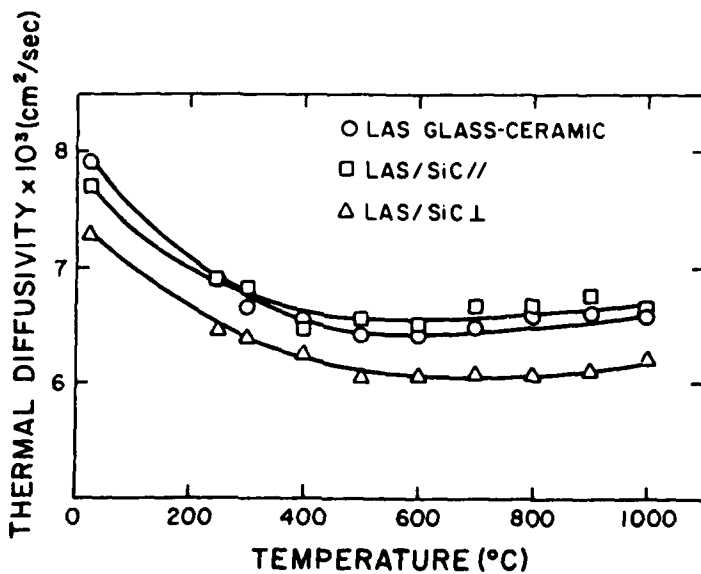


Fig. 3. Experimental data for the thermal diffusivity as a function of temperature for lithium-alumino-silicate glass-ceramic matrix with 0, 48 and 49 vol. % SiC fibers for specimen thicknesses of 1.32, 1.29 and 1.29 mm, parallel and perpendicular to the fiber axis, respectively.

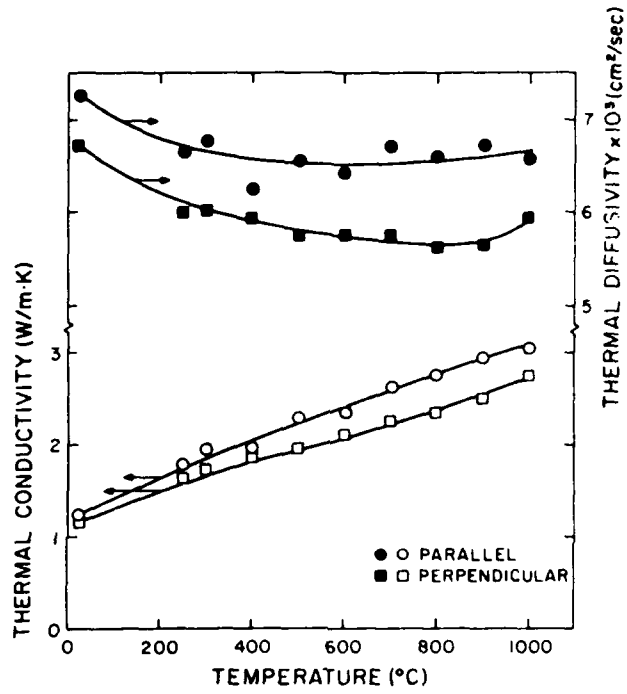


Fig. 4. Temperature dependence of the thermal conductivity and diffusivity of amorphous silicon carbide fibers calculated from the composite data shown in Fig. 3.

CHAPTER X

THERMAL STRESS IN MATERIALS HEATED INTERNALLY BY RADIATION ABSORPTION

J. R. Thomas, Jr., J. P. Singh, and D. P. H. Hasselman

Department of Mechanical Engineering
and Materials Engineering
Virginia Polytechnic Institute and State University
Blacksburg, Virginia 24061

Analysis and results are reported for thermal stress in materials heated internally by radiation absorption. Two modes of heating are considered: radiation suddenly applied from one side and held constant thereafter, and radiation incident from one side but having a periodic variation in time.

In both cases it is found that the radiation absorption coefficient plays a large role in determining the thermal stress, and conclusions are drawn concerning desirable optical thicknesses. With periodic heating, the stress can cycle between tensile and compressive values. This phenomenon could be especially significant for materials prone to cyclic fatigue failure.

1. INTRODUCTION

Structural materials for fusion reactors will be subjected to rather unusual conditions of transient heating, depending on their location and exposure. In many cases the heating will result from an incident surface heat flux or from the absorption of nuclear radiation, which generates heat internally. The heat source will almost certainly be of a pulsed nature, so thermal cycling can be expected. Many of the materials being considered for these applications^{1,2} include brittle materials, such as high temperature ceramics, which are susceptible to catastrophic failure when subjected to transient thermal stresses. Previous studies^{3,4} of thermal stresses in such situations have limited consideration to heating in the form of incident surface heat flux. The present authors and coworkers have recently been studying thermal stresses in materials generated by internal absorption of radiation.⁵ These investigations have yielded results of importance to several applications, such as partially transparent materials used in solar receivers, and aerospace structures or components such as radomes and IR-windows.

In the present paper, we wish to highlight some of the results of our previous work which appear to be of significance in fusion materials considerations, and to report some more recent results for pulsed heating which should have more direct application to fusion reactor materials. The broad objective of the work has been to understand the role of the various physical properties which affect the nature and the magnitude of thermal stress, in order to encourage intelligent design and materials selection. For this reason we have considered only plate geometry so that solutions for the transient temperature and thermal stress distributions may be obtained explicitly by

analytical means. These analytical solutions often reveal the importance of the various material properties with greater clarity than would numerical solutions for complicated geometries.

2. SUDDENLY APPLIED RADIATION

In order to provide background for understanding our results for a periodic heat source, we would like first to review some previous results. We have considered thermal stresses arising from heating by normally incident radiation arriving on either side of a flat plate of thickness $2a$, which is cooled on one side by convection. The radiation begins suddenly at time $t = 0$ and is held constant thereafter. The radiation is attenuated exponentially as it passes through the plate, and leads to a volumetric heat source which is mathematically described as

$$u(x) = u_0 e^{-\lambda(x+a)}, \quad t > 0, \quad (1)$$

for radiation incident from the left. Here $u(x)$ is the energy generation rate per unit volume at location x , measured from the centerline, and λ is the linear attenuation coefficient. For an absorbing material with surface reflectance r_p ,

$$u_0 = (1 - r_p) q_0,$$

where q_0 is the incident radiation flux. For convenience we set $\lambda = 1 - r_p$.

To determine the resulting thermal stress, we solved the heat conduction equation

$$\frac{\partial^2 T}{\partial x^2}(x,t) + \frac{\partial T}{\partial t} = \frac{1}{\alpha} \frac{\partial u}{\partial t}(x,t) \quad (2)$$

where $T(x,t)$ is the temperature at location x at time t , k the thermal conductivity and κ the thermal diffusivity. The general solution of Eq. (2) was required to satisfy boundary conditions appropriate to the cooling mechanism. For convective cooling on the right, the conditions are

$$\frac{\partial T}{\partial x}(-a,t) = 0 \quad (3)$$

and

$$-k \frac{\partial T}{\partial x}(a,t) = h [T(a,t) - T_\infty], \quad (4)$$

where h is the convective film coefficient and T_∞ is the fluid temperature. Also required is an initial condition, which we chose for simplicity as

$$T(x,0) = T_\infty. \quad (5)$$

Once $T(x,t)$ was determined, an expression for the thermal stress distribution was developed from the equation

$$\begin{aligned} \sigma_{y,z} = & \frac{\alpha E}{1-\nu} [-T(x,t) + \frac{1}{2a} \int_{-a}^a T(\xi,t) d\xi \\ & + \frac{3x}{2a} \int_{-a}^a T(\xi,t) \xi d\xi], \quad (6) \end{aligned}$$

where α is the coefficient of thermal expansion, E is Young's modulus, and ν is Poisson's ratio. The detailed expression is given in Ref. 7 and will not be repeated here.

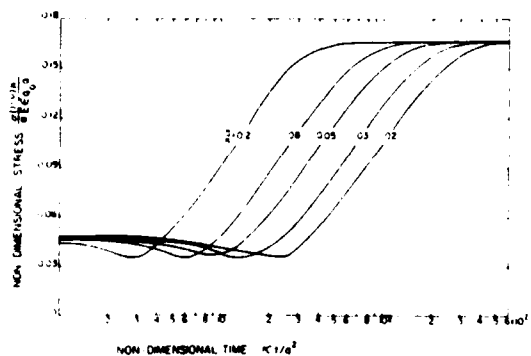


Figure 1. Time dependence of Maximum tensile stress in a partially absorbing flat plate with $2\alpha a = 3$, $\kappa = 0.3 \text{ W/cm}^2\text{C}$, and $a = 1 \text{ cm}$.

In Figure 1 we show the maximum tensile thermal stress, for the case described above, as a

function of time for various values of h . Note that as steady state is approached, the maximum stress becomes independent of h , whereas for intermediate times, the stress is roughly proportional to h . The stress distribution for $t = \infty$ is shown in Figure 2 for various values of optical half-thickness $2\alpha a$. Here it is seen that the stress is tensile at either face, and compressive near the center. The largest stress occurs at the hotter face, a somewhat unexpected result which is discussed more thoroughly in Ref. 7. It is also apparent that the stress is largest for $2\alpha a = 2.0$.

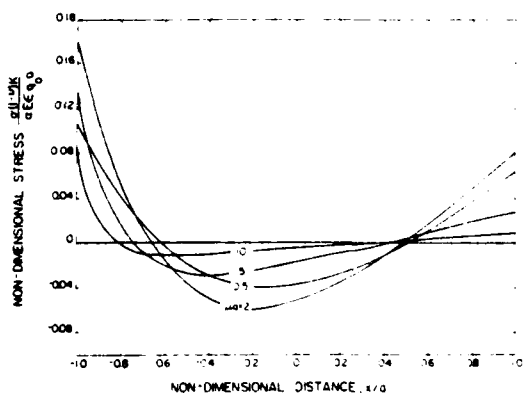


Figure 2. Spatial distribution of steady state ($t = \infty$) thermal stresses for various values of $2\alpha a$ in a partially absorbing flat plate with $k = 0.3 \text{ W/cm}^2\text{C}$ and $a = 1 \text{ cm}$.

For very small values of h , the plate is effectively insulated. Since no heat is removed the temperature increases indefinitely, but soon achieves a time-invariant profile. In Figure 3 we show the stress distribution for this case for various values of $2\alpha a$. Note that the stress profile is reversed, as compared to that shown in Figure 2 for finite h . Note also that the largest stresses now occur for $2\alpha a = 1.0$ instead of $2\alpha a = 2.0$.

The implications of these results for the selection of materials may be summarized as follows: for non-zero film coefficient h , intermediate values of optical thickness, i.e., $2\alpha a = 4.0$, should be avoided; $2\alpha a = 0$ or $2\alpha a = \infty$ yield greatly reduced thermal stress. The fact that the maximum tensile stress occurs at the hotter surface could be of considerable importance for environmental conditions which promote fatigue by stress corrosion or similar mechanisms.

These results were obtained for a suddenly applied radiation field which remains constant after time $t = 0$. We now treat in more detail the case of an oscillating source of radiation which should be more representative of fusion reactor applications.

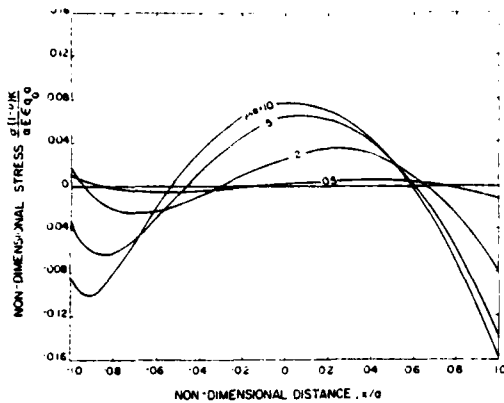


Figure 3. Spatial distribution of steady state ($t = \infty$) thermal stresses for various values of αa , $h = 0$, $k = 0.3 \text{ W/cm}^\circ\text{C}$, and $a = 1 \text{ cm}$.

3. OSCILLATING RADIATION SOURCE

3.1 Analysis

We consider a slab as before, but subjected to radiation from the left which oscillates in time with frequency ω . We thus seek the solution of Eq. (2) subject to the same boundary and initial conditions (3-5), but with a heat source

$$u(x) = u_0 e^{-\mu(x+a)} [1 + \epsilon \sin(\omega t)]. \quad (7)$$

Here $\epsilon < 1$ is the amplitude of the oscillation in the heat generation rate, and all other symbols are as previously defined. We find the solution by standard techniques¹ to be

$$T(x,t) = T_\infty + \sum_{n=1}^{\infty} B_n(t) \cos(\lambda_n x), \quad (8)$$

where

$$B_n(t) = \frac{G_n e^{-\lambda_n a}}{\lambda_n^2 + (\lambda_n^2/n)^2} \left[e^{-\lambda_n^2 t/n} \cos(\lambda_n t + \frac{\lambda_n^2}{n} \sin \omega t) \right] + \frac{G_n}{\lambda_n^2} (1 - e^{-\lambda_n^2 t/n}). \quad (9a)$$

with

$$G_n = \frac{u_0}{cN_n} \frac{e^{-2\lambda_n a} (\frac{h}{k} - \lambda_n) \cos(2\lambda_n a) + \lambda_n}{\lambda_n^2 + \frac{\lambda_n^2}{n}}, \quad (9b)$$

$$N_n = \frac{1}{2\lambda_n} \{ \sin(2\lambda_n a) \cos(2\lambda_n a) + 2\lambda_n a \}, \quad (9c)$$

and where the eigenvalues are the solution of the transcendental equation

$$\lambda_n \tan(2\lambda_n a) = \frac{h}{k}.$$

In Eq. (9b), ρ and c are the density and heat capacity of the material, respectively. The temperature distribution (8), when substituted into Eq. (6), yields an explicit expression for the thermal stress distribution. The result is identical to that given in Ref. 7 with $B_n(t)$ given by Eqs. (9) above, and thus will not be repeated here.

3.2 Discussion

The temperature distribution given by Eqs. (8) and (9) is very similar to that found for suddenly applied radiation, except that a sinusoidal variation is superimposed on the time variation. The amplitude of this oscillation is greatest in the front face of the plate ($x = -a$) of course, and there is a phase shift between the temperature oscillations at the front and back face. This difference in amplitude can be seen in Figure 4, where the envelope of the temperature oscillation is plotted in nondimensional form at long times - i.e. near steady-state conditions. This phase shift is reflected in the thermal stress distribution which is shown as a function of time in nondimensional form in Figure 5. This plot was also constructed to show the long-time behavior when near steady-state conditions prevail. Although the amplitude of the stress oscillation is nearly the same at the front face as in the center, at the center the oscillation is between tensile and compressive values, whereas the stress in the front face remains tensile throughout the oscillation. Of potentially greatest importance is the large swing in the stress on the rear face, which also oscillates between tension and compression. Materials prone to cyclic fatigue failure are thus more likely to fail at the back face of the plate which is in contact with the cooling medium.

It is recognized that the operating cycle of a fusion reactor will likely consist of flat-topped pulses separated by somewhat longer downtimes, and is thus not accurately modeled by a sinusoidal variation. However the purpose of the present study was to investigate the effects of periodically applied radiation in the simplest possible mathematical format. Future studies will consider more realistic radiation-source operating cycles.

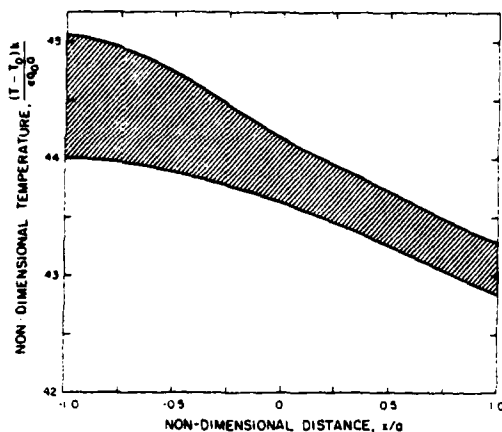


Figure 4. Envelope of the non-dimensional temperature oscillation; $\mu a = 3.0$, $h = 0.006$ $W/cm^2\text{-}^\circ C$.

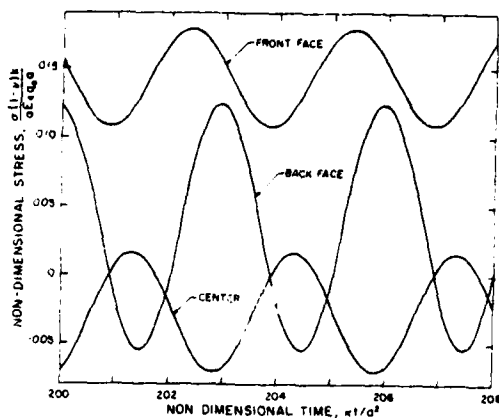


Figure 5. Time dependence of the thermal stress; $\mu a = 3.0$, $h = 0.006$ $W/cm^2\text{-}^\circ C$.

4. SUMMARY AND CONCLUSIONS

Thermal stresses in materials absorbing nuclear radiation may be studied by first solving the heat conduction equation with the appropriate heat source term, boundary and initial conditions. The resulting expression for the time-dependent temperature profile is then used in Eq. (6) to derive an explicit expression for the thermal stress as a function of position and time.

For stresses resulting from suddenly applied radiation on the left side of a slab cooled on

the right, the maximum steady-state stress occurs on the side facing the radiation source. In addition to the usual dependence on E , μ , λ , thickness a , and thermal diffusivity α , the magnitude of the stresses is rather strongly dependent on the absorption coefficient, with intermediate values of the optical thickness producing greater stresses. Stresses resulting from an oscillating radiation source also have an oscillatory character, with the maximum swing at the rear face where the plate is cooled. Both near the center and at the rear face the stresses oscillate between tension and compression, which could have important implications for materials in which fatigue failure is a problem.

ACKNOWLEDGEMENT

This work was supported in part by the Office of Naval Research under contract N00014-74-C-09431.

REFERENCES

- [1] Clinard, F. W., Jr., Ceramics for Applications in Fusion Systems, *J. Nucl. Mater.* 85 & 86 (1979) 393-404.
- [2] Trantina, G. G., Ceramics for Fusion Reactors-Design Methodology and Analysis, *J. Nucl. Mater.* 85 & 86 (1979) 415-420.
- [3] Hasselman, D. P. H., Thermal Shock by Radiation Heating, *J. Amer. Ceram. Soc.* 46 (1963) 229-234.
- [4] McKelvey, T. E., Koniges, A. E., Marcus, F., Sabado, M., and Smith, K., Proceedings 8th Symposium Engineering Problems of Fusion Research II (1979) 1827-1831.
- [5] Hasselman, D. P. H., Thomas, J. R., Kamat, M. P., and Satyamurthy, K., Thermal Stress Analysis of Partially Absorbing Brittle Ceramics Subjected to Radiation Heating, *J. Amer. Ceram. Soc.* 63 (1980) 21-23.
- [6] Singh, J. P., Thomas, J. R., Jr., and Hasselman, D. P. H., Thermal Stresses in Partially Absorbing Flat Plate Symmetrically Heated by Thermal Radiation and Cooled by Convection, *J. Thermal Stresses*, 3 (1950) 341-49.
- [7] Thomas, J. R., Jr., Singh, J. P., and Hasselman, D. P. H., Analysis of Thermal Stress Resistance of Partially Absorbing Ceramic Plate Subjected to Asymmetric Radiation, II: Convective Cooling at Rear Surface, *J. Amer. Ceram. Soc.* 64 (1981), 163-169.
- [8] Singh, J. P., Satyamurthy, K., Thomas, J. R., and Hasselman, D. P. H., Analysis of Thermal Stress Resistance of Partially Absorbing Ceramics: Three-dimensional

Asymmetric Radiation II: Convective
Cooling at Front Surface, J. Amer. Ceram.
Soc. 64 (1981), 169-173.

- [9] Rust, James H., Nuclear Power Plant
Engineering (Haralson Publ. Co., Buchanan,
GA 1979).
- [10] Boley, B. A. and Weiner, J. H., Theory of
Thermal Stresses (John Wiley and Sons, New
York, 1960).
- [11] Arpaci, V. S., Conduction Heat Transfer,
(Addison-Wesley, Reading, MA, 1966).

December 1981

BASIC DISTRIBUTION LIST

Technical and Summary Reports

<u>Organization</u>	<u>No. of Copies</u>	<u>Organization</u>	<u>No. of Copies</u>
Defense Documentation Center Cameron Station Alexandria, Virginia 22314	(12)	Naval Construction Battalion Civil Engineering Laboratory Port Hueneme, California 93043 Attn: Materials Division	(1)
Office of Naval Research Department of the Navy Attn: Code 471 Code 102 Code 470	(1) (1) (1)	Naval Electronics Laboratory Center San Diego, California 92152 Attn: Electron Materials Science Division	(1)
Commanding Officer Office of Naval Research Branch Office 495 Summer Street Boston, Massachusetts 02210	(1)	Naval Missile Center Materials Consultant Code 3312-1 Point Mugu, California 93041	(1)
Commanding Officer Office of Naval Research Branch Office 536 South Clark Street Chicago, Illinois 60605	(1)	Commanding Officer Naval Surface Weapons Center White Oak Laboratory Silver Spring, Maryland 20910 Attn: Library	(1)
Office of Naval Research San Francisco Area Office One Hallidie Plaza, Suite 601 San Francisco, California 94102	(1)	David W. Taylor Naval Ship R&D Center Materials Department Annapolis, Maryland 21402	(1)
Naval Research Laboratory Washington, D.C. 20390 Attn: Code 6000 Code 6100 Code 6300 Code 6400 Code 2627	(1) (1) (1) (1) (1)	Naval Undersea Center San Diego, California 92132 Attn: Library	(1)
Naval Air Development Center Code 302 Warminster, Pennsylvania 18974 Attn: Mr. F. S. Williams	(1)	Naval Underwater System Center Newport, Rhode Island 02840 Attn: Library	(1)
Naval Air Propulsion Test Center Trenton, New Jersey 08628 Attn: Library	(1)	Naval Weapons Center China Lake, California 93555 Attn: Library	(1)
		Naval Postgraduate School Monterey, California 93940 Attn: Mechanical Engineering Dept.	(1)
		Naval Air Systems Command Washington, D.C. 20360 Attn: Code 52031 Code 52032	(1) (1)

BASIC DISTRIBUTION LIST (Cont'd)

<u>Organization</u>	<u>No. of Copies</u>	<u>Organization</u>	<u>No. of Copies</u>
Naval Sea System Command Washington, D. C. 20362 Attn: Code 035	(1)	NASA Headquarters Washington, D. C. 20546 Attn: Code RRM	(1)
Naval Facilities Engineering Command Alexandria, Virginia 22331	(1)	NASA Lewis Research Center 21000 Brookpark Road Cleveland, Ohio 44135 Attn: Library	(1)
Scientific Advisor Commandant of the Marine Corps Washington, D.C. 20380 Attn: Code AX	(1)	National Bureau of Standards Washington, D.C. 20234 Attn: Metallurgy Division Inorganic Materials Division	(1) (1)
Naval Ship Engineering Center Department of the Navy Washington, D.C. 20360 Attn: Code 6101	(1)	Defense Metals and Ceramics Information Center Battelle Memorial Institute 505 King Avenue Columbus, Ohio 43201	(1)
Army Research Office P.O. Box 12211 Triangle Park, N.C. 27709 Attn: Metallurgy & Ceramics Program	(1)	Office of Naval Research, Branch Office 1030 East Green Street Pasadena, CA. 91106	(1)
Army Materials and Mechanics Research Center Watertown, Massachusetts 02172 Attn: Research Programs Office	(1)	Metals and Ceramics Division Oak Ridge National Laboratory P.O. Box X Oak Ridge, Tennessee 37380	(1)
Air Force Office of Scientific Research Bldg. 410 Bolling Air Force Base Washington, D.C. 20332 Attn: Chemical Science Directo rate Electronics and Solid State Science Directo- rate	(1) (1)	Los Alamos Scientific Laboratory P.O. Box 1663 Los Alamos, New Mexico 87544 Attn. Report Librarian Argonne National Laboratory Metallurgy Division P.O. Box 229 Lemont, Illinois 60439	(1) (1)
Air Force Materials Lab (LA) Wright-Patterson AFB Dayton, Ohio 45433	(1)	Brookhaven National Laboratory Technical Information Division Upton, Long Island New York 11973 Attn: Research Library	(1)
Library, Bldg 50, Rm 134 Lawrence Radiation Laboratory Berkeley, CA 94720	(1)		

BASIC DISTRIBUTION LIST (Cont'd)

<u>Organization</u>	<u>No. of Copies</u>	<u>Organization</u>	<u>No. of Copies</u>
Director Applied Physics Laboratory (1) University of Washington 1013 Northeast Forthieth Street Seattle, Washington 98105			

SUPPLEMENTARY DISTRIBUTION LIST

Technical and Summary Reports

Dr. P. Heitman
Detroit-Diesel Allison
Mail Stop W5
P.O. Box 894
Indianapolis, IN 46206

Dr. M. E. Gulden
INESCO
11077 N. Torrey Pines Rd.
La Jolla, CA 92037

Mr. Charles P. Blankenship
Chief, Materials Division
Mail Stop 188M
NASA-Langley Research Center
Hampton, VA 23665

Dr. J. J. Brennan
United Technologies Research
Center
East Hartford, CT 06108

Dr. R. J. Palicka
CERADYNE, Inc.
3030 South Red Hill Avenue
Santa Ana, CA 92705

Dr. C. O. Hulse
United Technologies Research
Center
East Hartford, CT 06108

Dr. W. R. Prindle
Research and Development
Corning Glass Works
Corning, NY 14830

Dr. S. Rangaswamy
METCO, Inc.
1101 Prospect Avenue
Westbury, NY 11590

Dr. K. H. Styhr
AiResearch Casting Co.
2525 W. 190th St.
Torrance, CA 90509

Dr. E. M. Anderson
Research and Engineering
Exxon Corporation
P.O. Box 101
Florham Park, NJ 07923

Dr. Donald M. Curry, ES32
Thermal Technology Br.
National Aeronautics and
Space Administration
Lyndon B. Johnson Space Center
Houston, TX 77058

Dr. Fred Schmidt
E. I. DuPont
Engineering Dept. E-304
Experimental Station
Wilmington, DE 19898

SUPPLEMENTARY DISTRIBUTION LIST (Cont'd)

Advanced Research Project Agency
Materials Science Director
1400 Wilson Boulevard
Arlington, VA 22209

Mr. George Boyer
Sensor Systems Program
Office of Naval Research
Code 222
Arlington, VA 22217

Professor R. Bradt
Ceramics Section
Materials Sciences Department
The Pennsylvania State University
University Park, PA 16802

Professor L. E. Cross
The Pennsylvania State University
Materials Research Laboratory
University Park, PA 16802

Dr. A. G. Evans
Department Materials Science
and Engineering
Hearst Mining Building
University of California
Berkeley, CA 94720

Dr. Gene Haertling
Motorola Corporation
3434 Vassar, NE
Albuquerque, NM 87107

Dr. L. L. Hench
Department of Metallurgy
University of Florida
Gainesville, FL 32603

Dr. A. A. Heuer
Professor of Ceramics
Case Western Reserve University
University Circle
Cleveland, OH 44106

Dr. Paul Jorgensen
Stanford Research Institute
333 Ravenswood Avenue
Menlo Park, CA 94025

Dr. R. N. Katz
Army Materials and Mechanics
Research Center
Watertown, MA 02172

Dr. H. Kirchner
Ceramic Finishing Company
P.O. Box 498
State College, PA 16801

Dr. B. G. Koepke
Honeywell, Inc.
Corporate Research Center
10701 Lyndale Avenue South
Bloomington, MN 55420

Mr. Frank Koubek
Naval Surface Weapons Center
White Oak Laboratory
Silver Spring, MD 20910

Dr. J. Lankford
Southwest Research Institute
8500 Culebra Road
San Antonio, TX 78284

Professor P. B. Macedo
The Catholic University of America
Washington, DC 20017

Dr. N. Perrone
Code 474
Office of Naval Research
800 N. Quincy Street
Arlington, VA 22217

Dr. R. Rice
Naval Research Laboratory
Code 6360
Washington, DC 20375

SUPPLEMENTARY DISTRIBUTION LIST (Cont'd)

Mr. R. T. Swann
MD-Materials Research Branch
Mail Stop 396
NASA Langley Research Center
Hampton, VA 23665

Dr. K. H. Holko, Manager
Materials Applications
General Atomic Company
P.O. Box 81608
San Diego, CA 92138

Dr. W. Bakker
EPRI
3412 Hillview Avenue
P.O. Box 10412
Palo Alto, CA 94303

Dr. P. A. Miles, Research
Raytheon Company
28 Seyon Str.
Waltham, MA 02154

Dr. J. Ritter
University of Massachusetts
Dept. of Mech. Engr.
Amherst, MA 01002

Professor T. J. Rocket
University of Rhode Island
Kingston
RI 02881

Dr. G. E. Youngblood
MERDI
Butte, MT 59701

Dr. E. G. Kobetich
Experimental Station, Bldg. 302
E. I. DuPont Company
Wilmington, DE 19898

Dr. M. A. Adams
Jet Propulsion Laboratory
California Institute of Technology
4800 Oak Grove Drive
Pasadena, CA 91103

Dr. Clifford Astill
Solid Mechanics Program
National Science Foundation
Washington, DC 20550

Dr. R. J. Gottschall
U.S. Dept. of Energy
Div. of Materials Science
Mail Stop J309
Washington, DC 20545

Prof. R. Roy
Pennsylvania State Univ.
Materials Research Lab.
University Park, PA 16802

Dr. R. Ruh
AFML - WPAFB
Dayton, OH 45433

Hague International
3 Adams Street
South Portland, ME 04106

Mr. J. D. Walton
Engineering Exp. Station
Georgia Inst. of Technology
Atlanta, GA 30332

Dr. W. F. Adler
Effects Technology, Inc.
5383 Hollister Avenue
P.O. Box 30400
Santa Barbara, CA 92105

Mr. D. Richarson
Airesearch Manufacturing Company
4023 36th Street
P.O. Box 5217
Phoenix, AZ 85010

Dr. N. MacMillan
Materials Research Laboratory
Pennsylvania State University
College Park, PA 16802

Mr. W. B. Harrison
Honeywell Ceramics Center
1885 Douglas Drive
Golden Valley, MN 55422

SUPPLEMENTARY DISTRIBUTION LIST (Cont'd)

Dr. J. H. Rosolowski
General Electric Company
Research and Development Center
P.O. Box 8
Schenectady, NY 02301

Dr. J. H. Simmons
Catholic University of America
Washington, DC 20064

Dr. P. L. Smith
Naval Research Laboratory
Code 6361
Washington, DC 20375

Dr. R. W. Timme
Naval Research Laboratory
Code 8275
Underwater Sound Reference Division
P.O. Box 8337
Orlando, FL 32806

Dr. Charles C. Walker
Naval Sea Systems Command
National Center #3
2531 Jefferson Davis Highway
Arlington, VA 20390

Dr. Paul D. Wilcox
Sandia Laboratories
Division 2521
Albuquerque, NM 87115

Dr. Murray Gillen
Australian Embassy
Washington, DC 33801

Dr. R. N. Kleiner
Coo Porcelain Company
17750 W. 32nd Avenue
Golden, CO 80401

Dr. S. M. Wiederhorn
Physical Properties Section
Bldg. 223, Rm. A355
National Bureau of Standards
Washington, DC 20234

Dr. P. F. Becher
Code 6362
U.S. Naval Research Laboratory
Washington, D.C. 20375

Dr. R. Jaffee
Electric Power Research Institute
3412 Hillview Avenue
P.O. Box 10412
Palo Alto, CA 94303

Dr. B. A. Wilcox
Metallurgy and Materials Division
National Science Foundation
Washington, DC 20550

Dr. H. E. Bennett
Naval Surface Weapons Center
Research Department Code 601
China Lake, CA 93555

Dr. R. J. Charles
General Electric Company
Research and Development Center
Schenectady, NY 12301

Dr. A. R. C. Westwood
Martin-Marietta Laboratories
1450 South Rolling Road
Baltimore, MD 21227

Dr. N. S. Corney
Ministry of Defense
(Procurement Executive)
The Adelphi
John Adam Street
London WC2N 6BB
UNITED KINGDOM

Dr. D. E. Niesz
Battelle Memorial Institute
505 King Avenue
Columbus, OH 43201

Dr. R. E. Engdahl
Deposits and Composites, Inc.
318 Victory Dr.
Herndon, VA 22070

Professor W. D. Kingery
Ceramics Div. Rm. 13-4090
MIT
77 Mass. Avenue
Cambridge, MA 02139

SUPPLEMENTARY DISTRIBUTION LIST (Cont'd)

Dr. A. M. Alper
GTE Sylvania Inc.
Towanda, PA 18848

Dr. W. H. Rhodes
GTE Laboratories Inc.
40 Sylvan Rd.
Waltham, MA 02154

Dr. D. C. Larson
IIT Research Inst.
10 W. 35th Street
Chicago, IL 60616

Dr. B. Butler, Chief
Materials Branch
Solar Energy Research Institute
1536 Cole Blvd
Golden, CO 80401

Dr. M. Berg
AC Spark Plug Division
General Motors Corp.
1601 N. Averill Avenue
Flint, MI 48556

Dr. F. E. Kennedy
Thayer School of Engineering
Dartmouth School of Engineering
Hanover
NH 03755

Dr. R. J. Bratton
R&D Center
Westinghouse Electric Corp.
Pittsburgh, PA 15235

Dr. W. Reilly, Director
PPG Industries
P.O. Box 31
Barberton, OH 44203

Dr. D. J. Godfrey
Admiralty Materials Laboratory
Ministry of Defense
(Procurement Executive)
Holton Heath
Poole, Dorset
BH16 6 JU
UNITED KINGDOM

Dr. Wm. Kessler
AFML
Wright-Patterson Air Force Base
OH 45433

Dr. S. F. Galasso
United Aircraft Research Laboratories
East Hartford, CN 06108

Dr. M. Srinivasan
The Carborundum Comp.
P.O. Box 1054
Niagara Falls, NY 14302

Dr. W. D. Tuohig
Bendix Research Laboratories
Southfield, MI 48076

Dr. Robert Ruh
AFML/LLM
Wright-Patterson AFB
OH 45433

Mr. J. Schuldies
Airesearch Manufacturing Company
P.O. Box 5217
Phoenix, AZ 85010

Dr. S. Musikant
General Electric Company
3198 Chestnut Street
Philadelphia, PA 19101

Dr. D. W. Richerson
Airesearch Man. Comp. Code 503-44
Garrett Corp.
111 S. 34th Str., Box 5217
Phoenix, AZ 85034

Dr. Frank Recny
General Electric Company
Court Street
Plant Building C
Box 1122
Syracuse, NY 13201

Globe-Union, Inc.
5757 North Green Bay Avenue
Milwaukee, WI 53201
Attn: G. Goodman

SUPPLEMENTARY DISTRIBUTION LIST (Cont'd)

Mr. J. F. McDowell
Sullivan Park
Corning Glass Works
Corning, NY 14830

Dr. E. K. Beauchamp, Div. 5846
Sandia Laboratories
Albuquerque, NM 87185

Dr. J. A. Rubin
Kyocera International, Inc.
8611 Balboa Avenue
San Diego, CA 92123

Dr. W. V. Kotelesky
Materials Technology Department
TRW, Inc.
One Space Park
Redondo Beach, CA 90278

Dr. N. N. Ault
NORTON Comp.
One New Bond Street
Worcester, MA 01606

Dr. Hayne Palmour III
Engineering Research Division
N.C. State University
P.O. Box 5995
Raleigh, NC 27650

Dr. D. Ulrich
AFOSR, Code NC
Chemical Sciences Div.
1400 Wilson Blvd.
Arlington, VA 22209

Dr. V. J. Tennery
Oak Ridge Nat. Lab.
Oak Ridge, TN 38730

Dr. E. D. Lynch
Lynchburg Research Center
Babcock and Wilcox Co.
Box 1260
Lynchburg, VA 24505

Dr. S. C. Dixon
SDD-Thermal Structure Branch
Mail Stop 395
NASA Langley Research Center
Hampton, VA 23665

Dr. F. W. Clinard, Jr.
Los Alamos Scientific Lab.
MS 546
P.O. Box 1663
Los Alamos, NM 87544

Dr. D. DeCoursin
Fluidyne Eng.
5900 Olson Memorial Hwy.
Minneapolis, MN 55422

Dr. F. F. Lange
Rockwell International
P.O. Box 1085
1049 Camino Dos Rios
Thousand Oaks, CA 91360

Dr. T. Vasilos
AVCO Corporation
Research and Advanced Development
Division
201 Lowell Str.
Wilmington, MA 01887

Dr. R. E. Rondeau
AFML-LDJ
Wright Patterson-Air Force Base
OH 45433

Dr. S. Dutta
NASA-Lewis Research Center
Mail Stop 49-3
21000 Brookpark Rd.
Cleveland, OH 44135

Mr. B. Probst
NASA-Lewis Research Center
21000 Brookpark Rd.
Cleveland, OH 44135

Dr. S. W. Freiman
Deformation and Fracture Group
Physical Properties Section, Bldg 223
National Bureau of Standards
Washington, DC 20234

Mr. W. Trombley
Garrett Corporation
1625 Eye Str. NY
Suite 515
Washington, DC 20006

ATE
LMED
8-8